

**Liver-specific
overexpression of the IGF2 mRNA-binding
protein p62 induces a fatty liver disease phenotype**

Dissertation
zur Erlangung des Grades
des Doktors der Naturwissenschaften
der Naturwissenschaftlich-Technischen Fakultät III
Chemie, Pharmazie, Bio- und Werkstoffwissenschaften
der Universität des Saarlandes

vorgelegt von
Elisabeth Tybl

Saarbrücken
Dezember 2009

Tag des Kolloquiums:

Dekan:

Berichterstatter:

Vorsitz:

Akademischer Mitarbeiter:

Table of contents

Table of contents	1
Zusammenfassung	6
Abstract	7
1. Introduction	9
1.1 Hepatocellular carcinoma	9
1.2 NASH	11
1.3 The tumor-associated autoantigen <i>p62</i>	11
1.4 DNA methylation	12
1.5 Genomic imprinting	12
1.6 The imprinted genes IGF2 and H19	14
1.6.1 H19	14
1.6.2 IGF2	16
1.7 IGF2 downstream signalling pathways	19
1.7.1 Phosphoinositide 3-kinase (PI3-kinase)	19
1.7.1.1 AKT	21
1.7.1.2 PTEN	23
1.7.2 Impact of PTEN and pAKT on lipid and glucose metabolism	24
1.8 RNA interference	26
1.9 Mice	27
1.9.1 The tet system	27
1.9.2 <i>p62</i> transgenic mice	28
1.10 Aim of this work	29
2. Methods	30
2.1 Animals	30
2.1.1 Animal welfare	30
2.1.2 Generation of <i>p62</i> transgenic animals	30
2.1.3 Isolation of genomic DNA from mouse tails	32
2.2 Bacteria	32
2.2.1 Preparation of competent bacteria	32
2.2.2 Transformation of plasmid DNA in competent bacteria	32

2.2.3	Isolation of plasmid DNA	33
2.2.4	Determination of DNA concentration	33
2.3	Agarose gel electrophoresis	33
2.4	PCR (Polymerase Chain Reaction)	34
2.5	Reverse Transcription	37
2.6	Real-time quantitative RT-PCR	42
2.7	SNuPE analysis	46
2.8	Western Blot	47
2.8.1	Preparation of protein extracts from mouse liver tissue	48
2.8.2	Preparation of protein extracts from isolated mouse hepatocytes and hepatoma cell lines	48
2.8.3	Determination of protein concentration using the Bradford Assay	48
2.8.4	SDS polyacrylamide gel electrophoresis (SDS-PAGE)	49
2.8.5	Protein transfer onto PVDF membranes	49
2.9	Cell culture	51
2.9.1	Determination of cell amount and cell viability	52
2.9.2	Determination of living cells	52
2.9.3	Cell viability assay	53
2.9.4	Treatment of human hepatocellular carcinoma cell lines with siRNA	53
2.9.5	Preparation of siRNA	54
2.9.6	Transfection reagent	54
2.9.7	Transfection of human hepatocellular carcinoma cell lines	54
2.10	Isolation of primary murine hepatocytes	55
2.10.1	Collagenase perfusion	55
2.11	Caspase-3-like activity assay	57
2.11.1	Measurement of caspase-3-like activity in murine hepatocytes	57
2.11.2	Measurement of caspase-3-like activity in mouse liver tissue	58
2.12	Actinomycin D treatment and mRNA half-live estimation	58
2.13	Histological staining	59
2.13.1	Fixation and embedding of liver tissue	59
2.13.1.1	Cryostat histology	59
2.13.1.2	Paraffin histology	59
2.13.1.3	Preparation of slides	60

2.13.1.4	Embedding of stained slides	60
2.13.2	Routine staining	60
2.13.2.1.	Periodic acid Schiff staining (PAS)	60
2.13.2.2.	Scharlach Red staining	61
2.13.2.3.	Counter-staining	61
2.13.3	Immunostaining	61
2.13.3.1	Heat-induced epitope retrieval (HIER)	62
2.13.3.2	Peroxidase pre-treatment	63
2.13.3.3	Biotin block	63
2.13.3.4	CSA II kit staining procedure	63
2.13.3.5	Detection using the DAKO REAL™ EnVISION™ detection system	64
2.13.3.6	Quality control	64
2.14	Intraperitoneal glucose tolerance test (IP-GTT)	65
2.15	Laboratory chemistry	66
2.15.1	Enzymes	66
2.15.1.1	Transaminases	66
2.15.1.1.1	ALT (GPT)	67
2.15.1.1.2	AST (GOT)	67
2.15.2	Substrates and metabolites	68
2.15.2.1	Cholesterol and HDL	68
2.15.2.2	Triglycerides	68
3.	Results	70
3.1	Liver specific expression of <i>p62</i>	70
3.1.1	Genotyping of <i>p62</i> mice	72
3.1.2	Genotyping of <i>p62/LT2/SD7</i> mice by allele-specific PCR	72
3.1.3	<i>p62</i> expression	74
3.2	Induction of a fatty liver disease phenotype	74
3.2.1	HE	74
3.2.2	Scharlach Red	75
3.2.3	PAS	76
3.3	Increased liver to body weight ratio	77
3.4	Absence of liver damage	78
3.4.1	Serum lipids	78

3.5	Absence of inflammatory parameters	79
3.5.1	Serum transaminases	79
3.5.2	Immunohistology of NF- κ B	80
3.6	Increased expression of IGF2 and H19	82
3.7	Localisation of <i>p62</i> and IGF2	84
3.8	No alteration of IGF2 and H19 mRNA stability	85
3.9	Monoallelic expression of IGF2 and H19	87
3.10	Correlation between <i>p62</i> and IGF2 and H19 in human hepatoma cell lines	92
3.11	Increased phosphorylation of the protein kinase AKT	95
3.12	Act D/TNF- α -induced apoptosis protection	96
3.13	Decreased PTEN expression	98
3.13.1	PTEN in <i>p62</i> transgenic mice	98
3.13.2	PTEN in HepG2 cells	100
3.14	Intraperitoneal glucose tolerance test (IP-GTT)	100
4.	Discussion	103
4.1	The <i>p62</i> protein and HCC	103
4.1.1	<i>p62</i> transgenic mice	103
4.2	Phenotypic alterations	105
4.2.1	Appearance of basophilic cell foci	105
4.2.2	Fatty liver phenotype	106
4.2.3	Disturbance in glycogen storage	107
4.2.4	Metabolic alterations	108
4.2.4.1	Increased liver to body weight ratio	109
4.2.4.2	Alteration of serum levels	109
4.2.5	Non-inflammatory phenotype	110
4.2.5.1	Absence of inflammatory parameters	110
4.2.5.2	Absence of NF- κ B translocation	111
4.3	Increased IGF2 and H19 expression	112
4.3.1	Absence of transcriptional stability changes	112
4.3.2	Monoallelic expression of IGF2 and H19	114
4.3.3	Silencing of <i>p62</i>	116
4.4	IGF2 downstream effects	116

4.4.1	Decreased PTEN expression	116
4.4.2	Increased phosphorylation of AKT/protein kinase B	118
4.4.3	Apoptosis protection	119
4.5	Improved glucose tolerance	120
5.	Summary	121
6.	Outlook	122
7.	Supplement	123
7.1	PCR primer	123
7.2	Taq Man probes	124
7.3	Real-time PCR conditions using Taq Man probes	124
7.4	Real-time PCR conditions using SYBR green	124
7.5	Antibodies	125
7.6	siRNA	125
7.7	Molecular weight markers	125
7.8	Solutions and buffers	126
7.8.1	Cell culture media	126
7.8.2	Solutions for primary murine hepatocyte isolation	126
7.8.3	Solutions for Western Blotting	128
7.8.4	Solutions for caspase measurements	129
7.8.5	Material for SnuPE analysis	130
8.	Bibliography	132
9.	Publications	161
9.1	Abstracts	161
9.2	Original Publications	162
10.	Curriculum vitae	163
11.	Acknowledgement	164

Zusammenfassung

Im Rahmen dieser Arbeit sollte erstmals die Rolle des Autoantigens *p62*, das in HCC Tumoren nachgewiesen werden konnte, mit Hilfe eines Mausmodells untersucht werden. Hierzu wurden Mäuse generiert, die das humane *p62* Protein unter Kontrolle des liver enriched activator proteins (LAP) leberspezifisch exprimieren.

Aufgrund der postulierten insulin-like growth factor 2 (IGF2) mRNA-bindenden Eigenschaft von *p62* wurde vermutet, dass *p62* die Expression des metabolischen Wachstumsfaktors IGF2 regulieren könnte.

In der Tat zeigten Untersuchungen einen starken Anstieg der IGF2 und H19 Expression in *p62* transgenen Tieren. Dabei übt *p62* weder einen Einfluss auf die mRNA Stabilität aus, noch verursacht es eine Änderung der Allel-spezifischen Expression von IGF2 und H19.

Mit Auftreten der höchsten IGF2 Expression in *p62* transgenen Tieren konnte gleichzeitig der Phänotyp einer Fettleber zu einem frühen Alterszeitpunkt gezeigt werden.

Untersuchungen von Zielstrukturen, die IGF2-vermittelt reguliert werden, konnten eine Aktivierung von AKT sowie eine Inaktivierung von PTEN zeigen. Nachdem diese Ergebnisse einen anti-apoptotischen Phänotyp vermuten ließen, wurde die Apoptoserate anhand der Caspase-3-Aktivität bestimmt. In Hepatozyten aus *p62* transgenen Tieren konnte in der Tat ein Schutz vor induzierter Apoptose nachgewiesen werden.

Der Zusammenhang zwischen erhöhter *p62*, IGF2 und H19 Expression konnte abschließend mit Hilfe eines RNA-Interferenz Ansatzes im menschlichen System untermauert werden.

Abstract

Although *p62* was originally identified to be highly expressed in HCC tissue, its potential functional implications in liver disease have as yet been completely unknown. Therefore, aim of this work was to elucidate functional implications of hepatic overexpression of the tumor-associated autoantigen *p62*. This is why liver-specific *p62* transgenic mice were generated, which express *hup62* under control of the liver enriched activator protein (LAP).

Due to the IGF2 mRNA-binding properties of *p62*, a potential regulation of IGF2, a metabolically active growth factor, was hypothesized.

In fact, a highly increased expression of IGF2 and the closely associated H19 RNA, with which it shares an imprinting control region, could be demonstrated.

Investigations on IGF2 and H19 mRNA stability in isolated hepatocytes employing the transcription inhibitor actinomycin D (ActD) revealed no alterations in mRNA turnover upon *p62* expression. Since IGF2 and H19 are imprinted genes, allele-specific expression of both genes was investigated. However, no changes in allele-specific expression could be determined upon expression of *p62*.

Histological examinations showed the phenotype of a fatty liver in *p62* transgenic mice at a very early age when also IGF2 expression was highest.

Regarding potential IGF2 downstream targets, PTEN was downregulated in *p62* transgenic animals, whereas an increase in the phosphorylation of AKT was demonstrated.

Since a respective signalling status might exert anti-apoptotic actions, apoptotic cell death was determined, measured as caspase-3-like activity. In fact, a decrease upon ActD/TNF- α induced apoptosis manifested in hepatocytes from *p62* transgenic mice.

In order to investigate the causal correlation between increased IGF2 and H19 and *p62* overexpression also in a human system, siRNA-mediated knockdown of *p62* was

performed in human hepatoma cell lines confirming *p62* as a regulator of both IGF2 and H19.

In summary, these results for the first time characterize functional implications of *p62* overexpression and suggest the induction of an anti-apoptotic, fatty liver phenotype.

1. Introduction

1.1 Hepatocellular carcinoma

Hepatocellular carcinoma (HCC) and cholangiocellular carcinoma (CCC) are primary malignant liver cancers. HCC is the sixth most common cancer worldwide in terms of numbers of cases (5.7%) and the third most common cause of death from cancer. 500,000 to 800,000 incidences per year are observed with areas of high incidence (50-150 cases per 100,000 inhabitants) in parts of South East Asia and Africa (Figure 1). In Germany, each year 6,000 newly diagnosed cases are registered. The overall sex ratio (male: female) is around 2.4 (Parkin, Bray et al. 2005).

In most cases, HCC is developing from chronic liver cirrhosis caused by Hepatitis B and C virus infection, chronic alcohol consumption or hemochromatosis. Aflatoxins promote tumorigenesis in the case of an existing Hepatitis B, which might be a reason for the high incidence in the tropical areas of the world where food is frequently contaminated with the fungus *Aspergillus* (Yeh, Yu et al. 1989).

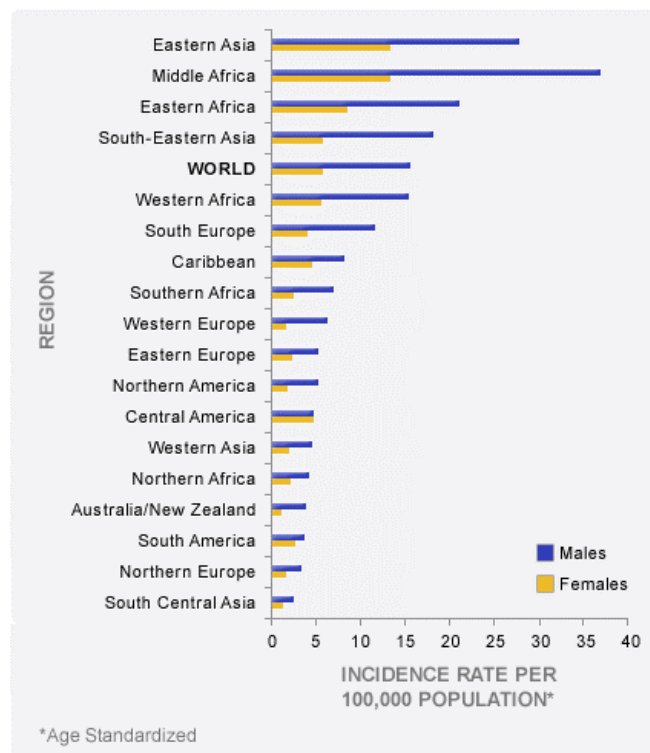


Figure 1: Age standardized incidence for liver cancer. Data show incidences per 100,000 by sex (source:<http://rafscience.com>).

Recently, states of insulin resistance like obesity, diabetes mellitus, non-alcoholic fatty liver disease (NAFLD), and non-alcoholic steatohepatitis (NASH) have increasingly shown to represent metabolic risk factors contributing to HCC.

These diseases might explain the rise in incidence, which doubled in men and women in the industrialized countries including the U. K. and Germany over the past 20 years (Cancer Research UK) (Figure 2).

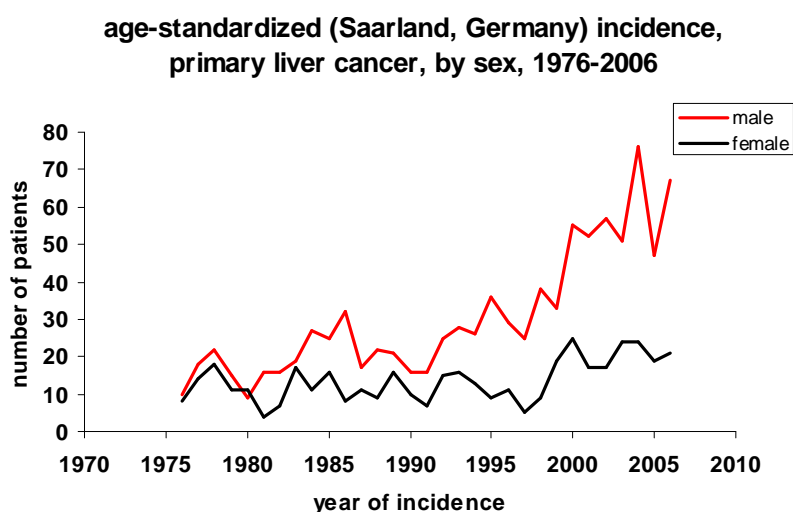


Figure 2: Rates of incidence of primary liver cancer in Saarland, Germany between 1976 and 2006 (source: www.krebsregister.saarland.de)

Overall survival (3-5%) shows a poor prognosis due to the lack of efficient systemic treatment options, leading to an average life span of about six month after diagnosis. As the molecular factors and interactions involved in hepatocarcinogenesis are poorly understood, it is necessary to gain an understanding of the pathogenesis to improve therapeutic treatment. Malignant transformation of hepatocytes may occur through an increase in liver cell turnover due to chronic liver injury and regeneration in a context of inflammation, immune response, and oxidative DNA damage, leading to genetic alterations. This may result in the activation of oncogenes, the inactivation of tumor suppressor genes or the overexpression of growth factors (Yang and Rogler 1991).

1.2 NASH

NAFLD encompasses a wide spectrum of diseases ranging from triglyceride accumulation in hepatocytes (hepatic steatosis) without and with inflammation (steatohepatitis), fibrosis, and cirrhosis (Neuschwander-Tetri and Caldwell 2003). NAFLD is more and more recognized as a major cause of liver-related morbidity and mortality due to its potential to promote the development of metabolic disorders, resulting in liver cirrhosis and HCC (Teli, James et al. 1995). NAFLD resembles the pathological picture of an alcohol induced liver disease but it is found in patients who do not abuse alcohol (Neuschwander-Tetri and Caldwell 2003). Meanwhile, this disease affects approximately 30 million Americans (Clark, Brancati et al. 2002) and prognosis prevalence is bad due to an increase in the epidemics diabetes and obesity.

Day et al. proposed a “two-hit” model to explain the progression of NAFLD (Day and James 1998). The “first hit” constitutes the deposition of triglycerides in the cytoplasm of the hepatocyte whereas the “second hit” includes additional cellular events, e. g. inflammation, cell death and fibrosis, which progress the disease.

1.3 The tumor-associated autoantigen *p62*

p62 belongs to the family of insulin-like growth factor 2 (IGF2)-mRNA binding proteins (IMPs) containing two types of RNA-binding motifs, the consensus sequence RNA binding domain (CS-RBD) and four human heterogeneous nuclear (hn) RNP K homology (KH) domains. These mRNA binding proteins contribute to tumorigenesis by regulating mRNA stability and localisation. Nielsen et al. showed in 1999 that IMPs bind to the 5'-sequence of the IGF2 leader 3 mRNA, thereby causing a translational repression of IGF2 expression (Nielsen, Christiansen et al. 1999). A potential regulation of IGF2 mRNA by *p62* is of special interest since IGF2 has been shown to be overexpressed in HCC (Su, Schröder et al. 1998) and has been shown to promote tumors in transgenic mice (Christofori, Naik et al. 1994). *p62* was originally isolated in 1999 (Zhang, Chan et al. 1999) as a 62 kDA autoantigen located in the cytoplasm of HCC tumor cells. It was demonstrated that *p62* is developmentally regulated, i.e. it is expressed in malignant cancer cells as well as in

fetal tissue but it could not be detected in normal, non-neoplastic hepatocytes (Zhang, Zhu et al. 2001).

1.4 DNA methylation

DNA methylation is a type of chemical modification that can be inherited and subsequently removed without changing the original DNA sequence. Methylation and demethylation events of DNA are central to the epigenetic regulations in development (Russo, Tommasi et al. 1996). Beyond, DNA methylation is implicated in the regulation of transcription, in maintaining genome stability (i. e. by establishing the allele-specific expression status) and in the inactivation of the X-Chromosome (Li, Beard et al. 1993; Bestor 2000). The mechanisms controlling these events are of fundamental importance in developmental cell biology but also seem to be implicated in carcinogenesis and tumour progression (Patra, Patra et al. 2002). Only DNA methylation typically occurs in a CpG dinucleotide context. CpG stands for cytosine and guanine separated by a phosphate (—C—phosphate—G—), which links the two nucleosides together in DNA. 2-3 % of the mammalian genome contains methylated cytosines, whereby in mammals, most prominent is the methylation of the DNA on cytosine at the 5'-position in CpG dinucleotides, catalysed by DNA methyltransferases (DNMTs). Two enzyme classes are known, from which DNMT1 is responsible for methylation of the newly synthesized strand, thereby being essential for the maintenance of the DNA methylation pattern (Bestor 2000). DNA methylase MBD2 performs the reverse reaction (Bhattacharya, Ramchandani et al. 1999).

Although DNMT2 shares high sequence homology with members of the DNA methyltransferase family, it was shown to have no DNA methyltransferase activity (Yoder and Bestor 1998). Surprisingly, DNMT2 represents an active RNA methyltransferase (Goll, Kirpekar et al. 2006).

1.5 Genomic imprinting

For the majority of genes both copies, one inherited from the father, one from the mother, are functional. However, in a small subset of genes, one copy is switched off in a parent-of-origin specific manner. These genes are called imprinted because one

copy is epigenetically marked leading to a monoallelic expression of the gene. Imprinting can vary between developmental stages, tissues, and species (Reik and Walter 2001). Paternally expressed imprinted genes tend to promote growth while it is suppressed by those genes that are maternally expressed.

A genome-wide search for imprinted genes in the human genome with the use of computer-learning algorithms resulted in the identification of 156 novel candidate imprinted genes (Luedi, Dietrich et al. 2007). In 2008, the “catalogue of imprinted genes and parent-of-origin effects in humans and animals” contained 219 imprinted genes (<http://igc.otago.ac.nz/Summary-table.pdf>).

The majority of imprinted genes show differences in DNA methylation between the parental alleles. Usually, a high density of cytosine-guanine dinucleotides (CpG) islands characterise imprinted genes.

In 1983, Feinberg and Vogelstein reported differences in DNA methylation at CpG islands in tumors for the first time (Feinberg and Vogelstein 1983). A dysregulation of this functional haploid state by a single epigenomic change can cause tremendous health effects making imprinted genes a susceptible target for human pathologies. Imprinting associated diseases occur through early development (e. g. Beckwith-Wiedemann, Prader-Willi or Angelman syndrome) or as cancer (e.g. breast, lung, liver, colorectal cancer) when altered later in life (Jirtle 1999). Moreover, imprinting disorders have an impact on metabolic diseases like diabetes mellitus or obesity.

Allele-specific expression of genes was first detected in 1991 for the fetal growth-factor IGF2, its receptor IGF2R and for H19 by restriction-fragment-length polymorphisms and RNase protection assays (DeChiara, Robertson et al. 1991).

Interestingly, imprinted genes are often arranged in clusters, i. e. imprinted genes are in vicinity of other imprinted genes. Activation of H19 expression on the maternal chromosome leads to the inactivation of the IGF2 gene, giving one example of two promoters competing for the same enhancer element, leading to a reciprocal gene expression. On the paternal allele, the IGF2 promoter drives IGF2 gene expression while at the same time inactivating H19 (Leighton, Saam et al. 1996). The imprinting

of IGF2 and H19 is controlled by a region located 4 kb upstream from the H19 transcription unit, defined as the H19 differentially methylated region (DMR) or imprinting control region (ICR) (Thorvaldsen, Duran et al. 1998).

1.6 The imprinted genes IGF2 and H19

The genes for both IGF2 and H19 are mapped to a 90 kilobase (kb) region in a gene cluster on human chromosome 11p15.5 (Zemel, Bartolomei et al. 1992) and on the distal region of chromosome 7 in mice (Pachnis, Belayew et al. 1984). In the majority of human tissues, only the maternal allele of the H19 gene is expressed and only the paternal allele of the IGF2 gene is expressed. In liver, IGF2 is monoallelically expressed at birth, with a switch to biallelic expression during the first year of postnatal life (Ohlsson, Nystrom et al. 1993; Davies 1994; Ekström, Cui et al. 1995). In contrast, H19 is imprinted in normal human liver throughout life (Ekström, Cui et al. 1995). Biallelic expression of IGF2 and H19 has been demonstrated in several paediatric (e. g. Wilms' tumor) and adult malignancies (e.g. lung cancer) (Glassman, de Groot et al. 1996; Ross, Schmidt et al. 1999).

1.6.1 H19

The H19 gene encodes for a 2.3 kb non-coding RNA (Brunkow and Tilghman 1991). It was originally identified as a fetal liver-specific mRNA whose repression after birth paralleled that of the α -fetoprotein (AFP) gene (Pachnis, Belayew et al. 1984).

Both genes are under the control of two trans-acting loci in the mouse, termed *raf* and *Rif* (Pachnis, Belayew et al. 1984). These loci determine the adult basal and inducible levels, i. e. they affect the transcription of H19 mRNA. The H19 gene is composed of five exons, along with four very small introns. Preceding the translation initiation codon are four ATG codons, each of which is followed shortly thereafter by translation terminator codons (Pachnis, Brannan et al. 1988). This leads to H19 RNA transcription, splicing and poly-adenylation but probably not to translation. The localization of the H19 RNA to a cytoplasmic ribonucleoprotein (RNP) particle led to the conclusion that this RNA does not encode a protein (Brannan, Dees et al. 1990).

To identify the function of H19, several mouse models were established. The overexpression of H19 is lethal: mouse embryos die between day 14 and birth (Brunkow and Tilghman 1991). Loss of function of H19 does not lead to embryonic death in mice (Leighton, Saam et al. 1995). The overgrowth phenotype of H19 deficient mice is most likely due to the biallelic expression of IGF2 (Ripoche, Kress et al. 1997). This is why H19 is supposed to act as a regulator of IGF2 (Leighton, Saam et al. 1995).

The controversy whether H19 acts as a tumor suppressor or whether it promotes carcinogenesis has not yet been resolved, as numerous tumors display either overexpression or lack of H19 expression (Matouk, DeGroot et al. 2007; Yoshimizu, Miroglio et al. 2008).

Certain known carcinogens increase the level of H19. In this context diethylnitrosamine, a known carcinogen of the liver, has been regarded to induce H19 RNA expression in a mouse model (Graveel, Jatkoa et al. 2001). Also the c-Myc proto-oncogene plays an important role in the development of HCC (Coulouarn, Gomez-Quiroz et al. 2006) and is known to induce H19 expression (Barsyte-Lovejoy, Lau et al. 2006). H19 RNA is upregulated in HBV-associated HCC (Iizuka, Oka et al. 2002). Furthermore, a biallelic expression of the H19 gene was found in human HCC patients (Kim and Lee 1997).

Due to observations from Beckwith-Wiedemann syndrome, an overgrowth syndrome with an increased risk for embryonic tumors, it has been hypothesized that tumor predisposition is related to the 11p15.5 chromosomal region and the imprinting status at the H19-IGF2 locus, with a loss of imprinting (LOI) leading to a higher tumor risk (Rump, Zeegers et al. 2005).

As a result of this observation, the H19-IGF2 locus can be looked upon as a tumor suppressor candidate. *In vitro* experiments support initial evidence that underline this hypothesis (Hao, Crenshaw et al. 1993). *In vivo*, the acceleration in the latency of appearance of SV40 induced tumors in mice was revealed in the absence of H19 expression (Yoshimizu, Miroglio et al. 2008).

In addition, loss of the maternal and duplication of the paternal copy of the chromosomal region bearing the IGF2 and H19 genes occur at high frequency in HCC (Casola, Ungaro et al. 1995). These genetic events resemble the loss of heterozygosity (LOH) occurring at chromosome 11p15.5 loci in human cancers, result in the induction of IGF2, and lack of H19 expression.

1.6.2 IGF2

Insulin-like growth factor 2 (IGF-2) plays a key role in mammalian growth, influencing foetal cell division and differentiation and possibly metabolic regulation (Figure 3) (Nielsen 1992; O'Dell and Day 1998).

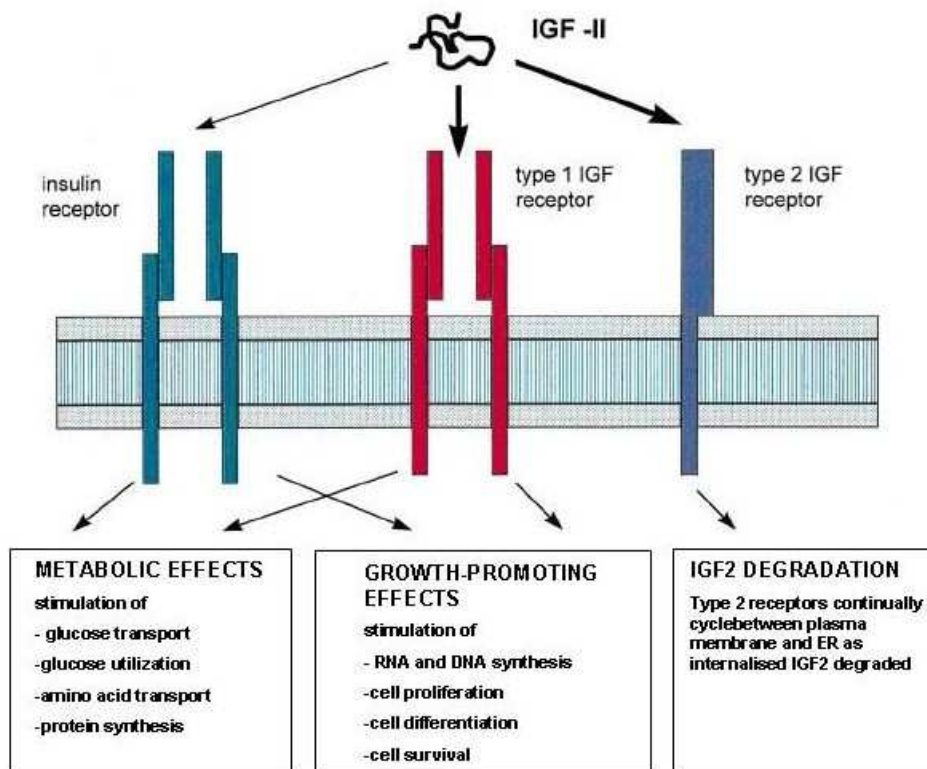


Figure 3: Interaction of IGF2 with its receptors and the multiple effects upon activation (source: (O'Dell and Day 1998))

The gene extends over approximately 12 kb of mouse chromosome 7 including six exons (Rotwein and Hall 1990). Exons 1-3 encode distinct 5'-untranslated regions and are transcribed by three different promoters, P1, P2, and P3, into three IGF2 mRNAs sharing common coding and 3' untranslated sequences. Exons 4-6 code for

the 180 amino-acid IGF2 precursor and exon 6 contains a 3'-untranslated region, which ends at a single poly-adenylation site (Rotwein and Hall 1990).

The mature 67 amino acid peptide shares sequence homology with both insulin and IGF1. The liver is the main endocrine source of IGFs, but autocrine/paracrine activity is found in most tissues (Moses, Nissley et al. 1980; Milner and Hill 1984). IGF2 stimulates growth through the insulin-like growth factor I receptor (IGF-IR), a ligand-activated tyrosine kinase (Baker, Liu et al. 1993). The IGF2 receptor appears to negatively regulate growth by targeting IGF2 to digestive lysosomes (Oka, Rozek et al. 1985).

Heterozygous knockout of the IGF2 gene led to fetal growth restriction in mice (DeChiara, Efstratiadis et al. 1990). Transmission through the male germline resulted in heterozygous progeny, which were smaller than wild-type littermates (about 60% of normal body weight). In contrast, if knockout transmission occurred through the female germline, the offspring was phenotypically normal.

Overexpression of IGF2 was detected in many tumours and for more than 20 years, it has been known that IGF2 contributes to tumorigenesis (Reeve, Eccles et al. 1985) through its anti-apoptotic and growth-stimulating effects (Pavelic, Bukovic et al. 2002).

Differential methylation of DNA in CpG islands is of fundamental importance in the maintenance of monoallelic gene expression (Li, Beard et al. 1993; Ward, Fisher et al. 1997). Transcription of the IGF2 gene is regulated by the H19 DMD region. On the paternal chromosome, the H19 DMD is methylated leading to the depression of the IGF2 promoter, while on the maternal chromosome the H19 DMD region is unmethylated. Loss of imprinting (LOI), resulting from the methylation of the maternal H19 DMD, leads to promoter activation on both alleles with the consequence of a biallelic IGF2 expression. This LOI might be a reason for IGF2 overexpression in tumors (Cui, Niemitz et al. 2001; Nakagawa, Chadwick et al. 2001).

Moreover, three CpG-rich, differentially methylated regions (DMR 1, DMR 2 and DMR 3) are located in the IGF2 locus, playing a role in monoallelic expression during

embryogenesis (Feil, Walter et al. 1994; Moore, Constancia et al. 1997). Whereas DMR 1 has been shown to be a methylation sensitive silencer, methylation of DMR 2 results in the upregulation of the IGF2 gene expression (Murrell, Heeson et al. 2001). In contrast to DMR 2, deletion of DMR 1 leads to silencing of IGF2 (Constancia, Dean et al. 2000). DMR 3 becomes temporarily demethylated before returning to the allele-specific pattern (Kuroiwa, Sakamoto et al. 2009).

Christofori et al. (Christofori, Naik et al. 1995) observed that endogenous IGF2 gene expression was activated in precancerous lesions and islet cell carcinomas of the pancreas in transgenic mice, which express SV40 large T-antigen under regulation of the rat insulin promoter. To test the hypothesis that IGF2 has a functional role in the development of pancreatic tumors, SV40 T-antigen transgenic mice were crossed with IGF2-deficient mice (DeChiara, Efstratiadis et al. 1990; Christofori, Naik et al. 1995). When tumors occurred in the animals, a direct correlation was observed between the IGF2 gene and the volume of tumors formed in the pancreas. There was a fivefold higher apoptotic index in tumors which lacked IGF2, suggesting that IGF2 plays a role in suppressing apoptosis.

Evidence of IGF2 involvement in hepatocarcinogenesis was deduced from animal models as well as in human HCC. IGF2 reexpression in four independent mouse lines may contribute to hepatocarcinogenesis through an autocrine mechanism (Schirmacher, Held et al. 1992). Transforming-growth factor α (TGF- α) is reactivated during hepatocarcinogenesis. In TGF α - transgenic mice 100% of HCC expressed IGF2 with the paternal allele silent and the maternal allele activated (Harris, Rogler et al. 1998). A 40- to 100-fold increase in the level of IGF2 mRNA was detected in 22% of primary liver cancers (Cariani, Lasserre et al. 1988). This increase in liver IGF2 transcripts is consistent with what was observed in a human hepatocellular carcinoma derived cell line (HepG2) (Koufos, Hansen et al. 1985).

Growth promoting effects of IGF2 are mediated through binding to the IGF-IR. This binding induces activation through auto-phosphorylation of intracellular tyrosine residues. This follows the induction of downstream signal transduction pathways involved in differentiation, proliferation and apoptosis (O'Connor 1998): IGF-IR mediated signalling mainly induces the ERK 1/2 kinases and the PI3-kinase.

The hydroxyl residues of the inositol molecule can be phosphorylated *in vivo* at the 3'- and 5'-position. Hence, these phosphorylated molecules are called phosphoinositides (PI). Phosphate transfer is mediated through PI-kinases. PI3-kinase transfers the terminal phosphate of adenosinotriphosphate to the 3'-position of inositol (Divecha and Irvine 1995). Upon activation, these enzymes phosphorylate inositol lipids at the D-3 position of the inositol ring to generate the 3-phosphoinositides, phosphatidylinositol 3-phosphate [PtdIns(3)P], phosphatidylinositol 3,4-bisphosphate [PtdIns(3,4)P₂] and phosphatidylinositol 3,4,5-trisphosphate [PtdIns(3,4,5)P₃]. Phosphorylation at the D3 position is necessary for binding to the pleckstrin-homology domain of AKT.

The tumor suppressor protein PTEN is able to downregulate PI3-kinase lipid formation by its lipid phosphatase activity (Figure 5).

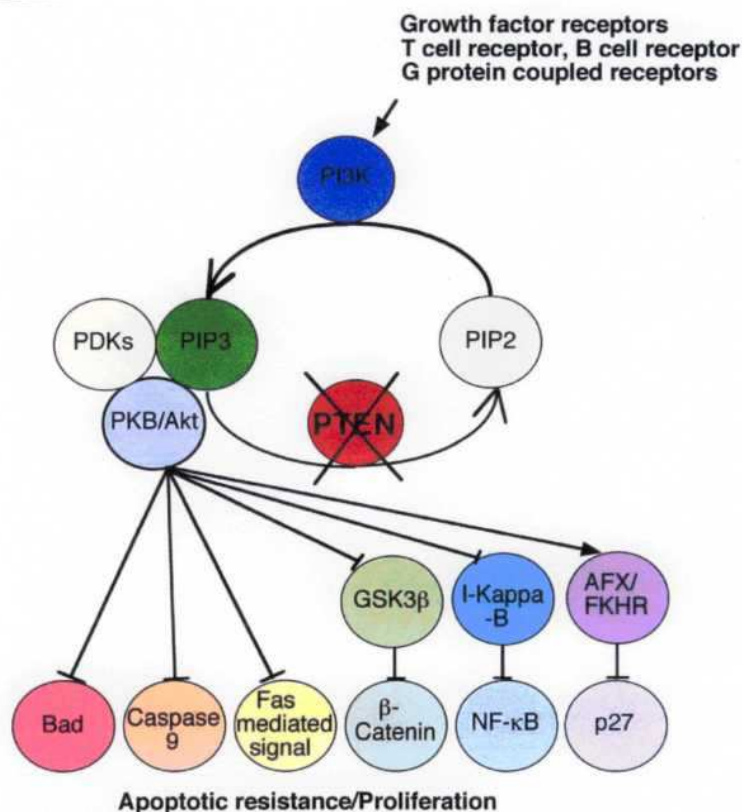


Figure 5: Schematic representation of the PI3-kinase pathway.

Numerous cell surfacemolecules initiate PI3-kinase signalling. Upon phosphorylation PIP3 is formed, which in turn activates the AKT pathway. Thereby, certain downstream effectors are mediated. In the absence of PTEN, the AKT pathway is hyperactivated, leading to an increase in apoptosis resistance and enhanced cell proliferation (source: (Kishimoto, Hamada et al. 2003))

Three classes of PI3-kinases have been defined on the basis of their primary structure, regulation, and *in vitro* lipid substrate specificity. Class I consists of four p110 catalytic isoforms which associate with the p85 family of regulatory subunits (Stephens, Eguinoa et al. 1997). Class II enzymes are large proteins, which all contain a characteristic C-terminal region with homology to C2 domains. Class III enzymes only contain a catalytic and a phosphoinositide kinase domain (Vanhaesebroeck, Leever et al. 1997).

1.7.1.1 **AKT**

In mammals, three isoforms of AKT (also referred to as protein kinase B =PKB) are encoded: AKT1, AKT2 and AKT3. All genes have greater than 85% sequence identity and share a common structure that consists of an N-terminal regulatory domain resembling the pleckstrin homology domain (Franke, Tartof et al. 1994), a kinase domain with serine-threonine specificity (Ahmed, Franke et al. 1993), and a C-terminal region required for the induction and maintenance of its kinase activity (Chan, Rittenhouse et al. 1999). It is postulated that the three isoforms are functionally redundant (Franke 2000).

The function of the PI3-kinase/AKT pathway in cell survival was first published in 1995 by Yao and Cooper (Yao and Cooper 1995). The mechanism by which PI3-kinase protects cells from programmed cell death involves the downstream activation of the protein kinase AKT. PtdIns(3,4)P₂ and PtdIns(3,4,5)P₃ lipids produced by PI3-kinase are able to bind AKT through its pleckstrin homology domain and recruit the kinase to the plasma membrane.

PKB/AKT is cytosolic and moves to the plasma membrane following PI3-kinase induction. At the membrane, Ser473 phosphorylation occurs through autophosphorylation or by PDK2. This region forms the docking site for PDK1, which binds and phosphorylates Thr308 (Persad, Attwell et al. 2001) (Figure 6 a).

Another model of activation after growth factor stimulation of PI3-kinase implicates that the pleckstrin homology domain binds to PtdIns (3,4,5) P₃ (PIP₃), thus allowing PDK1 to phosphorylate Thr 308 (Andjelkovic, Alessi et al. 1997). Subsequent activation of AKT promotes autophosphorylation of Ser473 or PDK2 (Figure 6 b).

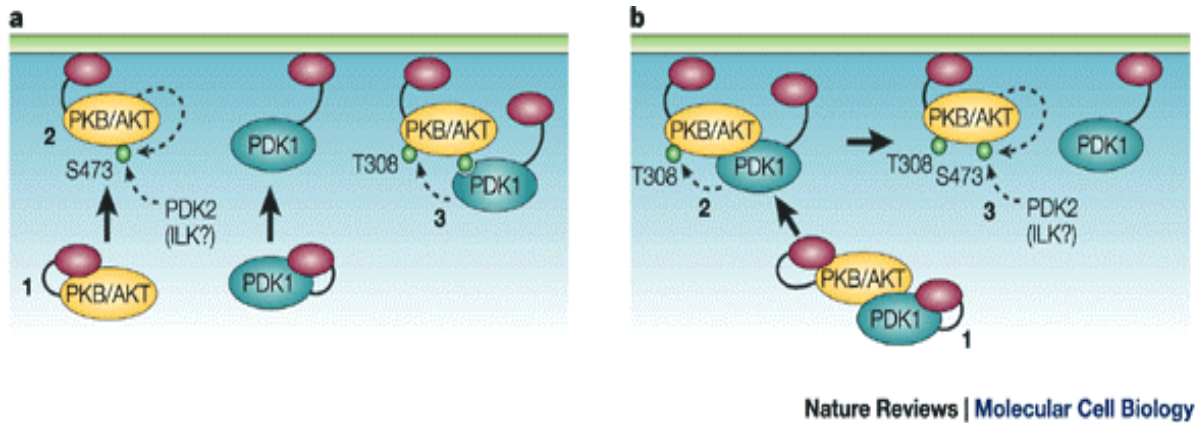


Figure 6: Two models of AKT activation.

In response to PI3 kinase induction, AKT is activated through PDK1 and PDK2 through phosphorylation of Thr308 and Ser473 residues (source: (Scheid and Woodgett 2001))

AKT has several downstream targets, which mediate cell survival. One of these targets is the Bcl-2 family member BAD, a pro-apoptotic protein, which is phosphorylated by AKT and thereby inhibition of anti-apoptotic Bcl-2 molecules is exerted (Datta, Dudek et al. 1997).

AKT also phosphorylates and thereby inactivates the death protease caspase-9. A decrease in apoptosis is caused by a reduced release of cytochrome c from the mitochondria, controlled by caspase-9 (Cardone, Roy et al. 1998).

Increased proliferation after AKT activation is mediated by glycogen synthase kinase-3 (GSK-3), which is involved in cell cycle regulation. Inactivation of GSK-3 through AKT mediated phosphorylation leads to the stabilization of cyclin D1 (Diehl, Cheng et al. 1998).

The metabolic function of AKT as a regulator of glucose metabolism is exerted by enhancing the uptake of glucose through an increase of endocytosis (Foster, Li et al. 2001). Glucose uptake is enhanced through AKT, which also affects glucose transporters by an induction of GLUT1 and GLUT3 expression and a translocation of GLUT4 to the plasma membrane (Cong, Chen et al. 1997; Barthel, Okino et al. 1999). The inactivation of GSK3 in turn leads to an AKT mediated increase in glycogen synthesis (Cross, Alessi et al. 1995).

Knock-out of AKT in mice led to a significant retardation in growth and to reduction of body weight (after AKT1 deletion) (Chen, Kim et al. 2001). Defects in the regulation of blood glucose levels following insulin stimulation (after AKT2 disruption) (Cho, Thorvaldsen et al. 2001) were detected in a mouse model.

After the overexpression of activated AKT in mouse mammary glands, apoptosis was suppressed, and confirmed the requirement of AKT activity in apoptosis suppression (Hutchinson, Jin et al. 2001). It is suggested that AKT expression itself does not promote oncogenic transformation but it is required to promote anti-tumorigenic properties of PTEN (Moorehead, Fata et al. 2001; Stiles, Gilman et al. 2002). In a mouse model, the overexpression of IGF2 lead to a reduction of apoptosis, accompanied by sustained phosphorylation of AKT.

Taken together, these results demonstrate that an increase in copy number or a molecular mutation of specific PI3-kinase genes leading to a 'gain of function' results in an oncogenic transformation of many cell types.

1.7.1.2 PTEN

The phosphatase and tensin homolog deleted from chromosome 10 (PTEN), also known as MMAC1 (mutated in multiple advanced cancers), is a tumor suppressor gene that is mutated in a large number of cancers at high frequency. It is located on human chromosome 10q23, a genomic region that suffers loss of heterozygosity (LOH) in many human cancers (Cantley and Neel 1999).

PTEN contains a protein tyrosine phosphatase (PTP) domain, which is able to dephosphorylate both tyrosine and serine/threonine residues. PIP3 is the main PTEN substrate. PTEN specifically cleaves the D3 phosphate produced by PI3-kinase activity (Maehama and Dixon 1998). Accumulation of PIP3 allows recruitment of AKT. In this context, the role of PTEN is to keep the levels of PIP3 low. Loss of PTEN function results in AKT hyperphosphorylation, leading to protection from apoptotic stimuli (Stambolic, Suzuki et al. 1998). It has to be emphasized that PTEN counteracts the cell survival of activated PI3-kinase or AKT co-expression. On the

other hand, activated PI3-kinase or AKT efficiently antagonize PTEN-mediated growth suppression.

PTEN inactivation might also result in an increase in cell cycle progression mediated through GSK-3 inactivation, which leads to cyclin D1 stabilization. Reduced cyclin D1 levels were revealed upon PTEN overexpression (Paramio, Navarro et al. 1999).

Heterozygosity of PTEN leads to the development of a broad range of tumors derived from prostate, lung, brain, bladder, breast carcinomas (Steck, Pershouse et al. 1997; Teng, Hu et al. 1997). Heterozygous mice also developed signs of autoimmune diseases (Di Cristofano, Kotsi et al. 1999). Homozygous knockout led to embryonic lethality at day E 9.5 (Di Cristofano, Pesce et al. 1998; Suzuki, de la Pompa et al. 1998).

Several studies revealed a correlation between HCC and PTEN inactivation. Loss of a PTEN allele was identified in 20-30% of patients with HCC (Kawamura, Nagai et al. 1999; Fujiwara, Hoon et al. 2000). Moreover, PTEN heterozygous mice exhibited neoplasms in the liver, suggesting that loss of PTEN may participate in liver carcinogenesis (Di Cristofano, Pesce et al. 1998).

1.7.2 Impact of PTEN and pAKT on lipid and glucose metabolism

In mice, hepatocyte-specific PTEN deficiency resulted in non-alcoholic steatohepatitis (NASH) with triglyceride accumulation followed by liver cirrhosis and HCC (Horie, Suzuki et al. 2004). Upon inactivation of PTEN, the inversely correlated AKT pathway is stimulated. The promotion of chronic inflammation, resulting from NF- κ B translocation, might contribute to the onset of hepatitis (Watanabe, Horie et al. 2007).

Vinciguerra et al. showed that unsaturated free fatty acids decreased PTEN expression in HepG2 cells through activation of a signaling complex made of mTOR and translocation of NF- κ B/p65 into the nucleus (Vinciguerra, Veyrat-Durebex et al. 2008).

The interplay between lipid and glucose metabolism is mediated by the reciprocal relationship of substrate availability and consumption between liver and peripheral tissues (Abel, Smuts et al. 2001; Yang, Lin et al. 2001). Glucose homeostasis is, in part, regulated by the insulin-stimulated uptake of glucose in adipose tissue (Abel, Smuts et al. 2001; Minokoshi, Kahn et al. 2003).

The failure in the insulin-like growth factor signaling cascade causes insulin resistance and metabolic disease, such as glucose intolerance, obesity and dyslipidemia. Upon receptor activation, PIP3 is generated, which in turn activates the AKT pathway. AKT controls diverse cellular substrates that are involved in glucose homeostasis (Brazil, Yang et al. 2004). Figure 7 illustrates the effects of AKT on glucose metabolism.

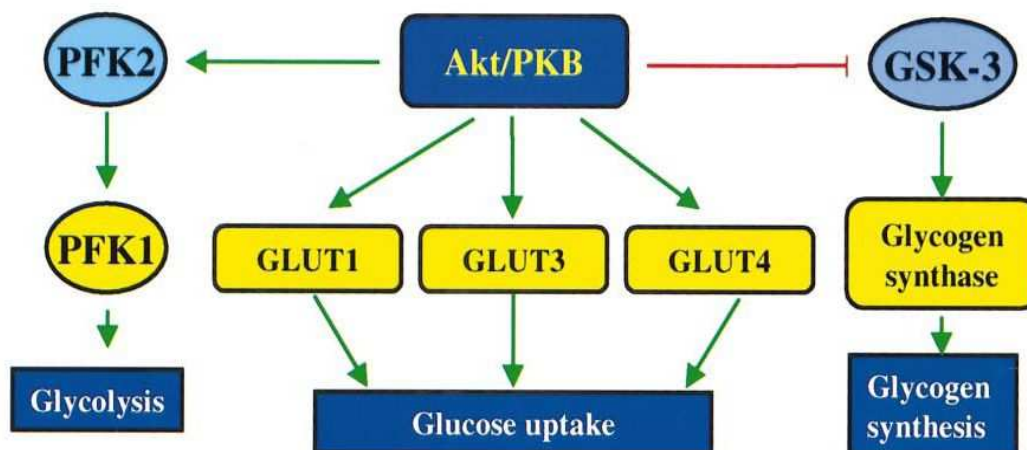


Figure 7: Regulation of glucose homeostasis by AKT.

Enhancement of glucose uptake is mediated by affecting Glucose transporters (GLUT). Glycogen synthesis is stimulated by inhibition of glycogen synthase kinase-3 (GSK-3). Through a general increase in endocytosis glucose uptake is activated (source:(Kandel and Hay 1999))

Liver-specific PTEN deficient mice display enhanced glycogenesis, demonstrated by an improved glucose clearance and lower glucose levels (Stiles, Wang et al. 2004).

A hint for the role of PTEN in glucose metabolism was found after *in vivo* administration of antisense oligonucleotides, which improved hyperglycemia in diabetic mice (Butler, McKay et al. 2002).

All these data from the literature implicated a participation of IGF2 in glucose and lipid homeostasis and a set of experiments was performed to clarify the possible role of *p62* in metabolic liver regulation due to its upregulation of IGF2 expression.

1.8 RNA interference

In 1998, Fire and Mello described a new technology based on specific gene silencing by double-stranded RNA (dsRNA) (Fire, Xu et al. 1998). Two types of small RNA molecules are central to RNA interference, micro RNAs (miRNA) and small interfering RNAs (siRNA). RNA interference is a defense mechanism protecting against the integration of foreign genetic material into the host genome.

RNA interference is initiated by the enzyme Dicer which catalyses the cleavage of long dsRNA to 21-23 nt siRNA products (Bernstein, Caudy et al. 2001). One of the two strands is then introduced to the RISC protein complex and sequence-specific mRNA degradation is facilitated (Pellino and Sontheimer 2003) (Figure 8).

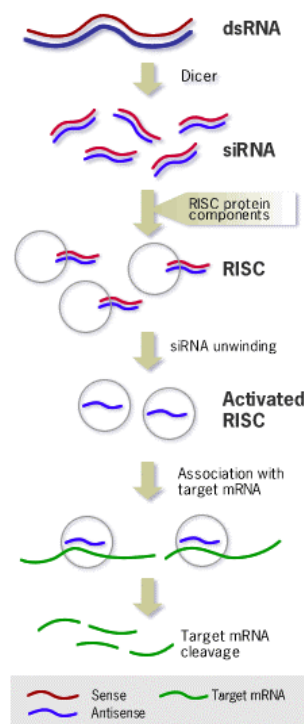


Figure 8: Mechanism of RNA interference.

Cleavage of dsRNA by Dicer initiates genesilencing by generating siRNA molecules, by incorporation of a single strand of the RNA molecule into the RISC complex, post-transcriptional gene silencing is facilitated (source: <http://www.borc.cn>)

After specific gene silencing of the *p62* mRNA in human hepatoma cell lines, investigations were made on the expression of IGF2 and H19. As the upregulation of both genes in *p62* transgenic mice is accompanied by *p62* overexpression, the question occurred whether the expression levels of IGF2 and H19 would decrease after siRNA-mediated mRNA degradation of *p62*.

1.9 Mice

Mice are a powerful tool for biological and medical researchers. After targeted changes of genes, occurring phenotypes can be reduced to a defined endogenous gene. Either overexpression of foreign genes or deletion of endogenous genes, as well as the introduction of point mutations, are possible strategies in gene targeting experiments.

1.9.1 The tet-system

The regulatory elements of the tetracycline-dependent expression systems were adapted from the tetracycline resistance of *E. coli* having its origin in the operon of transposon 10. In bacteria, the binding of the dimeric Tet-repressor (*tetR*) to the specific operon sequence (*tetO*) of the tetracycline promoter prevents transcription of the tetracycline resistance gene (*tetA*). Binding of tetracycline to the *tetR* is followed by a conformational change of the repressor, leading to its dissociation from the operon, thereby allowing transcription of the *tetA* gene (Hillen and Berens 1994).

Gossen et al. generated a tetracycline transactivator (*tTA*) through the fusion of the tetracycline repressor with the *Herpes simplex* virus (Gossen and Bujard 1992). The *tTA*-dependent promoter consists of the human cytomegalovirus (CMV) 'immediate early promoter' (Boshart, Weber et al. 1985) and a tet-operator sequence (Baron and Bujard 2000).

In the presence of tetracycline, or its analogon doxycycline (dox), *tTA* is prevented from binding to the promoter, whereas its absence results in the contrary (Figure 9).

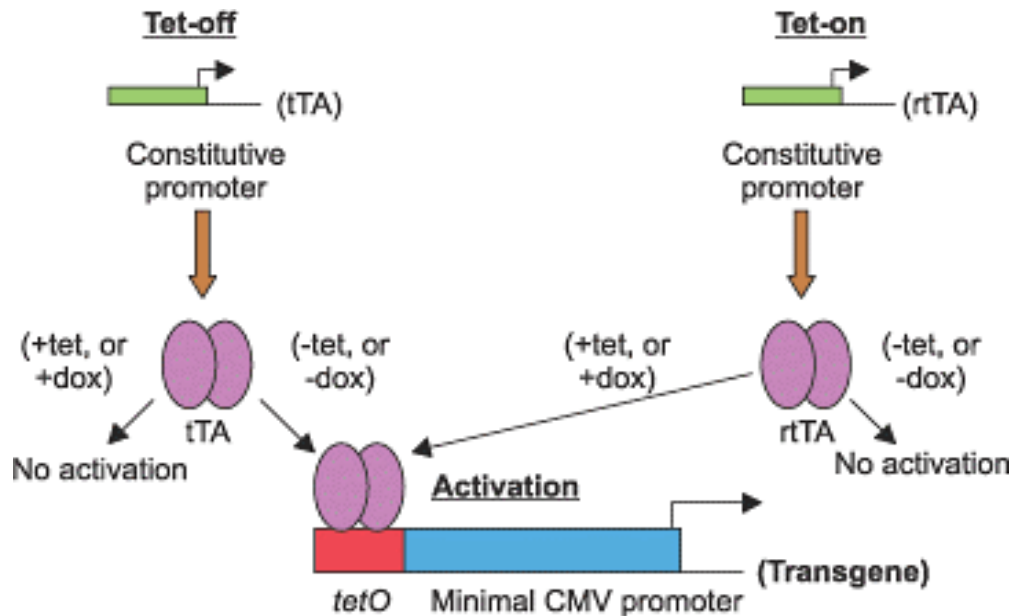


Figure 9: Gene regulation by the tet system.

Tet-off: The TRE is located upstream of the minimal immediate early promoter of the cytomegalovirus (CMV_{min}) which is silent in the absence of activation. tTA binds to the TRE, thereby activating gene transcription in the absence of tetracycline.

Tet-on: The Tet repressor reverses the protein response to tetracycline. As a result, transcription is activated in the presence of tetracycline (source: (Romano 2004))

1.9.2 *p62* transgenic mice

To elucidate the function of the hepatic *p62* protein expression, *p62* transgenic mice were generated in Prof. Eng M. Tan's group at the Scripps Research Institute (La Jolla, California, USA).

The targeting vector construct was designed in a way that put the human *p62* protein under control of the transrepressive responsive element cytomegaly virus (TRE- CMV_{min}) promoter, ensuring that the livers of *p62* transgenic mice did not express *p62* mRNA due to repression of the promoter sequence within the targeting construct itself. Expression of the transgene was realized by crossing LT2 mice with *p62* transgenic mice. LT2 mice carry a cis-acting locus control-like element called liver enriched activator protein (LAP) under control of a tetracycline regulatory element (*tTA*) (Kistner, Gossen et al. 1996). The *tTA* activates the TRE- CMV_{min} promoter leading to its activation, followed by *p62* mRNA expression. The LAP promoter accounts for an exclusive and liver-specific *p62* expression. Moreover, the *tTA* allows

that overexpression of the *p62* protein in the *p62* x LT2 offspring is suppressed by the application of doxycycline to the drinking water (Kistner, Gossen et al. 1996) (Figure 10).

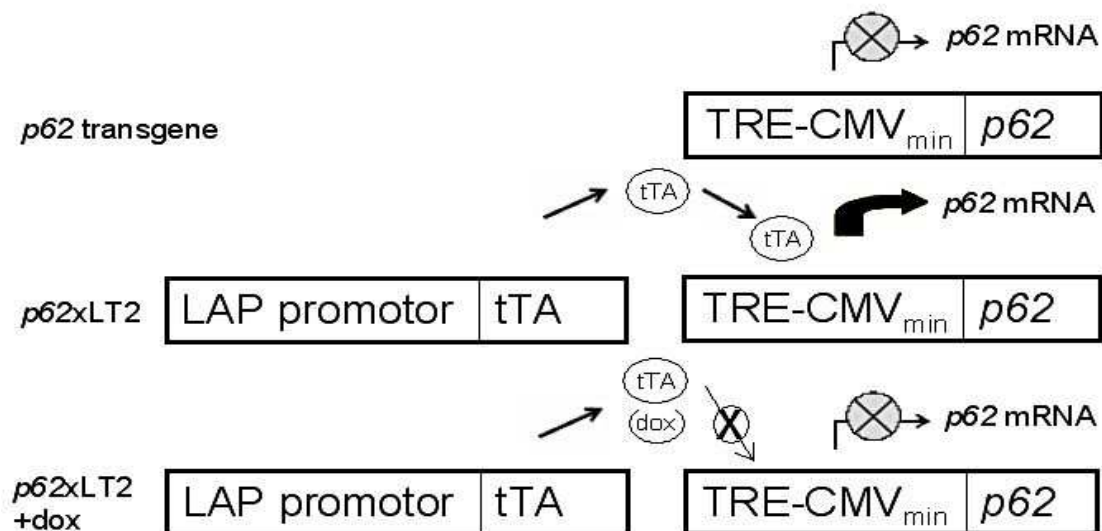


Figure 10: Generation of *p62* transgenic mice and mechanism of doxycycline-dependent regulation of hepatic *p62* expression.

No expression of *p62* mRNA in livers of mice transgenic for *p62* under TRE-CMV promoter control (upper panel). Liver-specific expression of *p62* mRNA mediated through the tTA modulation of the TRE-CMV promoter in double-positive *p62*⁺/LT2⁺ mice (middle panel). Application of doxycycline inhibits transgene expression (lower panel). TRE-CMV_{min}: transrepressor responsive element cytomegaly virus; tTA: tetracycline transactivator; LAP: liver enriched activator protein; dox: doxycycline

1.10 Aim of this work

In order to investigate the functions of the hepatic expression of the tumor-associated autoantigen *p62*, transgenic mice were generated showing a liver-specific *p62* expression.

Aim of this work was to elucidate phenotypic alterations induced by *p62* overexpression.

2. Methods

2.1 Animals

2.1.1 Animal welfare

The animals were maintained on a standard 12 h light-dark-cycle, at a constant temperature (22 ± 2 °C) and a relative humidity of $55\pm 10\%$ with free access to water and chow (Altromin, Lage, Germany). All animals received human care. The study was registered with the local animal welfare committee. The animals' stock breeding was performed at the animal laboratory at the Institute of Genetics (Saarland University).

For identification, animals received an ear tag with a three-digit number, at the same time a biopsy of the tail was taken for DNA isolation.

2.1.2 Generation of *p62* transgenic animals

Mice were generated at the Scripps Research Institute in Prof. Eng M. Tan's group. Using the tetracycline gene transcription system allows a repression/ derepression of the liver-specific expression of the *p62* transgene. A liver-specific Tet-system is established in a mouse model constructed by Kistner et al. (Kistner, Gossen et al. 1996). Therefore, it was necessary to generate a mouse carrying the *p62* DNA sequence under control of the TRE-CMV promoter.

The first step was to insert the sequence of the TRE-CMV_{min} promoter and the human endogenous DNA sequence of *p62* flanking exon 1 (ENSG00000073792 (1862 bp), leading to an insert of 2248 bp in total, into the targeting vector pUHG10-3/p-*p62* (5548 bp).

In a second step, embryonic stem cells were transfected with the targeting construct. Southern Blot experiments were performed to screen recombinant embryonic stem cells (data not shown). The recombinant clone was microinjected into pronuclei of 0.5 day old oocytes, which were implanted into a pseudo-foster mother. Microinjection was performed onto B6D2 mice. The target integration into the genome occurs in a

randomized order. Germ-line transmission was confirmed by Southern Blot (data not shown). The offspring were chimeric. Male chimeric mice were mated with female mice. This led to mice being heterozygous for the transgene.

As the expression the *p62* transgene is repressed by the TRE-CMV promoter, it is necessary to cross them with LT2 mice, which carry a transactivator, leading to a depression of the promoter, thereby allowing *p62* expression in the $p62^+/LT2^+$ offspring.

Male and female *p62* transgenic mice and their non-transgenic control littermates as well as the LT2 mice were obtained from Prof. Dr. Eng M. Tan, The Scripps Research Institute, La Jolla, USA. *p62* transgenic mice show a liver-specific expression of the human *p62* autoantigene.

For SNUPE analysis, SD7 mice (carrying the *mus spretus* IGF2-H19 region, (Guenet, Nagamine et al. 1990) (courtesy provided by Prof. Dr. Jörn Walter, Institute of Genetics, Saarland University) were crossed with *p62* transgenic mice. Male or female heterozygous LT2 mice were crossed with homozygous SD7 males or females to produce reciprocal progeny (LT2 x *Mus spretus*). F1 hybrids were mated to homozygous SD7 to produce heterozygous F2 offspring. For imprinting studies, *p62* transgenic females were mated with F2 hybrid males. Mice, carrying no *p62* transgene but the heterozygous LT2/SD7 background served as control. The offspring carried single nucleotide primer polymorphisms (SNPs) for IGF2 and H19 on chromosome 7. For the experiments, livers from both sexes were removed on postnatal days P0 and P16.

Livers of 2.5 up to 10 week old animals were used for gene and protein expression analysis; for histological staining of paraffin- and cryo-embedded liver sections, as well as for SNUPE analysis.

Instantly after organ removal, livers were placed in safe-lock Eppendorf tubes and frozen in liquid nitrogen. For long term storage, tissues were stored at -80°C. Paraffin-embedded livers were put into 4% formalin for 24 h straight after withdrawal. The processing and preparation of paraffin tissue blocks was kindly taken over by the

Institute of Pathology (University Hospital, Saarland University, Homburg/Saar, Germany).

Isolated hepatocytes were examined in mRNA stability and caspase-3-like activity assays.

2.1.3 Isolation of genomic DNA from mouse tails

For genotyping of mice under the age of 3 weeks, a tail biopsy was taken during organ extraction. Elsewise, an approximately 0.5-1 cm biopsy from the tail of 3-week old mice was incubated in 100 µl water/10x Taq buffer (9:1) at 55°C for several hours while shaking. Addition of 1 µl Proteinase K (20 mg/ml) guaranteed degradation of proteins. After heat-inactivation of Proteinase K at 95°C for 15 min, 1 µl of the supernatant was used in the PCR reaction.

2.2 Bacteria

2.2.1 Preparation of competent bacteria

A bacterial culture was incubated in 50 ml LB medium o. n. at 37° C in a shaking incubator. The next morning, 1 ml of this culture was transferred into 100 ml LB medium and allowed to grow up to an OD₆₀₀ of 0.3. Subsequent, cells were cooled down to 4°C and centrifuged for 5 min at 4,000 x g. The pellet was resuspended in 50 ml 50 mM CaCl₂ and stored on ice for 20 min. After an additional centrifugation step for 5 min at 4,000 x g, the pellet was resuspended in 10 ml of a solution of CaCl₂ containing 15% Glycerol. Cells were aliquoted, frozen in liquid nitrogen and stored at -80°C.

2.2.2 Transformation of plasmid DNA in competent bacteria

5 ng of the transforming plasmid were mixed with an aliquot of the chemically competent bacteria. After incubation on ice for 30 min, heatshock was performed at 42°C for 30 sec, subsequently followed by the addition of 1 ml LB medium. Bacteria

were shaken for 30 min in at 37°C in an incubator, before they were plated onto a LB agar plate.

2.2.3 Isolation of plasmid DNA

In order to allow absolute quantification in real-time RT-PCR, fragments of the target genes cloned into the pGEMTeasy® (Promega, Mannheim, Germany) vector were used as a standard. A 1:10 dilution series of the plasmid DNA was prepared, starting at a concentration of 20 attomol/μl (S1). Standards S1-S7 were run on each PCR plate in duplicates.

The plasmids were amplified in competent bacteria (XL-1 Blue) and isolation was carried out with the MiniPrep kit (Qiagen, Hilden, Germany).

7 ml of LB broth medium containing 14 μl ampicillin (50 μg/ml stock solution) were inoculated with a single clone of the designated colony and incubated at 37°C and 225 rpm o. n. The bacterial culture was transferred into a centrifuge tube and spun down at 4,000 x g for 10 min. The supernatant was discarded and the pellet was processed using the QIAprep Miniprep Kit (Qiagen, Hilden, Germany). To dissolve the plasmid DNA, 50 μl TE buffer was added to the tube.

2.2.4 Determination of DNA concentration

The concentration of the nucleic acids was determined by photometric analysis. An OD₂₆₀ of 1 corresponds to 50 μg/ml dsDNA. The quality of the isolation was verified by measuring the absorption at 280 nm, corresponding to the absorption maximum of proteins. The ratio of the two absorption values gives information on the purity of the sample, with optimal values ranging between 1.8 and 1.95.

2.3 Agarose gel electrophoresis

Agarose gel electrophoresis is a method to separate DNA molecules of 0.1 up to 25 kb by size. In an electric field, the negatively charged DNA molecules migrate through the agarose matrix towards the anode. DNA molecules are separated

according to their size, i. e. the bigger the DNA fragment, the slower it runs through the gel.

After boiling the agarose in 1x TBE in a microwave, the solution was stirred while cooling down below 56°C before 0.1-0.5 µg/ml ethidium bromide (3,8-diamino-5-ethyl-6-phenylphenanthridinium bromide) was added for later visualisation.

The dye intercalates into base pairs (inclusion within a distance of 10 bp) of the DNA molecule. For detection, the gel is exposed to UV light. Typically, DNA fragments appear as luminous bands whereas areas without nucleic acids are dark. For size determination, a DNA-ladder can be applied onto the gel.

In this work, a 1 kb-ladder from Invitrogen (Karlsruhe, Germany) as well as a 50 bp-ladder (Amersham, GE-Healthcare, Munich, Germany) in a amount of 5 µl were used (supplement 7.7).

DNA fragments obtained from PCR reactions were separated in 1.5% agarose gels in 1x TBE buffer. For the detection of polymorphisms, 2% agarose gels were employed. 10 µl of the PCR product were mixed in a ratio of 1:6 with 6x dye, containing bromophenol blue (migrates at the same rate as the 500 bp DNA fragment) and xylene cyanol (migrates at about the same rate as the 4,000 bp DNA fragment) as indicators that mark the process of gel electrophoresis. The mix was applied onto the gel and the run was carried out in a gel chamber with 1x TBE at 100 V for ~30 min.

2.4 PCR (Polymerase Chain Reaction)

PCR is an *in vitro* technique for the replication of DNA segments enframed by two sequence-specific oligonucleotides (primers) (Mullis and Faloona 1987). In a chain reaction, a thermally stable DNA polymerase amplifies the target DNA through the assembly of nucleotides to the primer sequences along the single-stranded, denatured DNA matrix. New DNA strands were synthesised. As the newly synthesised DNA strands serve as templates in each cycle, the copy numbers increase exponentially (Cornel 2008).

A basic PCR set up requires several components and reagents:

- the DNA matrix (template) that contains the DNA region to be amplified
- two oligonucleotides, i. e. short, single-stranded DNA molecules, that are complementary to the 5'- or 3'-end of the DNA-strain
- desoxynucleotidetriphosphates (dNTPs), the building blocks that are incorporated during the DNA synthesis
- DNA polymerase, usually Taq polymerase (thermally stable), for the synthesis of new DNA double strands
- polymerase buffer and Mg^{++} ions (important for incorporation of dNTPs, required for optimal polymerase activity and stability)

The PCR usually consists of a series of 25 to 40 repeated temperature cycles, each cycle typically consists of 2-3 discrete temperature steps.

- **Denaturation** step, causes melting of the doublestrand (ds), performed at 93-95°C
- **Annealing** step, single-stranded primers bind to the single-stranded template at 56-62°C. The polymerase binds to the primer-template hybrid and begins DNA synthesis.
- **Extension** step at 72°C, the DNA polymerase synthesizes a new DNA strand by adding dNTPs to the template in 5'- to 3'-direction.

In this work, PCR was performed for:

- genotyping of transgenic mice
- generation of DNA fragments, serving as templates in the SNuPE analyses
- controlling the quality of cDNA after syntheses
- quantification of mRNA expression.

Used DNA matrices were either genomic DNA from mouse tails or cDNA from liver tissues or isolated hepatocytes.

PCR protocol:

The PCR reaction was carried out in a Px2 thermal cycler (Thermo Electron, Karlsruhe, Germany). Taq polymerase from GenScript (USA) was used as thermally stable DNA polymerase. Different PCR protocols were performed.

dNTPs (GenScript)	1.25 mM
dNTP 10 mM (stock)	125 μ l
H ₂ O	ad 1,000 μ l

Taq Polymerase 5 U/ μ l

primer A (10 pmol/ μ l)	1.0 μ l
primer B (10 pmol/ μ l)	1.0 μ l
dNTPs (1.25 mM)	2.0 μ l
10 x PCR buffer	2.0 μ l
polymerase (5 U/ μ l)	0.5 μ l
template DNA	1.0 μ l
H ₂ O	ad 20.0 μ l

PCR program for genotyping of *p62* mice:

95°C	5 min
95°C	30 sec
56°C	30 sec
72°C	30 sec (35x)
72°C	5 min

An aliquot of the PCR reaction (10 μ l) was applied onto an agarose gel and separated electrophoretically. Bands in the ethidium-bromide containing gel were visualized under UV-light.

2.5 Reverse transcription

RNA is isolated from the cells or tissue of interest and transcribed into a copy I DNA by the enzyme reverse transcriptase (RT).

Three different enzymatic activities are combined in the RT enzyme:

- RNA-dependent DNA polymerase (reverse transcription)
- ribonuclease (RNaseH, degradation of RNA in RNA/DNA hybrids)
- DNA-dependent DNA polymerase.

The enzyme RT was originally isolated from retroviruses. The combination of the three functions allows *in vivo* transcription of the retroviral RNA-genome into a ds-DNA. *In vitro*, only the first and third function is necessary for the synthesis of the cDNA. Amplification starts at the 3'-hydroxyl end.

Transcription of RNA into cDNA can be done with three different primers (Sellner 1992):

- random primer mix (hexanucleotide primer mix): mixture of short (6 bp long) primers, showing every possible sequence
- oligo (dT) primer mix: binds to the 3'-poly A-tail of mRNA
- sequence specific primers.

For the experiments described here, either random primers (used for templates from mouse tissues or from mouse derived tissue culture cells) or oligo (dT) primers (used for templates from human tissue culture cells) were applied.

Afterwards, the cDNA served either as template in the real time PCR using sequence-specific primers or in the SNUPE-HPLC analysis.

Performance:

1) RNA preparation

The one-step RNA isolation method is based on the GITC (guanidium-isothicyanat) method described by Chomczynski and Sacchi (Chomczynski and Sacchi 1987).

Trizol is a monophasic solution from phenol and GITC, stabilizing RNA, whereas cells and soluble cell components are lysed. GITC is a strong inhibitor of ribonucleases.

1a) Preparation of liver tissue from mice

Liver tissue was homogenized in 0.3 ml Trizol (Qiagen, Hilden, Germany) and subsequently filled up to 1.0 ml Trizol in an Eppendorf tube. After addition of 250 μ l Chloroform and shaking, samples were incubated for 3 min at RT.

1b) Preparation from tissue culture cells

Cells from 6-well plates were harvested by removing the tissue culture medium and washing twice with 1x PBS. Subsequently, 300 μ l Trizol was added and cells were scraped off the bottom of the well with a cell scraper, before the Trizol solution containing the RNA was transferred into an Eppendorf tube. After addition of 63 μ l Chloroform and shaking, samples were incubated for 3 min at RT.

The RNA is now in the upper phase of the solution due to the pH value. By separating and spiking of the upper phase, RNA was precipitated with 1/1 volume of isopropanol. The RNA precipitates were washed in 70% ethanol and finally dissolved in 15 μ l or 30 μ l DEPC water.

2) DNase treatment of isolated RNA

To ensure exclusive amplification of cDNA during PCR, it is necessary to eliminate contaminations of sample RNA with genomic DNA. Ambion DNA free kit (Applied Biosystems, Darmstadt, Germany) was used for DNase treatment: 1/10 volume of 10x DNase I buffer and 1 μ l DNase I were added to the RNA and incubated for 45 min at 37°C. Subsequently, 1/10 volume of DNase inactivating reagent was added. After centrifugation, the supernatant was transferred into a fresh Eppendorf tube.

3) Determination of the amount and quality of RNA in a photometric assay

RNA concentration was determined at a wavelength of 260 nm in a photometer (BioMate3, Thermo Electron Corporation, Karlsruhe, Germany). 40 µg RNA/ml corresponds to an optical density (OD₂₆₀) of 1.

Proteins have an absorption maximum at 280 nm. 1.8 mg/ml protein corresponds to an OD₂₈₀ of 1.

A ratio of 1.8 to 1.95 (for DNA), and of 1.9 to 2.0 (for RNA) of the measurements at 260 and 280 nm suggest a high purity of the sample. Lower values suggest protein or phenol contamination, higher values result from denatured DNA or contamination of genomic DNA in RNA samples.

4) Reverse transcription

The first step consists of the denaturation of RNA for 10 min at 70°C. Either random or oligo (dT) primers are now able to bind to the single-stranded template. cDNA corresponding the RNA matrix is synthesized by the enzyme RT. Afterwards, cDNA can be used to perform PCR experiments. All steps were prepared on ice.

The following **RT(+)** approach (total volume: 10 µl) was used:

10x RT buffer	2.0 µl
25x dNTP mix (100 mM)	0.8 µl
MultiScribe™ Reverse Transcriptase (50 U/µl)	1.0 µl
Rnase Inhibitor (10 U/µl)	1.0 µl
Nuclease-free H ₂ O	3.2 µl
10x RT random primers	2.0 µl or
oligo (dT) primers (10 µM)	2.0 µl

The RT(-) approach without enzyme was carried out with the same samples in order to check for leftovers of genomic DNA in a later β-actin PCR.

1 µg RNA in a total volume of 10 µl was reverse-transcribed. Incubation was done in a Px2 thermal cycler (Thermo Electron, Karlsruhe Germany).

The following **RT program** was used:

Step 1	25 min at 10°C
Step 2	120 min at 37°C
Step 3	5 sec at 85°C

followed by instant cooling of the cDNA samples to 4°C. The samples were diluted 1:5 to a final volume of 100 µl. cDNA was stored at -20°C, for long time storage at -80°C.

5) Alu-PCR

Using primers specific for repetitive sequences in the human genome ('Alu' elements), it is possible to test on genomic DNA residues in RNA samples. Did separation of samples by gel electrophoresis reveal no amplification products, the RNA quality was verified and RNA could be used for reverse transcription.

The following **approach** was set up:

10x Taq buffer	2.5 µl
10 mM dNTP mix	2.0 µl
Taq polymerase (5 U/µl)	0.5 µl
primer AS1 (50 µM)	0.5 µl
MgCl ₂ (50 mM)	1.25 µl
template RNA	100 ng
H ₂ O	ad 25.0 µl

As positive reaction, 5 ng genomic DNA from THP-1 cells (kindly provided by Jessica Hoppstädter, Pharmaceutical Biology, Saarland University) was used. The Alu PCR was carried out in a Px2 thermal cycler (Thermo Electron, Karlsruhe, Germany).

Alu PCR program:

94°C	5 min
94°C	1 min
56°C	1 min
72°C	1 min (30x)
72°C	10 min

Amplification products appear as several diffuse bands of heterogenous size on agarose gels.

6) β -actin PCR

To assure for RNA sample quality, a β -actin PCR was performed with the RT (-) preparation. In the case of detection of an amplification product after gel electrophoresis, the band must result from genomic DNA contaminants because no reverse transcriptase enzyme is added to the RT (-) mix.

The **reaction** included:

10x Taq buffer	3.0 μ l
10 mM dNTP mix	2.4 μ l
Taq polymerase (5 U/ μ l)	0.5 μ l
primer A (10 pmol/ μ l)	1.0 μ l
primer B (10 pmol/ μ l)	1.0 μ l
template RT(-)	1.5 μ l
H ₂ O	ad 30.0 μ l

The β -actin PCR was run in a PX2 thermal cycler.

PCR program:

94°C	3 min
94°C	30 sec
62°C	1 min
72°C	1 min (30x)
72°C	5 min

10 µl of the amplification product were separated on an agarose gel. RNA samples were used in the reverse transcriptase reaction when no bands could be visualized.

2.6 Real-time quantitative RT-PCR

For detection and simultaneous quantification of gene expression patterns, real-time RT-PCR (Q-PCR) is a widely-used technique. PCR based methods have the advantage of being fast and highly sensitive.

Real-time polymerase chain reaction is based on the use of fluorescence reporter molecules to observe product amplification during each cycle of the PCR. Fluorescence signal intensity increases proportionally to the amount of amplification product.

The threshold cycle (C_t), which represents the PCR cycle at which an increase in reporter fluorescence above background is first detected, is determined in the real time assay. The C_t value inversely correlates with the initial amount of template, i.e. the more is in the reaction tube, the earlier the C_t value can be measured. Moreover, the C_t value defines the exponential phase of the PCR reaction, within which the extrapolation to the initial amount can be done.

Detection can be verified with different methods (Figure 11):

- unspecific intercalation of fluorescent dyes (e.g. SYBR[®] green) into the DNA
- specific detection using fluorescent probes (TaqMan[®], molecular beacons, hybridised probes).

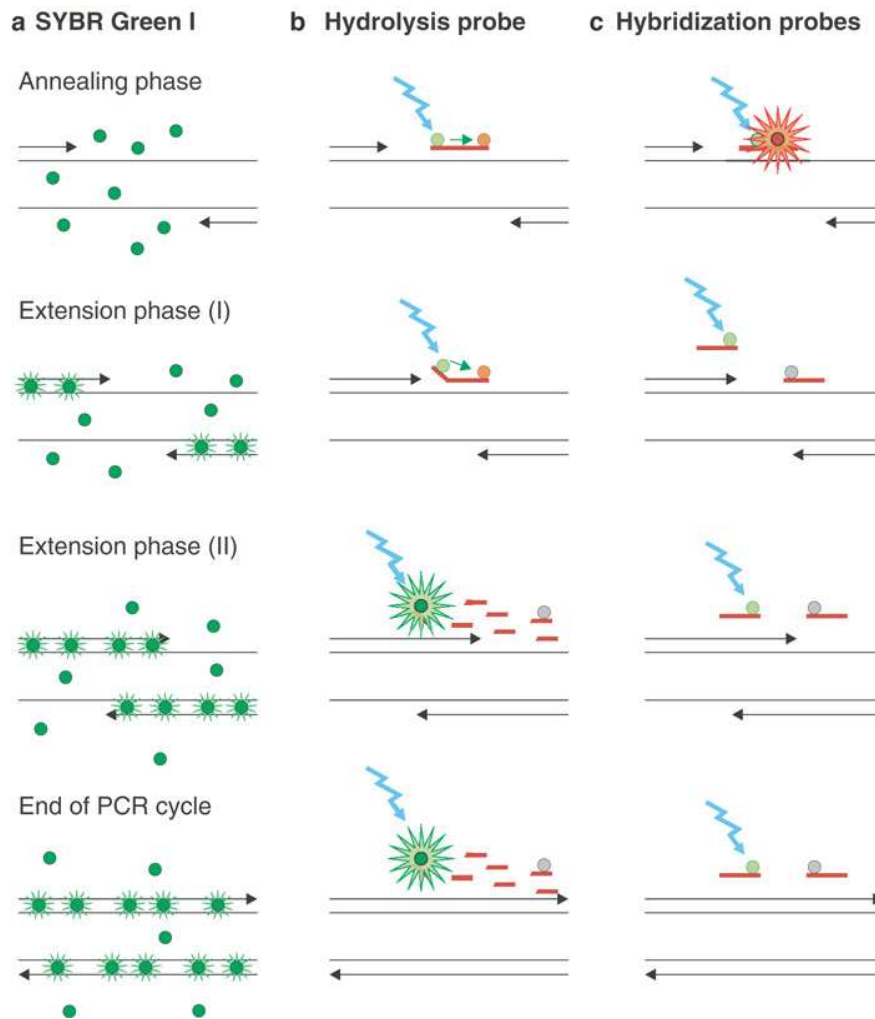


Figure 11: Principles of real-time RT-PCR techniques.

- a)** SYBR Green I technique. SYBR Green I fluorescence is enormously increased upon binding to double-stranded DNA.
- b)** Hydrolysis probe technique. The hydrolysis probe is conjugated with a quencher fluorochrome, which absorbs the fluorescence of the reporter fluorochrome as long as the probe is intact. Upon amplification of the target sequence, the hydrolysis probe is displaced and hydrolyzed by the *Taq* polymerase. Due to the separation of the reporter and quencher fluorochrome, the increase in fluorescence becomes detectable.
(http://www.nature.com/leu/journal/v17/n6/fig_tab/2402922f1.html)

Within this work, SYBR[®] green was used for all experiments performed on cDNAs derived from human material, whereas TaqMan[®] probes, carrying a fluorescent dye (FAM) at the 5'-end, were used for cDNAs derived from mouse material.

SYBR[®] green detection is based on the principle that the DNA-binding dye anneals to all ds-DNA in the PCR reaction, causing a fluorescence signal. An increase in DNA product during PCR leads to an increase in fluorescence intensity and is measured at

each cycle, thus allowing DNA concentrations to be quantified. As ds-binding dyes bind to all ds-DNA templates, it is necessary to perform a melting curve analysis after the end of the PCR reaction to distinguish specific from non-specific products.

For the detection using fluorescent probes, TaqMan[®] probes carry a fluorescent reporter at one end and a quencher of fluorescence at the opposite end. The close proximity of the reporter to the quencher prevents detection of its fluorescence. Both primers and probe anneal to the DNA target. Polymerisation of the new strand starts from the primers, and once the polymerase reaches the probe, breakdown of the probe due to the 5'- to 3'-exonuclease activity of the Taq polymerase decreases the reporter-quencher proximity and thus allows detection of fluorescence emission. An increase in the product targeted by the reporter probe at each PCR cycle causes a proportional increase in fluorescence.

The **two** following **approaches** were pipetted on ice:

a)	dNTPs (1.25 mM)	2.0 µl
	10x PCR buffer	2.5 µl
	primer A (10 pmol/µl)	1.25 µl
	primer B (10 pmol/µl)	1.25 µl
	Taq polymerase (5 U/µl)	0.5 µl
	MgCl ₂ (50 mM)	x µl
	TaqMan probe (1 pmol/µl)	x µl
	template DNA	5.0 µl
	H ₂ O	ad 25.0 µl

Amounts of the TaqMan[®] probes were 1.5 to 2.5 pmol. Concentrations for MgCl₂ differed from 3 to 5 mM depending on the approach (supplement 7.3).

b)	template DNA	5.0 µl
	Dynamo Flash SYBR [®] green qPCR kit	12.5 µl
	H ₂ O	ad 25.0 µl

Either cDNA or plasmid DNA served as template DNA in the PCR reaction.

PCR program for TaqMan[®] probe detection:

95°C	8 min
95°C	15 sec
60°C	15 sec
72°C	15 sec (40x- 45x)
72°C	3 min

PCR program for SYBR[®]green detection:

95°C	x min
94°C	x sec
60°C	x sec
72°C	x sec (40x)
55°C-95°C	7 sec in 0.5 temperature steps

Initial denaturing step varied from 5 to 10 min. Denaturing at 94°C lasted between 10 to 30 sec. Annealing and extension required 15 to 30 sec. Details regarding the cycling conditions are found in the supplement 7.3 and 7.4.

Real time PCR reactions were performed in an iQ5 cycler (BioRad, Munich, Germany). Each sample was run in duplicate or triplicate.

Quantification

Relative concentrations of DNA present during the exponential phase of the reaction are determined by plotting relative fluorescent units against cycle number showing an exponential curve. A threshold value for detection of fluorescence above background is determined by the software, called C_t . Since the quantity of DNA doubles every cycle during the exponential phase, relative amounts of DNA can be calculated, e.g. a sample whose C_t is 4 cycles earlier than another's has $2^4 = 16$ times more template.

Amounts of mRNA are determined by comparing the results to a standard curve produced by serial dilutions of a plasmid DNA. To accurately quantify gene expression, the measured amount of mRNA from the gene of interest is divided by

the amount of RNA from a housekeeping gene measured in the same sample to normalise for variations in the amount and quality between different samples. Providing unregulated expression of the reference gene transcript, normalization permits accurate comparison of the gene expression of interest (Bustin 2000).

2.7 SNUPE analysis

PCRs were performed in a 30 μ l reaction volume on cDNA.

The **reaction** included:

10x Taq buffer	3.0 μ l
10 mM dNTP mix	2.4 μ l
Taq polymerase (5 U/ μ l)	0.5 μ l
primer A (10 pmol/ μ l)	1.0 μ l
primer B (10 pmol/ μ l)	1.0 μ l
template cDNA	1.5 μ l

The IGF2 and H19 PCRs were run in a Px2 thermal cycler.

PCR program for IGF2:

95°C	5 min
94°C	30 sec
60°C	1 min
72°C	1 min (32x)
72°C	5 min

PCR program for H19:

95°C	5 min
94°C	1 min
60°C	1 min
72°C	30 sec (35x)
72°C	5 min

Successful PCR was checked by loading 5 µl of the reaction on a 1.5% agarose gel.

The following experimental procedure was kindly performed by Dr. Sascha Tierling, Institute of Genetics, Saarland University.

SNuPE primers were placed immediately adjacent to the polymorphic sites (**IGF2**: C: T SNP at position nt 1678 in the mRNA, **H19**: C: T SNP at position nt 2437 in the mRNA. 5 µl of PCR products were purified using an Exonuclease I/SAP mix (1U/9U, USB) for 30 min at 37°C followed by a 15 min inactivation step at 80°C. 14 µl primer extension mastermix was added and SNuPE reaction was performed.

SNuPE program:

96°C	2 min
96°C	20 sec (50x)
60°C	2 min

Obtained products were loaded on a DNASepTM (Transgenomic) column and separated at 50°C applying an acetonitrile gradient by continuously mixing buffer A and buffer B: **IGF2** 22-32% buffer B for 15 min, **H19** 17-30% buffer B for 15 min. The allele-specific expression index was determined by measuring the peak heights and calculating the ratio $hI / [hI + h(T)]$.

2.8 Western Blot

PTEN, pAKT and p62 protein levels were investigated by Western Blot analysis.

Western Blot is a technique used to identify and quantify specific proteins. Protein lysates are separated using denaturing SDS gel electrophoresis, allowing protein segregation according to the size.

After immobilisation of the proteins on a PVDF membrane, free protein-binding sites of the membrane have to be blocked by proteins, which cannot be detected by the antibody. This is necessary to eliminate unspecific binding of the antibody. To detect

specific binding of the antibody to the epitope of the antigen, species-specific antibodies conjugated to a fluorescent dye are used.

2.8.1 Preparation of protein extracts from mouse liver tissue

All work was performed on ice. 100 mg liver tissue were homogenised in 1 ml lysis buffer. After centrifugation (15 min, 4°C, 14,000 g) proteins remain in the supernatant.

After determination of protein concentrations by the method of Bradford (BioRad, Munich, Germany), each lysate was mixed 1:3 with Roti[®]-Load sample buffer (Carl Roth, Karlsruhe, Germany) before denaturation was performed at 95°C for 5 min.

2.8.2 Preparation of protein extracts from isolated mouse hepatocytes and hepatoma cell lines

Untreated or treated cells grown in tissue- culture plates were harvested by removing the cell culture medium before adding 100 µl lysis buffer. Cells were scraped off and the lysates were transferred to Eppendorf tubes. After centrifugation, the homogenates were treated as described above 2.8.1.

2.8.3 Determination of protein concentration using the Bradford assay

This is a spectroscopic method to measure protein concentrations based on a change in colour of the dye coomassie. After protein binding, the absorbance shifts to 595 nm due to coomassie red changes into coomassie blue.

Out of a BSA stock solution, a dilution series (2.5/5.0/7.5/10/15/20/25 µg/ml) was made according to the following scheme:

1.0 g BSA was dissolved in 100 ml H₂O. 10 ml of this solution was diluted in 90 ml H₂O to a concentration of 1 mg/ml (=stock). Aliquots of the dilution series were stored at -20°C.

Measurements were performed in a Sunrise™ multiplate reader (Tecan, Crailsheim, Germany) in 96-well tissue culture plates. 10 µl protein or BSA standard was mixed with 190 µl Bradford reagent (1:5) and detected in triplicate. Protein concentrations were assessed compared to the BSA standard protein curve.

2.8.4 SDS polyacrylamide gel electrophoresis (SDS-PAGE)

Due to negative charging of samples, migration through the gel towards the anode simply corresponds to the molecular weight of the proteins. Equal amounts of protein were loaded and separated by SDS-PAGE (Mini Protean chamber, BioRad, Munich, Germany). Proteins were stacked at 110 V for 10 min and resolved at 130 V for 60 min.

2.8.5 Protein transfer onto PVDF membranes

The blotting membrane (Immobilon PVDF-FL, Millipore, Schwalbach/Taunus, Germany) was cut to the size of the gel and equilibrated in methanol and subsequently in transfer buffer.

For the transfer set-up, a fibrous web and three pieces of moisturised filter paper were put on the cathode plate. On top, the gel and the membrane followed by another three pieces of moisturised filter paper and a fibrous web, everything forming an air bubble free stack, were placed (Figure 12). With the membrane directing towards the anode, blotting was performed at 170 mA for 150 min.

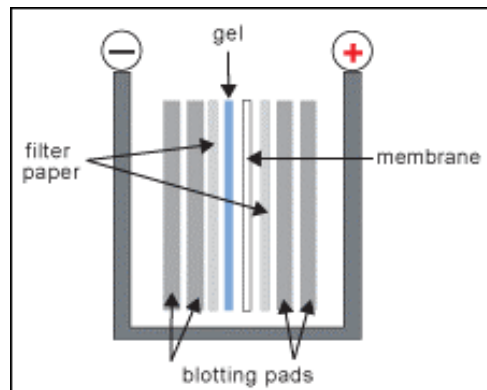


Figure 12: Western Blot setup.

Schematic representation of the assembly for the transfer of proteins onto a PVDF membrane. (www.bme.gatech.edu)

After the transfer, the membrane was incubated in Rockland Blocking Buffer (RBB) (Biomol, Hamburg, Germany) at room temperature for 60 min. The blocked membrane was incubated either at 4°C over night or at room temperature (10-60 min) with the adequate primary antibody in a dilution of 1:1,000 in RBB. Proceeding three washing steps in PBST, the specific secondary antibody was incubated for 30-60 min at room temperature under exclusion of light. After additional washing steps with PBST (2 x 20 min) and PBS (2 x 10 min), detection of immunoreactive bands was visualized by the Odyssey Infrared Imager (Licor Biosciences, Bad Homburg, Germany). To exclude loading differences, the blots were also probed with an antibody against the housekeeping protein α -tubulin (Sigma Aldrich, Munich, Germany).

To distinguish between protein expressions in lysates gained from control versus transgenic animals, samples were (semi-) quantified using the Odyssey software tool. The integrated intensity values for all samples were normalized to a housekeeping protein to adjust for uncontrolled variability.

Antibodies specific to phosphoAKT (Ser473), PTEN (both New England Biolabs, Frankfurt a. M., Germany), and anti α -tubulin (Sigma, Thermo Fisher Scientific, Karlsruhe, Germany) were incubated overnight at 4 °C in Odyssey Blocking buffer (LI-COR biosciences). Dilution factors can be found in the supplement 7.5.

For visualization of proteins with the Odyssey Infrared Imaging System (LI-COR Biosciences, Bad Homburg, Germany) membranes were blocked in Rockland Blocking buffer (Biomol). After washing, membranes were incubated with an IRdye680 conjugated goat anti-rabbit IgG secondary antibody (in case of PTEN and phosphoAKT detection) or with an IRdye800 CW conjugated goat anti-mouse antibody (in case of tubulin detection) in a 1/5,000 dilution in Odyssey Blocking Buffer (LI-COR Biosciences, Biomol, Hamburg, Germany). Secondary antibodies, goat anti-rabbit IRdye[®]680 and goat anti-mouse IRdye[®]800 CW, were purchased from Rockland (Biomol, Hamburg, Germany). After a subsequent washing step, proteins were detected and quantified with the Odyssey Infrared Imaging System.

2.9 Cell culture

Since cells were cultured under sterile conditions, all solutions were autoclaved or sterile filtered.

The human hepatocellular liver carcinoma cell lines HepG2, HUH7 and Alexander cells were originally isolated from male patients of different age and ethnicity, all suffering from primary liver carcinoma (Alexander, Bey et al. 1976; Aden, Fogel et al. 1979; Nakabayashi, Taketa et al. 1982). HepG2 and HUH7 cells show a higher expression of IGF2 compared to Alexander cells (Desbois-Mouthon, Baron et al. 2009). For H19 RNA, with which IGF2 is epigenetically closely related, low levels are reported in HepG2 and HUH7 (Banet, Bibi et al. 2000). Abnormal p53 gene expression is a frequent event associated with HCC. Alexander cells display greatly reduced p53 mRNA and protein expression levels in comparison to HepG2 and HUH7 cells (Bressac, Galvin et al. 1990). All three liver carcinoma cell lines were cultured in a humidified incubator at 37°C with 5% CO₂ in RPMI-1640 (PAA, Cölbe, Germany) containing 10% FCS gold (PAA, Cölbe, Germany), 2 mM L-glutamine (PAA, Cölbe, Germany) and 1% Penicillin/Streptomycin (P/S, PAA, Cölbe, Germany) to prevent bacterial contamination. Cultures at ~80% confluence were routinely passaged and subcultured to 80-90% confluence before any experimental procedures.

For thawing of cells, 8 ml RPMI medium was provided in a 25 cm² cell culture flask (Greiner Bio-one, Frickenhausen, Germany) before one cryovial of the appropriate cell line was added. Cultures at ~80% confluence were routinely split in a ratio of 1:3. Therefore, culture medium was removed and cells were washed with 1x PBS to remove dead cells, cell debris and to eliminate medium leftovers which would interfere with trypsin treatment. Approximately 5 ml 1x Trypsin/EDTA was added and cells were incubated at 37°C with 5% CO₂ until the cells were detached from the bottom of the flask. To inhibit trypsin activity, ~15 ml RPMI medium was added and cells were subsequently transferred into a Falcon tube to spin them down at 50 x g. After careful resuspension and separation of cell clusters, cells were plated to a new flask.

From early passages, cryostocks were generated by adding 20% DMSO to the RPMI medium. Cryovials, containing 1 ml cell suspension, were stored at -20°C and -80°C before they were frozen in liquid nitrogen for long-term storage.

2.9.1 Determination of cell amount and cell viability

Cell amount and viability were determined in an improved Neubauer counting chamber using trypan blue. As the dye penetrates through the cell membrane of dead cells, they can be distinguished from living cells.

A 1:10 dilution of cells was mixed 1:1 with trypan blue. The cell suspension was inserted into the chamber before counting of cells within one square of the grid.

2.9.2 Determination of living cells

amount of cells x 10,000 x dilution factor of cells = amount of living cells

In an improved Neubauer counting chamber, the total number of cells per ml can be defined after counting one corner square by multiplying the total number of cells found in the grid by 10⁴ (Figure 13).

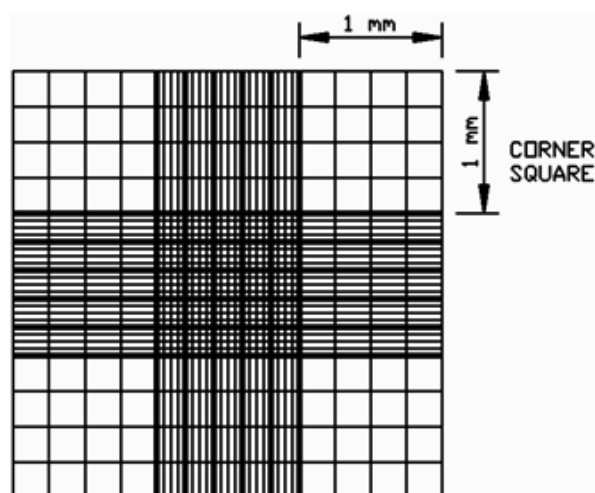


Figure 13: Improved Neubauer counting chamber.
(www.nexcelom.com)

2.9.3 Cell viability assay

Toxic effects of INTERFERin™ were tested in the colorimetric MTT assay. Yellow MTT (3-(4,5-Dimethylthiazol-2-yl)-2,5-diphenyltetrazolium bromide) is reduced to purple formazan only by living cells (Mosmann 1983).

200 μ l RPMI medium containing 1.5×10^4 cells were plated in a 96-well plate and incubated for 24 h. After removal of medium, cells were incubated for 20 h with different dilutions of the transfection reagent in RPMI. The supernatant was replaced by 150 μ l MTT solution (0.5 mg/ml). After 2 h incubation at 37°C with 5% CO₂, 100 μ l of the MTT solution was removed and cells were lysed by addition of 200 μ l of the lysis reagent dimethylsulfoxide (DMSO). After gentle shaking, the absorption was measured in an ELISA reader at 550 nm.

2.9.4 Treatment of human hepatocellular carcinoma cell lines with siRNA

For transfection experiments cells were harvested from a flask and transferred into a 12-well cell culture plate (Greiner Bio-One, Frickenhausen, Germany). Transfection was carried out with cells approximately 50% confluent. The high-purity, full-length siRNA against *p62* used in this work was purchased from Qiagen (Hilden, Germany). As a negative control, the random siRNA 'siGENOME non-targeting siRNA #2'

(Dharmacon, Thermo Fisher Scientific, Karlsruhe, Germany) was used. Sequences of both siRNAs used within this work are given in supplement chapter 7.6. 1 nM siRNA was determined to be the optimal working concentration for efficiently knock-down gene expression, avoiding 'off-target' effects.

2.9.5 Preparation of siRNA

Before using the siRNA for the first time, it was necessary to add 250 μ l siRNA suspension buffer (Qiagen, Hilden, Germany) to the lyophilisate of siRNA to obtain a 20 μ M solution (= stock). After incubation at 95°C for 1 min and at 37°C for 1 hour, suspension buffer was added to produce a 2 μ M solution of siRNA. Aliquots of 1 ml of the 2 μ M solution were stored at -20°C until use .

2.9.6 Transfection reagent

For siRNA delivery into the cell, INTERFERinTM (Biomol, Hamburg, Germany) was used. INTERFERinTM consists of a cationic lipid complex, able to bind negatively charged siRNA. The resulting complex overcomes the cell membrane *via* endocytosis. In the cytoplasm siRNA is released from the siRNA-INTERFERin complex and can mediate RNA interference (RNA_i). INTERFERinTM was stored at 4°C.

2.9.7 Transfection of human hepatocellular carcinoma cell lines

Experiments were carried out in 12-well cell culture plates using the reverse transfection method. In reverse transfections, the siRNA-transfection reagent complexes are prepared inside the wells. Thereafter, cells and medium are added (Figure 14).

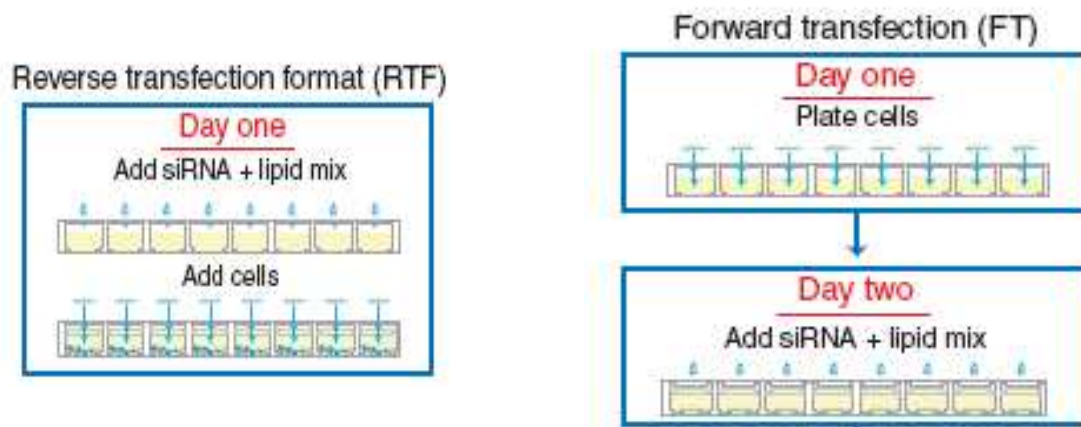


Figure 14: Workflow comparison of transfections formats.
(www.dharmacon.com/docs/RTF_Application_Note.pdf)

A volume of 2 μl INTERFERinTM/well was chosen due to low cytotoxicity determined in the MTT assay. 2 μl INTERFERinTM and 0.125 μl siRNA (=1 nM/well) were preincubated in 250 μl of FCS- and P/S-free RPMI medium, allowing complexation at RT for 10 min. To eliminate possible effects caused by the transfection reagent, some cells only received INTERFERinTM without siRNA (= IF control). The complex was provided in the 12-well plate and 125,000 cells, in P/S-free RPMI medium containing 10% FCS, were pipetted to each well. After cell adhesion to the bottom of the plate, medium was replaced the following day by fresh, P/S- and FCS-containing RPMI medium. Cells were maintained for 48 h or 72 h, at 37°C at 5% CO₂ until they were harvested for RNA and protein isolation.

2.10 Isolation of primary murine hepatocytes

For hepatocyte isolation, the collagenase perfusion method was used. Both sexes of *p62* transgenic and control mice aged 7-8 weeks were examined.

2.10.1 Collagenase perfusion

All buffer solutions were prepared freshly and tempered to 37°C until use. Collagenase A is added to the collagenase buffer directly before perfusion. Stock solutions were kept at RT or at 4°C and were replaced every 4 weeks (see supplement for detailed composition). As a peristaltic pump, maintaining the flow-

through of the perfusion solutions, the Sci-Q 323 from Watson-Marlow (Roth, Karlsruhe, Germany) was used.

Mice received an intra-peritoneal anaesthesia (Rompun 2%: Xylazinchloride 5-20 mg/kg b. w. + Ketamin 10%: Ketaminchlorid 75-100 mg/kg b. w.). As soon as no body reflexes were recognisable, the top skin layer was disinfected with 70% isopropanol and opened. Another disinfection step was carried out before the abdominal wall was opened. The inner organs were carefully put aside to gain access to the Vena cava inferior. A canula was introduced into the Vena cava after the vein was truncated with a scissor. Perfusion started with EGTA-buffer and soon after the liver was swelling due to buffer accumulation, a load-relieve was set into the Vena cava right under the heart. Perfusion with ~50 ml EGTA-buffer persisted 5 min at 25 rpm. Subsequently, the buffer was exchanged to collagenase buffer. After approximately 6 min of perfusion, the liver tissue was removed and placed in a cell culture dish containing suspension buffer. The bovine serum albumine (BSA) in this buffer efficiently inhibits the activity of collagenase A and therefore stops further digestion of the liver. The liver capsule is carefully minced with two forceps for hepatocyte release. Cells were transferred into a Falcon tube and put on ice.

The following experimental steps were done under sterile conditions under a laminar-air flow.

The hepatocyte cell suspension was carefully filtered through a cell strainer and transferred into a Falcon tube. Cells were washed with suspension buffer, followed by centrifugation for 5 min at $37 \times g$, before they were carefully resuspended in 10 ml suspension buffer. For determination of cell viability the suspension was diluted 1:5 with suspension buffer. This dilution was mixed 1:1 with trypan blue and living as well as dead cells were counted in an improved Neubauer counting chamber. Cells were cultured on collagen-coated plates for adjacent experiments when cell viability was 80% or more. Four hours after plating, when cells adhered to the collagen-coated bottom, medium was refreshed.

For mRNA stability and caspase-3-like activity experiments, medium was replaced by FCS-free William's medium E (Gibco, Invitrogen, Karlsruhe, Germany) two hours

before the experiments started and cells were maintained under serum-free conditions until harvest.

2.11 Caspase-3-like activity assay

In normal cells, caspases exist as inactive proenzymes that undergo proteolytic cleavage arranged in cascades during apoptosis. The downstream effector caspase-3 has been identified as being a key mediator of programmed cell death in mammalian cells (Hengartner 2000). It has been shown that caspase-3 cleaves PARP [poly-(ADP-ribose) polymerase], an enzyme that is involved in DNA repair and genomic maintenance. The upstream sequence of the PARP cleavage site, DEVD (N-acetyl-Asp-Glu-Val-Asp), is utilized as a basis for the highly specific caspase-3 substrate DEVD-AFC (7-amino-4-trifluoromethylcoumarin). Caspase-3 cleaves the tetra-peptide after the aspartate residue, thus releasing the dye which can be quantified by UV spectrofluorometry (extinction wave length: 400 nm / emission wave length: 505 nm). This assay is termed 'Caspase-3-like activity' due to the fact, that other downstream caspases besides caspase-3 (e. g. caspase-7) show similar substrate specificity.

2.11.1 Measurement of caspase-3-like activity in murine hepatocytes

Apoptosis in hepatocytes (500,000 cells/well; 6-well cell culture plate) from *p62* transgenic and control mice was induced by addition of 0.4 µg/ml Actinomycin D (Act D) for 15 min at 37°C with 5% CO₂, followed by incubation with TNFα (100 ng/ml) for 20 h in a humidified cell incubator. Medium was removed, cells were washed twice with 1x PBS, and 120 µl lysis buffer was added to each well. To complete cell lysis, cells were stored at -80°C o. n. Thawing was performed on ice. Cells were detached from the bottom of the plate with a cell scraper and transferred into Eppendorf tubes. After centrifugation at 13,000 x *g* at 4°C for 15 min, 10 µl of the supernatant was pipeted into a 96-well tissue culture plate. Subsequently 90 µl of the substrate buffer solution was added. Measurements of the generation of free AFC were performed in triplicates in a fluorometer multiplate reader (Wallac VICTOR², Perkin Elmer, Rodgau-Jügesheim, Germany). Protein concentration of the corresponding samples was measured with the Bradford assay using a BSA standard.

2.11.2 Measurement of caspase-3-like activity in liver tissue

Protein isolation from whole liver lysates, followed by the determination of the protein concentration was performed as described in 2.8.1. and 2.8.3. 10 µl of the protein lysate was pipeted into a 96-well tissue culture plate subsequently, 90 µl of the substrate buffer solution was added. Measurements were performed as described in 2.11.1.

2.12 Actinomycin D treatment and mRNA half-life estimation

Transcriptional arrest followed by the measurement of mRNA levels of the transcripts of interest after certain time points, using real-time RT-PCR, allows the determination of the stability of the corresponding mRNA. To illuminate the question whether the reduction in the mRNA expression level results from reduced mRNA stability or from reduced transcriptional activity, transcription in murine hepatocytes was blocked by actinomycin D (Act D) for up to 10 hours.

Act D blocks transcription through intercalation. By binding DNA during the elongation process, it prevents DNA-dependent RNA polymerase III from synthesis of the complementary mRNA strand.

1.0 mg/ml Act D was dissolved in 100% ethanol (=stock solution), stored at -20°C for a maximum of 4 weeks, and diluted in cell culture medium to a final concentration of 10 µg/ml.

Experiments were performed the day after cell isolation. All cells were treated at different time points, but harvested simultaneously (0/4/6/8/10 hours) after Act D incubation. Therefore, the cell culture medium was removed, cells were washed twice with 1x PBS and 500 µl Qiazol lysis reagent was added to each well. Cells were detached from the plate bottom with a cell scraper and transferred into Eppendorf tubes. Until RNA isolation, samples were stored at -80°C.

2.13 Histological staining

All histological staining were performed in the Institute of Pathology, Saarland University, Homburg/Saar (Germany) with kind assistance from Prof. Dr. Rainer M. Bohle, MTA Gertrud Walter and MTA Sieglinde Wagner.

2.13.1 Fixation and embedding of liver tissue

2.13.1.1 Cryostat histology

For preparation of cryostat sections, tissues have to be cut into small blocks of several mm length and shock frozen in liquid nitrogen. Fixation of the tissue block as done in paraffin histology is not necessary. Directly before cutting sections, the tissue block has to be placed on a holder, which is prepared with cryostat embedding liquid.

In this set of experiments sections were cut at 8 μm . Sections were mounted on Superfrost slides (Menzel GmbH, Braunschweig, Germany) and air-dried. Cyrosections were used for lipid staining and counter-stained with haematoxylin-eosin (HE).

2.13.1.2 Paraffin histology

Paraffin embedded tissues require a more complex reprocessing but result in a much better conservation of the tissue structure. Tissues were kept in 4% neutral buffered formaldehyde for fixation (24 h) immediately after organ removal. Formaldehyde is the most commonly used fixative for immunohistology. Fixed tissues have to be embedded before it is possible to cut sections. Routinely, this is done in paraffin.

After formalin fixation dehydration is carried out with an increasing alcohol series consisting of isopropanol 80%, 90% and 100%, followed by incubation in an intermediate medium like xylol, before the tissue blocks are embedded in paraffin.

Paraffin-embedding procedures were kindly performed at the Institute of Pathology. Paraffin blocks were stored at RT and protected from moisture.

2.13.1.3 Preparation of slides

For slide preparation a microtome is used. Hereby, it is possible to cut slides of 2 μm size. It is necessary to cool paraffin blocks down to -20°C before usage. The obtained section has to be straightened in a water bath (tempered 40°C) before it is mounted on a slide. Before immunostaining, slides have to be dried o. n. at $\sim 37^{\circ}\text{C}$.

Sections from *p62* transgenic mice were placed on the slide together with a section from a control mouse not expressing the transgene.

2.13.1.4 Embedding of stained slides

After staining is finished, slides have to be rinsed in water and dehydrated in a decreasing alcohol and xylol series before embedding for long-term storage in Entellan[®] (solution of synthetic resin-bound polymers in xylene) is performed. One to two drops of Entellan[®] are put on the slide and a coverslip is placed air-bubble free over the section.

2.13.2 Routine staining

To evaluate pathological changes in the architecture and physiology in tissues, several staining methods are used. Routinely, **HE-staining** is carried out. The cell nucleus is stained magenta-blue whereas the cytoplasm appears red-pink.

2.13.2.1 Periodic acid Schiff staining (PAS)

High proportions of carbohydrate macromolecules, e.g. glycoproteins, polysaccharides, glycolipids, phospholipids, and unsaturated fatty acids in the tissue can be visualised by PAS staining (Mulisch 1989). This method is primarily used to identify glycogen. The reaction of periodic acid selectively oxidizes the glucose residues, thereby creating aldehydes that react with the colourless acid fuchsin in Schiff reagent resulting in a purple-magenta color. Cell nuclei are counter-stained with haematoxylin.

As lipids are dissolved from the tissue by any alcohol treatment of the slide, PAS staining on paraffin sections can only detect lipids indirectly as cavities in the tissue structure.

2 µm thick paraffin tissue sections were produced and staining was performed automatically in a staining machine.

2.13.2.2 Scharlach Red staining

The principle of this method lies on the better solubility of the dye in the tissue lipids than in the moderately apolar solvent, in which it is solubilised (Mulisch 1989). The lysochrome diazo-dye Sudan IV is allowed to permeate into the highly apolar fat without the solvent solubilising the fat to be stained.

6-8 µm thick tissue sections were stained for 40 min in Scharlach Red and counter-stained for 3 min in haematoxyllin. Embedding was done with a 1:1 solution of glycerol-HCl.

2.13.2.3 Counter-staining

Specific detection methods require counter-staining, e.g. immune detection results in a specific brown colour of certain tissue areas. To emphasise this staining and to be easily able to distinguish positively from negatively stained structures, a haematoxylin or haemalaun counter-staining follows, which particularly stains cell nuclei blue.

2.13.3 Immunostaining

With this method, it is possible to detect antigens in the tissue by using specific antibodies directed against the antigen of interest. A secondary antibody carrying a marker is directed against the primary antibody.

The APAAP (alkaline phosphatase anti-alkaline phosphatase) method uses three antibodies. The primary binds to the antigen, the secondary is used as a “bridge” between the first and the third, binding to both. The third antibody is enzyme-marked

and directed against alkaline phosphatase. An advancement of this method is the so called DAKO REAL™ EnVision™ detection system method. Hereby, the secondary antibody is conjugated to a dextrane molecule carrying multiple horseradish-peroxidase (HRP) residues.

A second staining method applied in this work was 'CSA II Biotin-free Tryamide Signal Amplification' System (DAKO, Hamburg, Germany). The primary antibody is first detected with a peroxidase-conjugated secondary antibody. The next step utilizes the bound peroxides to catalyse oxidation of a fluorescein-conjugated phenol. Hereby, fluoresceyl-tryamide precipitates onto the specimen. The procedure is continued with the detection of bound fluorescein by a peroxidase-conjugated anti-fluorescein. Staining is completed using DAB/hydrogen peroxide for visualization (source: DAKO CSA II kit manual).

Both methods share the same visualisation technique. For detection, a transparent substrate diaminobenzidine (DAB) is applied on the slide. Through enzymatic reaction with peroxidase, a coloured precipitation is generated staining the tissue structures towards the primary antibody binds. For successful immune detection, it is necessary to perform several pre-treatments with paraffin-embedded tissue blocks.

2.13.3.1 Heat-induced epitope retrieval (HIER)

For the detection of several antigens, it can be necessary to treat samples with heat prior to staining. This is supposed to "renature" proteins, i.e. the sterical changes (e.g. protein cross-links) that proteins undergo during fixation, leading to epitope retrieval, are reversed. Slides were put in an open, heat-stable container containing citrate buffer, and incubated in a closed water bath for 20 min at 65°C. Slides are not allowed to run dry during the procedure. Afterwards, slides are cooled down to RT for 30 min.

Citrate buffer (pH 6.0)

Tri-sodium-citrate-dihydrate (10 mM)	2.94 g
Water ad	1.0 l

2.13.3.2 Peroxidase pre-treatment

Endogenous peroxidases have to be blocked as they would cross-react with the DAB reagent, resulting in false positive staining. This procedure was carried out by application of DAKO REAL™ peroxidase-blocking solution at RT for 15 min. During the incubation, it is important that slides are not covered.

2.13.3.3 Biotin block

If using the CSA II Signal Amplification System, it is necessary to block endogenous biotin in the tissue to eliminate potential background staining avoiding false positive signals. This procedure was carried out by application of serum-free protein block provided with the kit at RT for 5 min. The protein block was not rinsed off after treatment.

2.13.3.4 CSA II kit staining procedure

After the pre-treatment procedure, slides were incubated with the primary antibody for different incubation times.

For usage with rabbit primary antibodies it is necessary to apply the CSA II rabbit link (DAKO, Hamburg, Germany) after incubation of the primary antibody, because the system is originally intended for the use with primary antibodies from mouse. The CSA II rabbit link was applied to cover the specimen and incubated for 30 min. In a next step, the amplification reagent was incubated for 15 min at RT. During this procedure, slides were protected against light. This step was followed by the application of Anti-Fluorescein-HRP labelled secondary antibody for 30 min. Finally, staining was performed by DAB substrate chromogen (CHROM) application onto the specimen for 5 min. Counterstaining was realized with HE for 30 sec and slides were mounted.

During all incubation steps, slides were covered with coverslips and incubated in a humidified chamber to prevent them from drying out. Between all incubation steps,

the slides were carefully washed in 1x TBST. All steps in the procedure were carried out at RT. The kit was stored at 4°C and CHROM was prepared freshly every day.

2.13.3.5 Detection using the DAKO REAL™ EnVison™ detection system

In this work, also the DAKO REAL™ EnVison™ detection system with DAKO REAL™ DAB+ (1-5% of 3,3'-diaminobenzidine hydrochloride) chromogene as visualisation reagent was applied. The dextran backbone is linked to up to 100 of peroxidase (HRP) molecules and up to 20 secondary antibody molecules coupled to it. The secondary antibody reacts with rabbit and mouse immunoglobulins.

After the pre-treatment procedure, slides were incubated with the primary antibody for different incubation times at different temperatures (refer to supplement chapter 7.5). After binding of the second, polymer-coupled antibody at RT for 30 min, the DAB-containing substrate working solution (CHROM) was mixed according to the manufacturer's instruction manual and applied to the slides for 8-10 min at RT. Haematoxylin counter-staining was performed for 2 min at RT.

During all incubation steps, slides were covered with coverslips and incubated in a humidified chamber to prevent them from drying out. Between all incubation steps, the slides were carefully washed in 1x TBST. The kit was stored at 4°C and CHROM was prepared freshly every day.

2.13.3.6 Quality control

Unspecific binding can occur at different steps in the staining protocol, due to insufficient blocking of endogenous peroxidases, insufficient removal of paraffin or exhausted antigen retrieval. Usually, unspecific staining occurs because of undesirable binding of the primary antibody to unspecific structures in the tissue. Therefore, it is necessary to perform control experiments.

Each staining run should include a negative control omitting the primary antibody to exclude non-specific staining, assuring at the same time the specificity of the primary

antibody. If non-specific staining is present, this will be recognized as a rather diffuse, brown staining on the slides.

A positive control should ascertain a proper performance of all the applied reagents. Therefore, we stimulated mice with LPS for 15 and 30 min before tissue retrieval for the generation of positive control slides, supposing that the induction of the target antigen after LPS treatment was established (e.g. increase in NF- κ B activation). Positive control slides should result in specific verification of the desired antigen.

2.14 Intraperitoneal glucose tolerance test (IP-GTT)

The blood glucose level is regulated by the hormones insuline and glucagone. Insuline lowers blood glucose levels by stimulating glucose uptake into the liver and muscle, at the same time blocking gluconeogenesis and lipolysis. On the contrary, the antagonist glucagon increases glycolysis leading to higher blood glucose levels. Determination and clinical outcome control of blood glucose levels are associated with hyperglycemias, like diabetes mellitus

By performing intraperitoneal glucose tolerance tests (ip-GTT), it is possible to determine a time response of glucose decomposition *in vivo*. In this work, blood glucose was measured by the glucose dehydrogenase method using an Accu Check Aviva (Roche Diagnostics, Mannheim, Germany) glucometer. This method is based on the principle that glucose is converted into gluconolacton in the presence of a coenzyme (PQQ). During this reaction, released electrons build an electric current which is proportional to the glucose concentration in the sample.

To minimize value variations, mice were fasted for 4 hours with free access to water. Mice were weighed and their tails were slit slightly with a scissor. By gently massaging the tail, a drop of blood was sampled onto a glucometer strip. The value from the baseline blood sample (0 min) was taken as the fasting glucose value. Afterwards, 10 μ l/g body weight of a 20% glucose injection solution (Glucose-20% B. Braun, Melsungen, Germany) was administered intraperitoneally (i. p.). Subsequent blood samples were taken and glucose values were measured at 15 min, 30 min and 75 min after injection.

2.15 Laboratory chemistry

All serum parameters were determined by the 'Zentrallabor des Universitätsklinikums des Saarlandes' (Homburg, Germany) with kind assistance from MTA Marga Sand-Hill and Prof. Dr. Jürgen Geisel.

Mice were killed by cervical dislocation at the age of 2.5 weeks for blood sampling. To obtain the serum, whole blood was centrifuged for 10 min at 4,000 rpm before the supernatant was transferred into a fresh tube, diluted 1:3 with 0.9% NaCl, stored at -20°C and transported at 4°C until measurement.

All samples were measured in a PPE Modular analyser using Roche® reagents at a constant temperature of 37°C (Roche Diagnostics, Mannheim, Germany).

2.15.1 Enzymes

Enzymes are biomolecules which catalyze chemical reactions (i. e. by lowering activation energy, they increase the conversion rate of substrates). Enzymes are solved in the cytoplasm or bound to specific cell compartments. Higher plasma enzyme levels are caused either by a physiological increase in enzyme synthesis during growth or by pathophysiological lesions in the cell membrane. Enzyme activity measurements are usually based on the principle of a photometrically determined change in absorption which is proportional to the enzyme activity. The measurement unit of 1 U corresponds to the turnover of 1 µmol substrate per minute. Determination of plasma enzyme concentrations is important in the diagnosis of tissue damage as well as for the severity and dimension of the damage.

2.15.1.1 Transaminases

Transaminases, i. e. alanine amino transferase ALT (GPT) and aspartate amino transferase AST (GOT) belong to a group of enzymes, which reversibly convert amino acids into the corresponding α-keto acids by transferring amino groups to coenzymes. Both transaminases were determined according to the International

Federation of Clinical Chemistry (IFCC). 7 µl of serum were measured. In case of the analyser making a second dilution of 1:20, 14 µl were used.

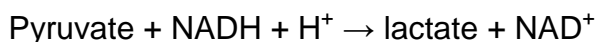
2.15.1.1.1 ALT (GPT)

ALT is located in the cytoplasm. Highest concentrations occur in the liver, followed by other organs like heart, kidney, skeletal muscle, pancreas, spleen and lung. ALT determinations are preliminary used for the diagnosis of liver parenchymal damage.

Test principle:

1. L-alanine + pyridoxalphosphate enzyme complex →
pyruvate + pyridoxaminphosphate enzyme complex
2. α- Ketoglutarat + pyridoxaminphosphate enzyme complex →
L-glutamate + pyridoxalphosphate enzyme complex

The increase in pyruvate is measured in the linked lactate dehydrogenase reaction.



The speed of the decrease in extinction at a wave-length of 340 nm is determined by the degradation rate of NADH which is proportional to the development of pyruvate and therefore to the ALT activity.

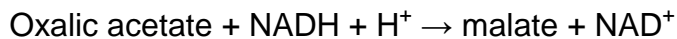
2.15.1.1.2 AST (GOT)

70% of AST is bound to the mitochondria whereas 30% are located in the cytoplasm. With an increase in severity of the damage, the fraction of AST from the mitochondria will rise. A pathophysiological increase in AST levels is observed during liver, heart and skeletal muscle damages as well as in haemolysis.

Test principle:

1. L-aspartate + pyridoxalphosphate enzyme complex →
oxalacetate + pyridoxaminphosphate enzyme complex
2. α- Ketoglutarat + pyridoxaminphosphate enzyme complex →
L-glutamate + pyridoxalphosphate enzyme complex

The increase in oxalic acetate is determined in the linked malate dehydrogenase reaction.



The speed of the decrease in extinction at a wave-length of 340 nm is determined by the degradation rate of NADH which is proportional to the development of oxalic acetate and therefore to the AST activity.

2.15.2 Substrates and metabolites

Substrates participate in metabolism. Physiological concentrations are normally kept up in the plasma. Often, the level of organ specific substrates does not change until metabolism and organ function are severely disturbed.

2.15.2.1 Cholesterol and HDL

Cholesterol is a lipidic steroid primarily synthesized *de novo* in the liver, required for membrane permeability and fluidity. Plasma cholesterol is bound to lipoproteins, which can be fractionized into low density lipoprotein (LDL), high density lipoprotein (HDL); very low density lipoprotein (VDL), and chylomicrons. HDL particles are thought to transport cholesterol back to the liver for excretion or to other tissues that use cholesterol to synthesize hormones.

High levels of cholesterol in the blood are strongly associated with atherosclerosis and with lipid metabolic disorders. Hypercholesterolemia is diagnosed with several diseases, among which are cholestasis, cirrhosis and diabetes mellitus, while high levels of HDL correlate with a better health outcome.

2.15.2.2 Triglycerides

Triacylglycerol is a glyceride in which glycerol is esterified with three fatty acids. High levels of triglycerides are linked to atherosclerosis, heart disease and stroke and pancreatitis. Triglyceride measurements are used for the diagnosis of lipid metabolic disorders and for the classification of hyperlipidemias.

Cholesterol and triglycerides were measured according to the CHOD-PAP method. Detergents release cholesterol and his esters from lipoproteins. Cholesterol esterase hydrolyzes cholesterol which is then oxidized by cholesteroloxidase. Thereby, hydrogen peroxide is built, which is in the presence of peroxidase and 4-aminoantipyrine, converted into chinonimine. Triglycerides were hydrolysed to glycerol and fatty acids. Glycerol is oxidized and thereby hydrogen peroxide is built.

The resulting dye is measured at a wave-length of 505 nm. The intensity of the colour is thereby proportional to the concentration of triglycerides. HDL was determined by a homogenic enzymatic test. For measurement of cholesterol and triglycerides 2 μ l serum and for measurement of HDL 2.1 μ l of serum were used.

3. Results

p62 was originally identified as tumor-associated autoantigen in HCC (Zhang, Chan et al. 1999) but biological actions of the protein have as yet been completely unknown.

Therefore, mice overexpressing *p62* exclusively in the liver were generated by the group of Dr. Tan (The Scripps Research Institute, La Jolla, USA) in order to investigate functional implications of hepatic *p62* expression.

3.1 Liver specific expression of *p62*

The chromosomal insertion of the transgene for the mouse lineage used for all experimental procedures is not known.

Northern and Western Blots revealed that neither $p62^+/LT2^-$ nor $p62^-/LT2^+$ mice but solely double-positive $p62^+/LT2^+$ mice from both lineages express *p62* in the liver (Figure 15, data kindly provided by Dr. Fu-Dong Shi and data not shown).

Doxycyclin administration abrogated *p62* expression (data not shown, experiments performed by PD Dr. Alexandra K. Kiemer).

All single- and double-transgenic mice are fertile and show normal development. No spontaneous occurrence of liver tumours for up to two years was observed.

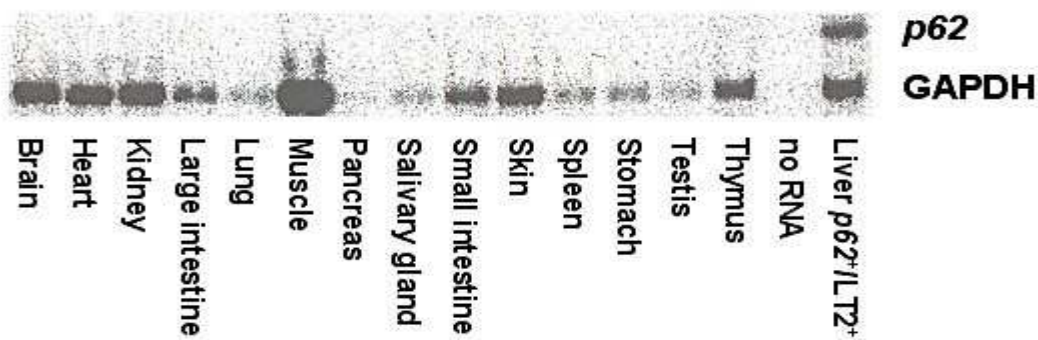


Figure 15: Northern Blot.
p62 expression in different mouse organs. Only in livers of *p62* transgenic mice the 2.0 kb band corresponding to *p62* mRNA could be detected.

All experiments were performed either in liver tissue or in isolated hepatocytes from *p62* transgenic mice (+/+; “*p62*”) in comparison to control mice (-/+; “*co*”) carrying the liver specific promoter but showing no overexpression of the *p62* transgene. Mice homo- and heterozygous of both groups were used for the experiments.

Figure 16 shows that *p62* expression is restricted to the cytoplasm and that the transgene is expressed in a high percentage of hepatocytes.

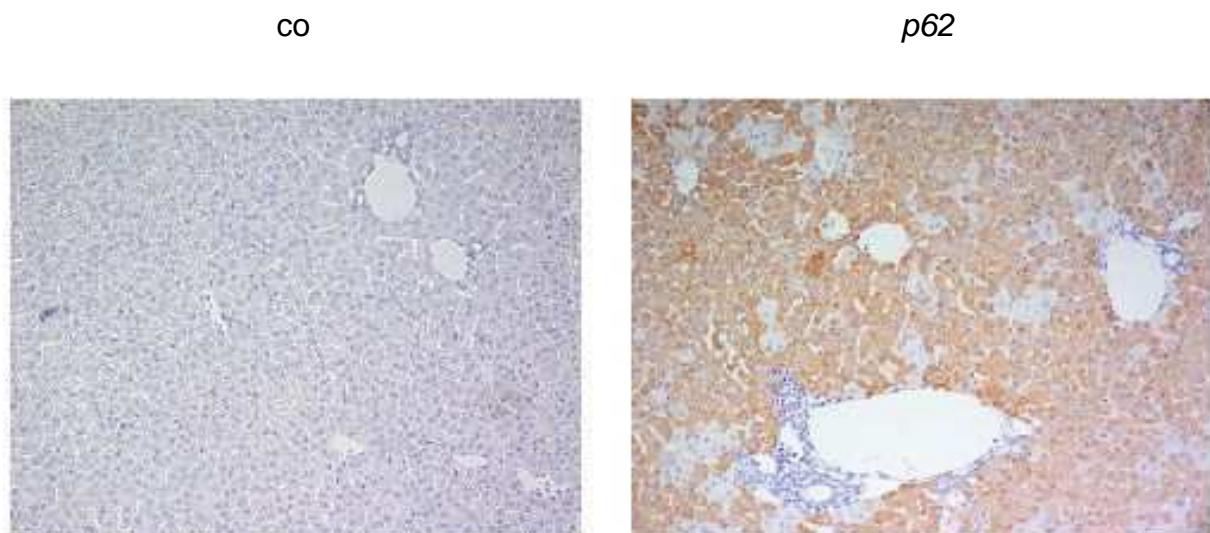


Figure 16: *p62* localization.
 Immunostaining of *p62* in liver tissue. An increase in cytoplasmic staining was detected in *p62* transgenic animals (right, *p62*) in comparison to controls (left, *co*) (paraffin-embedded; 20x original magnification).

3.1.1 Genotyping of *p62* mice

For genotyping of mice, a PCR was performed with two primer pairs, which allows detection of the *p62* transgene and the LT2 gene. With the primer pair “*p62* lower” and “*p62* upper” a band of 350 bp was detected, whereas the primer pair “LT2 lower” and “LT2 upper” detected a band of 500 bp in size. With the PCR reaction, all possible genotypes can be detected. Figure 17 illustrates the two possible amplification products.

In *p62*⁻/LT2⁺ mice only one band of 500 bp appeared, corresponding to the LT2 gene, whereas in *p62*⁺/LT2⁺ mice, two bands could be detected, one of 500 bp and one of 350 bp, the latter corresponding to the *p62* transgene. Also *p62*⁺/LT2⁻ mice were detected, corresponding to a 350 bp band in size in the absence of a 500 bp LT2 band (data not shown). These mice do not overexpress the transgene.

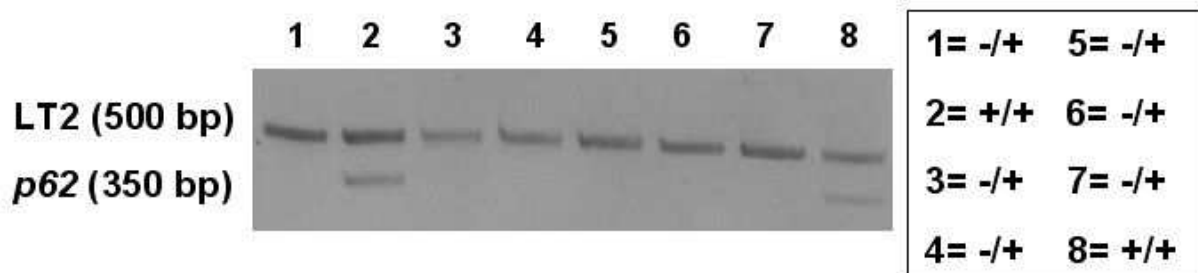


Figure 17: Genotyping of *p62* transgenic mice.

PCR products were loaded onto a 1.5% agarose gel. The 500 bp band corresponds to LT2, the 350 bp band matches *p62*.

3.1.2 Genotyping of *p62*/LT2/SD7 mice by allele-specific PCR

For the imprinting analyses, mice were selected for the insertion of the *Mus spretus* into the *Mus domesticus* background. SD7 mice carry the *Mus spretus* distal chromosome 7 on a C57BL/6 *Mus domesticus* background. By crossing these mice with mice on a *Mus domesticus* background, the inheritance of the parental alleles can be examined. To distinguish between the *Mus spretus* and the *Mus domesticus* background, two PCR reactions using microsatellite primers were performed to analyse the recombination events in the progeny of *p62* x SD7 mice.

Microsatellites (also called single sequences repeats, SSR) are sequences composed of tandem repeats from one to six bases in length, which are arranged head-to-tail without interruption (Hancock, Worthey et al. 2001).

The primer pair “D7 Mit 12 for” and “D7 Mit 12 rev” detected a band of 220 bp corresponding to the *Mus spretus* background, whereas a band of 197 bp was detected on the *Mus domesticus* C57BL/6 background (Figure 18 A). Only mice where both bands were detected in the genotyping PCR were selected for the experiments.

The primer pair “D7 Mit 140 for” and “D7 Mit 140 rev” detected a band of 125 bp corresponding to the *Mus spretus* background. The band of 137 bp appeared when a *Mus domesticus* background existed (Figure 18 B). Only mice showing both bands in the genotyping PCR were used for the experiments.

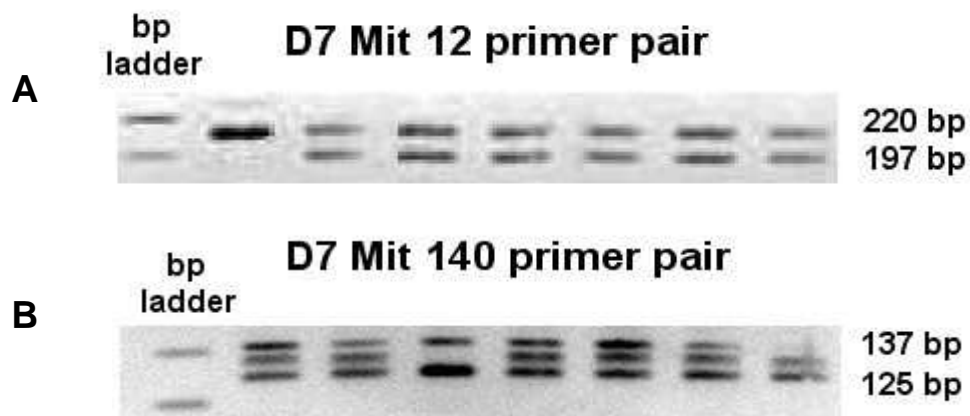


Figure 18: Genotyping of the progeny of *p62* x *SD7*.

- A** Bands show PCR products from “D7 Mit 12” amplification. The band of 220 bp in size corresponds to the *Mus spretus* origin of the parental allele. The band of 197 bp in size relates to the *Mus domesticus* origin.
- B** Bands show PCR products from “D7 Mit 140” amplification. The band of 125 bp corresponds to the *Mus spretus* origin, whereas the band of 137 bp relates to the *Mus domesticus* origin.

3.1.3 *p62* expression

Figure 19 show that 5 week old *p62* transgenic animals displayed the highest levels of *p62* mRNA.

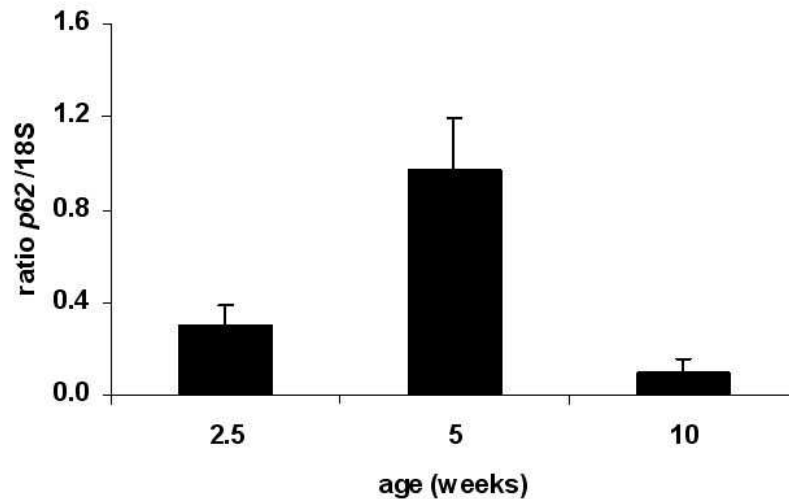


Figure 19: *p62* mRNA expression.

p62 expression was determined by real-time RT-PCR in *p62* transgenic mice ($n > 6$), expressed as the mean \pm S.E.M. A value of $p < 0.005$ (*) represented a statistically significant difference compared to controls using student's t-test.

3.2 Induction of a fatty liver disease phenotype

In order to investigate changes in liver morphology caused by *p62* overexpression, histological investigations were performed on liver tissue from *p62* transgenic and control mice. Mice at the age of 2.5 and 5 weeks were examined.

3.2.1 HE

HE staining of sections suggested morphological changes in *p62* transgenic livers. Stainings showed a homogenous distribution of HE in healthy tissue, whereas in *p62* transgenic livers the cytoplasm of eosinophilic cells, predominately located around the central veins (Rappaport zone 1), were stained stronger than pericentral and central-lobular (Rappaport zones 2 + 3) (Rappaport 1960; Rappaport 1976) cytoplasmic areas, where basophilic cells predominated (Figure 20).

Leukocyte infiltration was not observed with *p62* overexpression. Examination of livers from 5 week old animals displayed no such staining differences. Leukocyte infiltration was not elevated under *p62* overexpression in both groups.

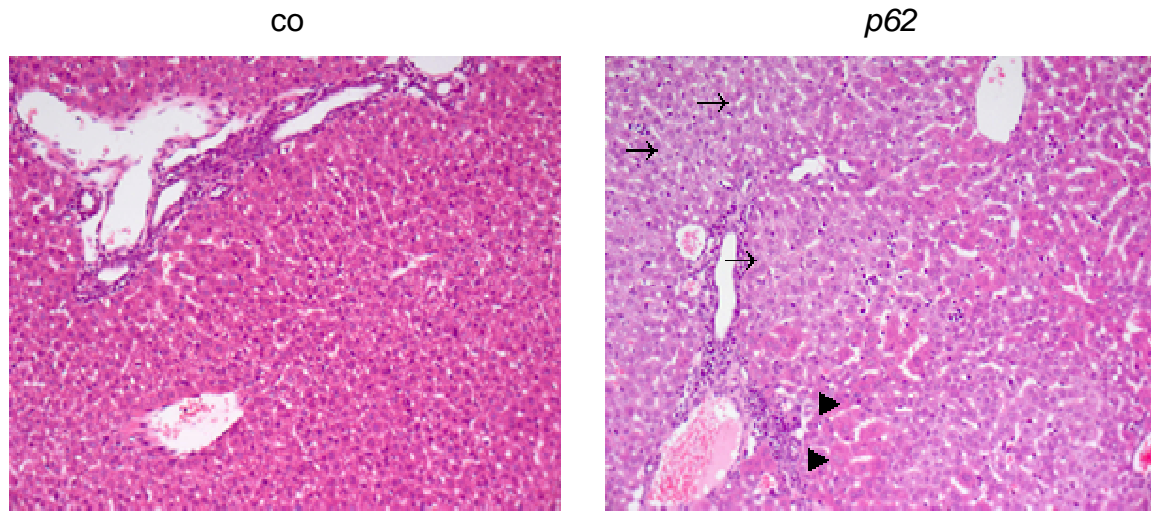


Figure 20: Histological alterations in 2.5 week old mice.

HE-stained liver tissue of control mice (left, *co*) in comparison to *p62* transgenic animals (right, *p62*) (paraffin-embedded, 20x original magnification). Basophilic cells are shown in both groups, whereas eosinophilic cells were only detected in *p62* transgenic animals. Areas of basophilic cells (→) are pericentrally located. (▶) displays accumulation of eosinophilic cells.

3.2.2 Scharlach Red

Liver architecture gave hints on an accumulation of fatty acids as presumed from the occurrence of empty vacuoles in paraffin-embedded liver tissue. Therefore, investigations on specific fat staining were performed. In comparison to controls, the *p62* transgenic tissue of 2.5 week old mice showed a significant increase in finely dispersed fat droplets without a zonal preference (Figure 21).

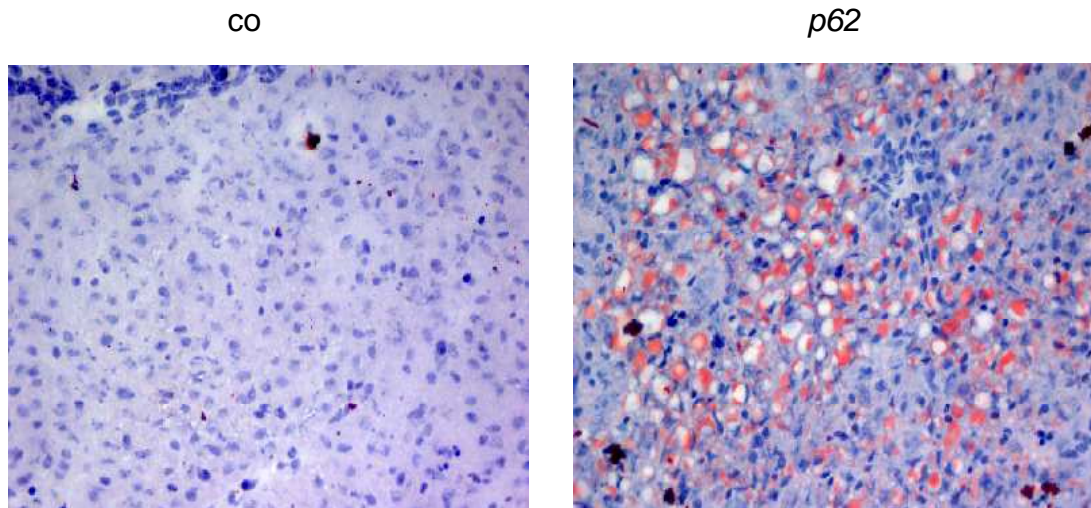


Figure 21: Fat droplets in 2.5 week old mice. Scharlach Red stained cryosected liver tissues of controls (left, *co*) in comparison to *p62* transgenic mice (right, *p62*) (cryosected; 40x original magnification). A microvesicular distribution of fatty acids occurred in hepatocytes of transgenic animals.

In 2.5 week old animals, 21 transgenic livers were stained and compared to 14 controls. 12 transgenic livers, i. e. 57% showed a strong reaction with Scharlach Red due to the accumulation of fat, revealing the phenotype of a fatty liver.

p62 transgenic females displayed a higher frequency in the occurrence of the fatty liver phenotype (66%) when compared to males (44%). In addition to microscopic differences, fatty livers macroscopically occurred with pale colour (data not shown).

For the age of 5 weeks, no significant difference was observed between the two experimental groups (data not shown).

3.2.3 PAS

Metabolic differences were also seen regarding carbohydrate macromolecules, i. e. glycogen. At the age of 2.5 weeks, a decrease in glycogen staining was observed in livers of *p62* transgenic mice (n=12) in comparison to controls (n=7) (Figure 22). Whereas an accumulation of glycogen in Rappaport zones 1 + 2 around the central veins could be detected in some transgenics (n=4), others displayed a homogenic distribution with no zonal preference (n=8).

For 5 week old mice, no significant changes between the two groups could be found (data not shown).

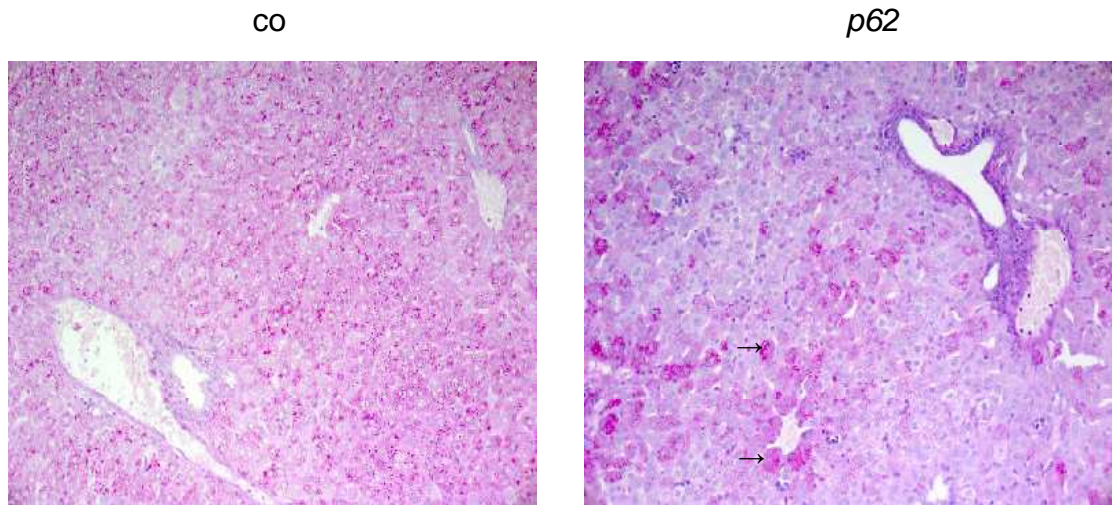


Figure 22: Glycogen staining. PAS-stained liver tissue of control animals (left, co) in comparison to *p62* transgenic animals (right, *p62*) (paraffin-embedded; 20x original magnification). (→) show the accumulation of glycogen around the central vein in *p62* transgenic animals.

3.3 Increased liver to body weight ratio

Fatty livers might result from higher body weight due to impaired hepatic lipid export and favoured hepatic triglyceride (TG) accumulation (Angulo 2002). As we could detect hints on pathological changes similar to steatosis and steatohepatitis occurring under *p62* overexpression, we were interested in potential changes in liver and/or body weight.

For neither body nor liver weight, we could detect any significant differences between both examined groups at the age of 2.5, 5 and 10 weeks. Moreover, no gender-specific differences were detected (data not shown).

Interestingly, at the age of 2.5 weeks when the phenotypic alterations caused by *p62* overexpression were highest, the liver to body weight ratio revealed a significant difference between control and transgenic mice (Figure 23).

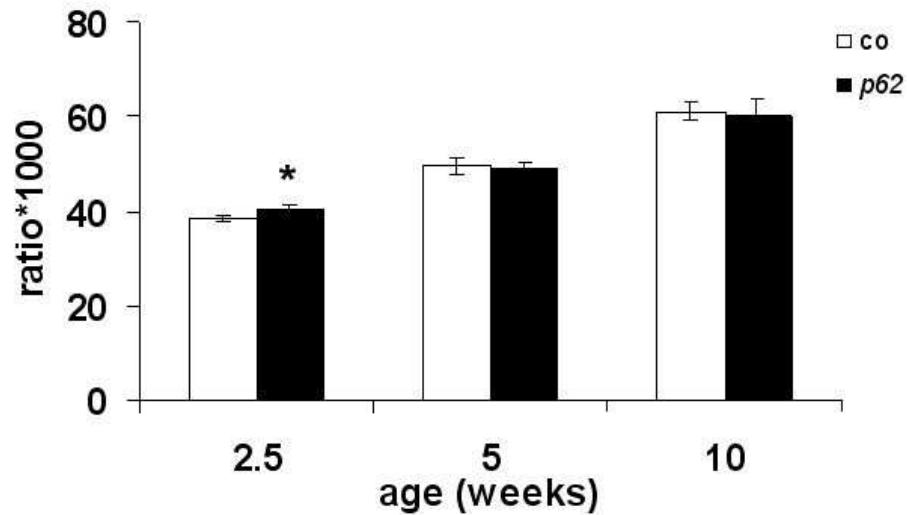


Figure 23: Liver to body weight ratio.

Liver to body weight ratio of 2.5 (co: n=26 / tr: n=29), 5 (co: n=12 / tr: n=12) and 10 (co: n=6/ tr: n=3) week old mice, expressed as the ratio*1000, representing the mean \pm S.E.M. A $p < 0.05$ (*) represents a statistically significant difference compared to controls using student's t-test.

3.4 Absence of liver damage

Since alterations in metabolism and liver architecture were revealed only in 2.5 week old mice, we decided to determine lipid (cholesterol, HDLC, triglycerides) serum parameters also in this age group. Since the incidence of fatty livers seemed higher in female animals, we also considered gender-specific differences.

3.4.1 Serum lipids

No relevant differences in cholesterol or HDLC values were revealed, neither with regard to gender-specificity nor to the experimental groups (Table 1).

Interestingly, a significant increase in triglyceride serum levels was found when *p62* transgenic male mice were compared to their corresponding control littermates (Table 1), whereas no difference was detected for females.

		HDLC	CHOL	TG
co	both sexes	87 ± 5	102 ± 6	104 ± 12
	male	102 ± 7	108 ± 7	73 ± 7
	female	84 ± 5	93 ± 5	144 ± 15
p62	both sexes	84 ± 6	103 ± 7	104 ± 13
	male	90 ± 9	90 ± 11	109 ± 8 (*p<0.05)
	female	86 ± 6	105 ± 5	125 ± 37

Table 1: Serum parameters of 2.5 week old *p62* transgenic mice.

Determination of lipid serum parameters in *p62* transgenic mice (n=10, of which n=6 male and n=4 female) after 4 hours of fasting vs. controls (n=16, of which n=9 male and n= 7 female). Serum parameters expressed in mg/dl, representing the mean ± S.E.M. A value of $p<0.05$ (*) was considered statistically significant from respective controls using student's t-test.

3.5 Absence of inflammatory parameters

Since *p62* transgenic animals developed histological liver alterations similar to a non-alcoholic fatty liver disease (NAFLD), we aimed to determine whether they also show characteristics of a non-alcoholic steatohepatitis (NASH), additionally encompassing inflammation.

3.5.1 Serum transaminases

Since alterations in liver architecture occurred in 2.5 week old mice only, serum transaminase (ALT, AST) parameters were examined only in this age group. Due to the preferred incidence of fatty livers in female animals, gender-specific differences were also considered.

ALT levels displayed a decrease in transgenic mice compared to controls, with a difference being most considerable in female animals.

Determination of serum AST levels, which would also indicate liver damage, showed the same non-significant result, with the most potent decrease in female transgenics´.

The *de Ritis* ratio showed a significant increase in *p62* transgenic females (Table 2). Although this single result might be interpreted as a hint on perturbations in liver function, the data do not suggest that a pronounced liver damage is induced in *p62* transgenic animals.

		ALT	AST	<i>De Ritis</i> ratio
co	both sexes	357 ± 40	2564 ± 299	6.29 ± 0.25
	male	312 ± 36	2289 ± 189	7.65 ± 0.55
	female	439 ± 112	2488 ± 592	4.02 ± 0.76
<i>p62</i>	both sexes	263 ± 43	1749 ± 254	5.99 ± 0.32
	male	278 ± 56	1972 ± 437	5.45 ± 1.35
	female	248 ± 27	1677 ± 840	6.81 ± 0.88 (*p<0.05)

Table 2: Transaminase levels.

Serum ALT and AST levels (U/l) determined after 4 hours of fasting of *p62* transgenic mice (n=7, of which n=4 male and n=3 female) vs. controls (n=14, of which n=9 male and n=5 female). Data are expressed as the mean ± S.E.M. A value of p<0.05 (*) was considered statistically significant from controls of the respective gender using student´ s t-test.

3.5.2 Immunohistology of NF-κB

Although the absence of leukocyte infiltration did not suggest any signs of inflammation, a potential activation/ translocation of NF-κB (p65 subunit) was investigated, which plays a pivotal role in the inflammatory response (Winwood and Arthur 1993; Luedde, Beraza et al. 2006).

15 min and 30 min LPS stimulated livers from C57BL/6 mice served as positive controls. Staining in LPS-treated positive control livers displayed an increase in nuclear staining of immune cells but neither in cytoplasmic nor nuclear staining of hepatocytes (Figure 24 A).

p62 transgenic livers did not show increased nuclear p65 staining, indicating inflammatory activity (Figure 24 B). Therefore, it can be concluded that *p62* does not

promote chronic inflammatory processes as already indicated by serum parameter values and by the absence of observed leukocyte infiltration.

Interestingly, an increase in cytoplasmic staining of hepatocytes in *p62* transgenic mice was revealed in 12 of 15 animals (80%). Moreover, about one third of the transgenic livers displayed a higher occurrence of positively stained hepatocytes in Rappaport zone 3.

For 5 week old mice, no difference in neither cytoplasmic nor nuclear staining of liver cells between both experimental groups could be revealed (data not shown).

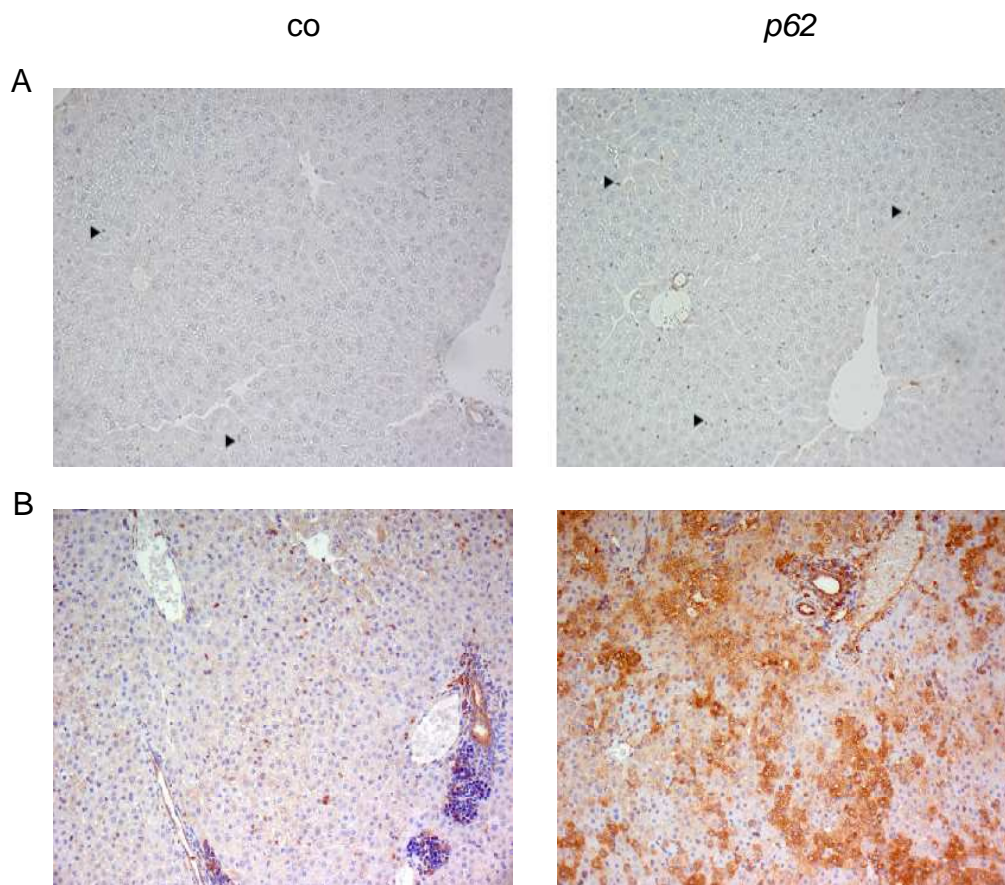


Figure 24: 20x original magnification of paraffin-embedded slides. Immunostaining of NF- κ B p65.

- A** NF- κ B (p65) stained liver tissues 15 min (left) and 30 min (right) after LPS treatment. The increase in nuclear staining of immune cells is indicated by arrows (►).
- B** NF- κ B (p65) stained liver tissue of *p62* mice (left: co), (right: *p62*). An increase in cytoplasmic hepatocyte staining was detected for *p62* transgenic animals.

3.6 Increased expression of IGF2 and H19

Since *p62* belongs to the family of IGF2 mRNA-binding proteins (Zhang, Chan et al. 1999) and due to the fact that IGF2 has been associated with metabolic disorders, we were interested in potential changes in IGF2 expression in *p62* transgenic mice. At the same time H19 was determined, due to the fact of the similar regulation of both genes by genomic imprinting (Sasaki, Ishihara et al. 2000).

For all investigated ages (2.5, 5 and 10 weeks) an upregulation of IGF2 and H19 could be shown for *p62* transgenic animals in comparison to controls (Figure 25).

Interestingly, however, expression of both IGF2 and H19 was highest at the age of 2.5 weeks when phenotypic alterations were most obvious.

At the age of 2.5 and 5 weeks a significant upregulation of IGF2 and H19 could be shown for *p62* transgenic mice in comparison to control animals. 10 week old animals followed that tendency.

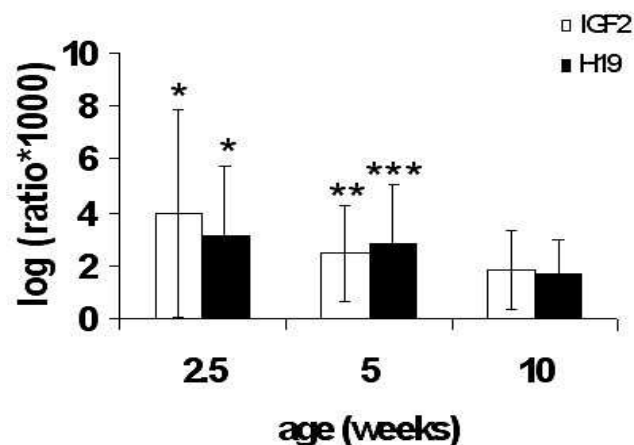


Figure 25: Time course of mRNA expression.

Log ratio of IGF2 and H19 to 18S in *p62* transgenic mice vs. controls, expressed as the mean \pm S.E.M. Experiments were performed for a minimum of $n=6$ mice per group. A value of $p<0.05$ (*), a $p<0.005$ (**) and a $p<0.001$ (***) was considered statistically different from controls at the respective age using student's t-test.

Correlation data revealed that with raised *p62* expression, the induction of IGF2 and H19 increased within one age group (Figure 26). Increased IGF2 expression was accompanied by elevated H19 expression. Noteworthy, female *p62* transgenic mice displayed higher levels of *p62*, IGF2 and H19 than their corresponding male littermates.

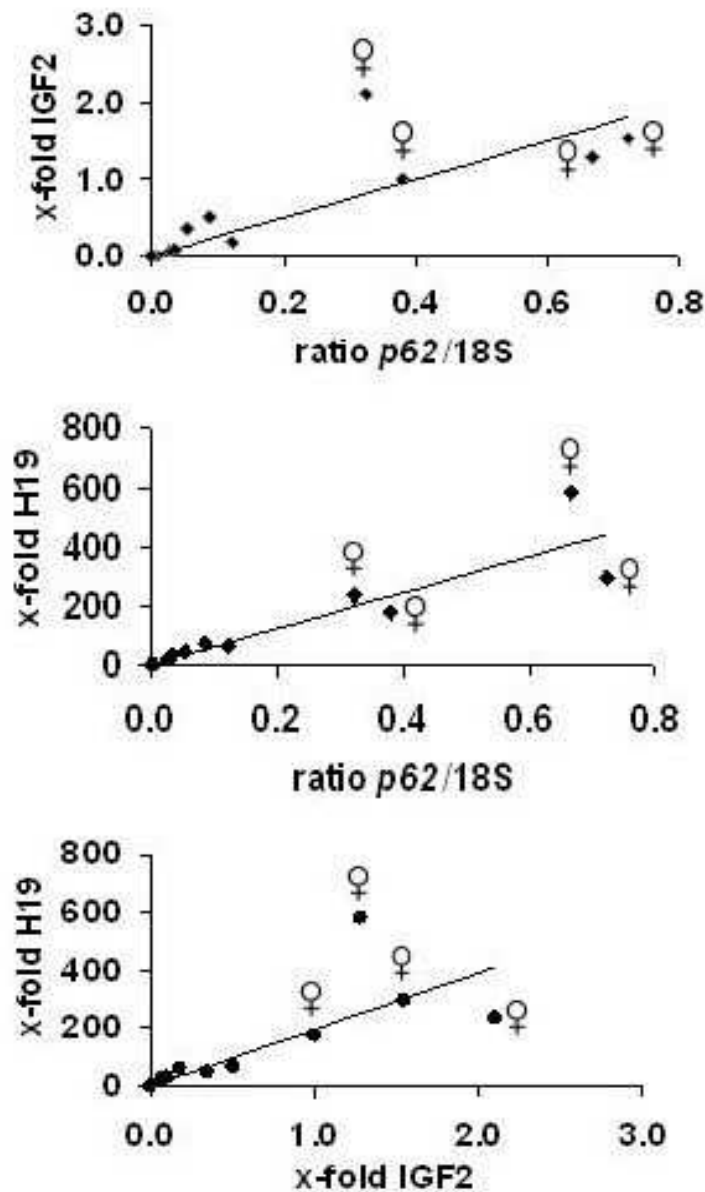


Figure 26: Correlation graphics of *p62*, IGF2 and H19 mRNA expression of 2.5 week old *p62* transgenic animals.

p62 is expressed as the ratio normalized to 18S and blotted against the x-fold values of IGF2 (B) or H19 (C) compared to controls. Correlation between IGF2 and H19 mRNA expression (D), expressed as x-fold values of control (n=4) and transgenic (n=9) mice. ♀ shows gene expression levels in female *p62* transgenic animals.

To exclude genetic predisposition, the correlation of *p62*, IGF2 and H19 gene expression was demonstrated after application of doxycycline to *p62* transgenic mice.

Doxycycline abrogated *p62* expression, and a reduction in mRNA expression of IGF2 and H19 could be verified by real-time RT-PCR (Figure 27, data kindly provided by Prof. Dr. A. K. Kiemer).

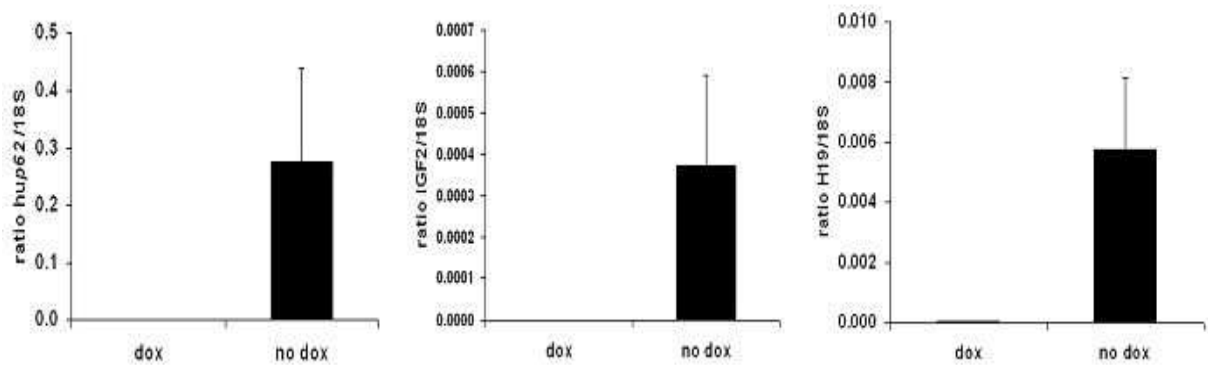


Figure 27: Time course of mRNA expression after doxycycline (dox) administration.

Ratio of *p62*, IGF2 and H19 normalized to 18S in *p62* transgenic mice (dox) vs. untreated *p62* transgenic animals (no dox), expressed as the mean \pm S.E.M.

3.7 Localisation of *p62* and IGF2

Staining of *p62* and IGF2 in *p62* transgenic livers revealed a diffuse pattern with areas of only weak staining and clusters of hepatocytes showing strong immunoreactivity within the cytoplasm and therefore high expression of *p62* and IGF2. Both proteins are located in the cytoplasm. No zonal preference was observed (Figure 28).

It is worth mentioning that immunostaining of *p62* and IGF2 in serial sections from *p62* transgenic livers demonstrated that hepatocytes, which display high expression levels of *p62* showed an increase in IGF2 protein, too (Figure 28).

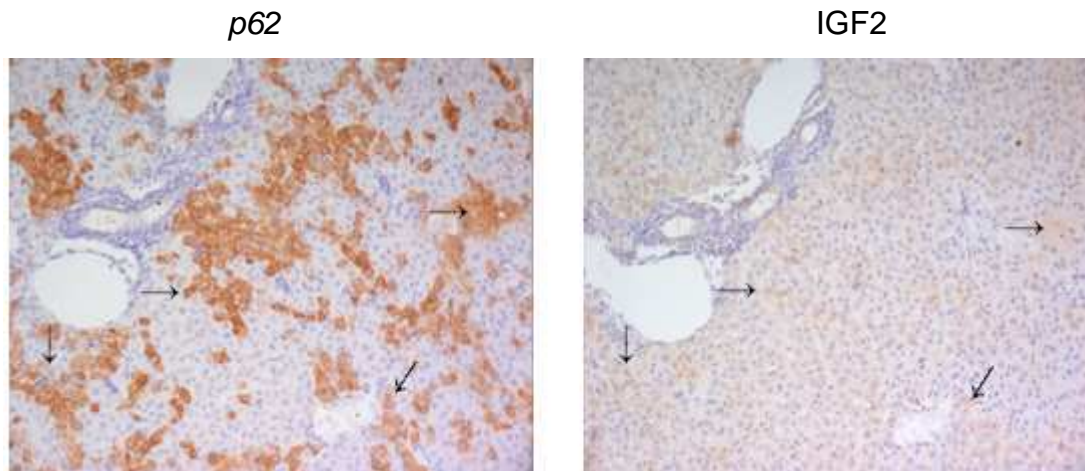


Figure 28: Immunostaining of *p62* and IGF2.

Serial sections of the tissue of a 2.5 week old *p62* transgenic liver, stained with an antibody against *p62* (left) and IGF2 (right) (paraffin-embedded; 20x magnification). Cells displaying strong immunostaining of *p62* also showed increased IGF2 expression, indicated by (→).

3.8 No alteration of IGF2 and H19 mRNA stability

p62 is known to belong to the family of insulin-like growth-factor 2 mRNA-binding proteins (Nielsen, Christiansen et al. 1999). mRNA-binding proteins can play a role in the regulation of mRNA stability.

Because of the fact that *p62* expression resulted in an upregulation of IGF2 and H19 mRNA levels and IMPs have been shown to bind also to H19 (Runge, Nielsen et al. 2000), mRNA stability of IGF2 and H19 in *p62* transgenic mice were estimated in isolated and actinomycin D (Act D) treated hepatocytes.

Figure 15 shows that steady-state levels of all mRNAs decreased after treatment with Act D, but more than 60% of mRNA levels were left after 10 h suggesting high mRNA half-lives for all three transcripts (Eberhardt, Doller et al. 2007). The decay of IGF2 and H19 was comparable between both experimental groups over the time course. These results indicate that both IGF2 and H19 stability is not altered by the presence of *p62* (Figure 29).

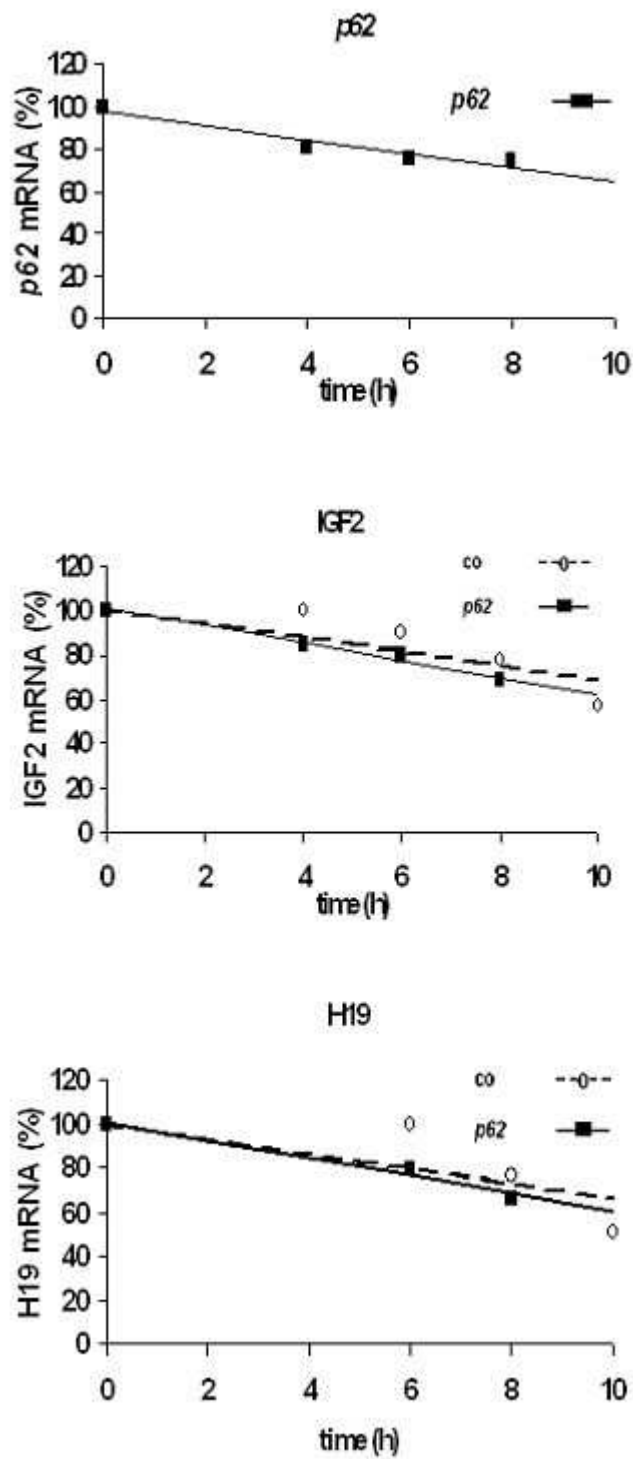


Figure 29: mRNA stability.

mRNA expression in hepatocytes isolated from *p62* transgenic (n=3) vs. control (n=3) mice. Data are expressed as the mean \pm S.E.M. relative mRNA expression after Act D (10 μ g/ml) treatment for 4, 6, 8 and 10 hours normalized to cyclophilin. Data expressed relative to untreated cells of the same isolation (0 h), set as 100%.

3.9 Monoallelic expression of IGF2 and H19

To elucidate allele-specific expression of IGF2 and H19, single-nucleotide primer extension (SNuPE)-HPLC analysis was performed on liver tissues from newborns and 2.5 week old mice.

To be able to distinguish between the origin of the paternal allele, SD7 mice (carrying the *Mus spretus* distal chromosome 7 on a C57BL/6 *Mus domesticus* background) were crossed with *p62* transgenic mice (Moore, Constancia et al. 1997). SD7 mice provide a source of single-nucleotide polymorphisms (SNPs) to distinguish expression of all the genes present on this gene locus, including IGF2 and H19.

For verification that endogenous, i. e. *mup62*, has no influence on allele-specific IGF2 or H19 expression, expression levels of *mup62* were examined by real-time RT-PCR (Figure 30). Results showed a non-significant decrease in *mup62* expression in transgenic mice, which may be evoked by *p62* overexpression.

Real-time RT-PCR experiments on the cDNA of livers derived from *p62* transgenic newborns showed only a weak increase in IGF2 and H19 compared to control animals (Figure 31). Since phenotypic alterations were most obvious when IGF2 and H19 expression was highest, a second set of experiments with 2.5 week old mice was performed.

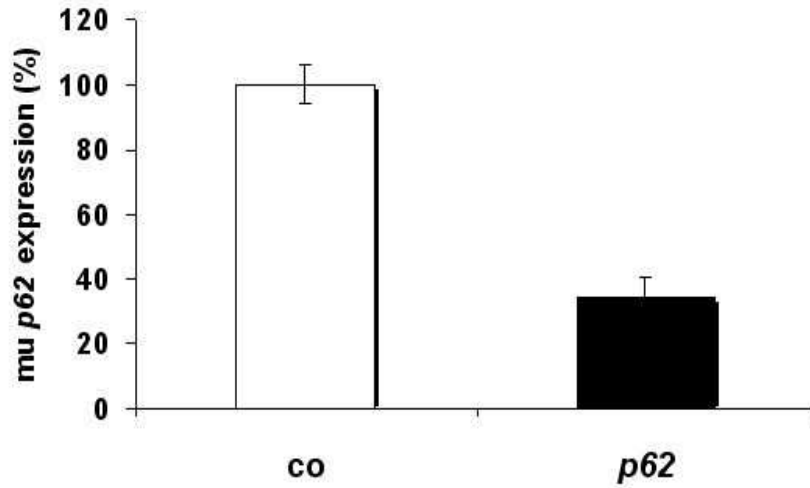


Figure 30: mRNA expression of *mup62* in newborn *p62/SD7* mice.

Data is expressed as the the relative expression \pm S.E.M. Results show 1 experiment, performed with a minimum of 4 animals per group.

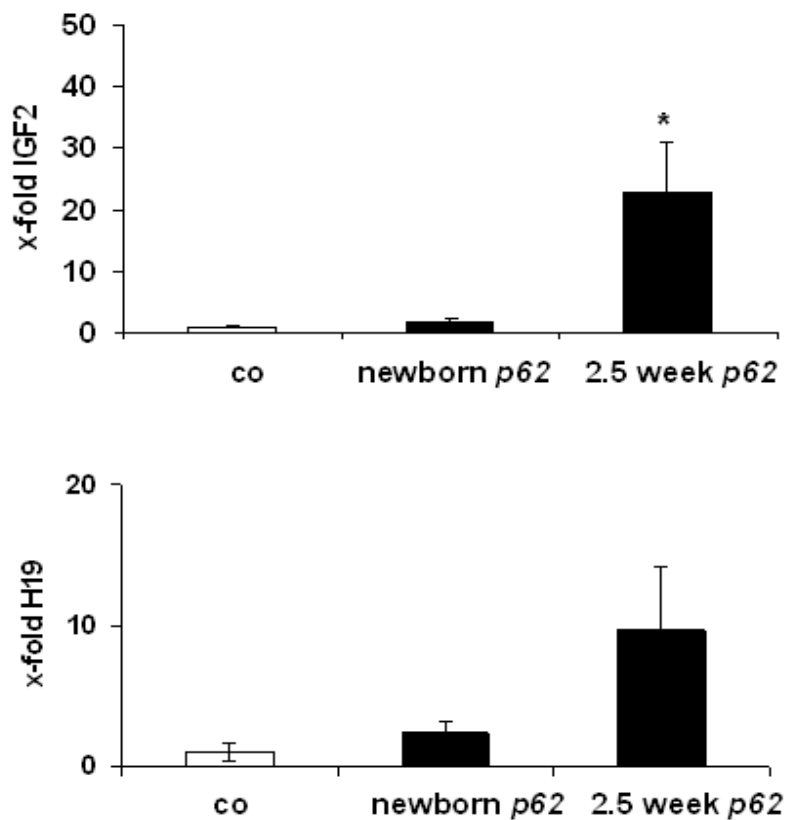


Figure 31: *IGF2* and *H19* mRNA expression in newborn and 2.5 week *p62/SD7* mice.

Data expressed as the x-fold values \pm S.E.M. of transgenic vs. control animals. (*) $p < 0.05$ statistically different from controls of the respective age using student's t-test.

Besides, cDNA was used for the amplification of IGF2 and H19 transcripts in SNUPE reactions. A 16 bp primer, which ends directly before the 3' end of the polymorphism, is annealed and elongated by exactly one allele-specific didesoxynucleotide (ddNTP). The reaction is aborted after incorporation of a ddNTP because ddNTPs do not carry a free hydroxyl group at the 3' residue and cannot be elongated.

An aliquot of the SNUPE reaction was loaded onto an HPLC column and eluted DNA was detected with a UV detector at 260 nm.

IGF2 products derived from the *Mus domesticus* background (*p62*) led to the addition of a ddTTP whereas IGF2 products derived from the *Mus spretus* background (*SD7*) resulted in a ddCTP.

H19 products reciprocally correlated with the IGF2 results: the ddCTP concluded for the *Mus domesticus* background whereas a ddTTP originated from *Mus spretus*.

After amplification three products can be distinguished from each other:

unextended primer 5' TCAGTGAATCAAATTA 3'

T-extended primer (*M. dom.*) 5' TCAGTGAATCAAATTAddTTP 3'
→ reaction stopp

C-extended primer (*M. spret.*) 5' TCAGTGAATCAAATTAddCTP 3'
→ reaction stopp

The three products can be distinguished according to their hydrophobicities, thereby following the principle that with increasing hydrophoby, elution occurs earlier, i. e. the unextended primer lacking a base compared to the extended ones leaves the column first. As cytosine (C) is more hydrophilic than thymidine (T), products carrying a **C** are eluted earlier than products carrying a **T**.

For both examined ages, a mono-allelic expression of IGF2 and H19 was shown (Figure 32) in control as well as *p62* transgenic mice: IGF2 is paternally and H19 is maternally expressed, as can be seen for values on the allele-specific index (Table 3).

	H19 MW	H19 ± SEM	IGF2 MW	IGF2 ± SEM
newborn transgenic mice	0.94	0.01	1.00	0.00
newborn control mice	0.92	0.02	1.00	0.00
2.5 week transgenic mice	1.00	0.00	1.00	0.00
2.5 week control mice	1.00	0.00	1.00	0.00

Table 3: Allele-specific index of H19 and IGF2 expression after SnuPE-HPLC detection.

Results are obtained by determination of the peak heights of the C- and T-extended primers and calculating the ratio $h(C)/h(C)+h(T)$ (newborn: *p62*: n=7, co: n=6; 2.5 week: *p62*: n=8; co: n=4). No statistically significant difference could be determined between both examined groups.

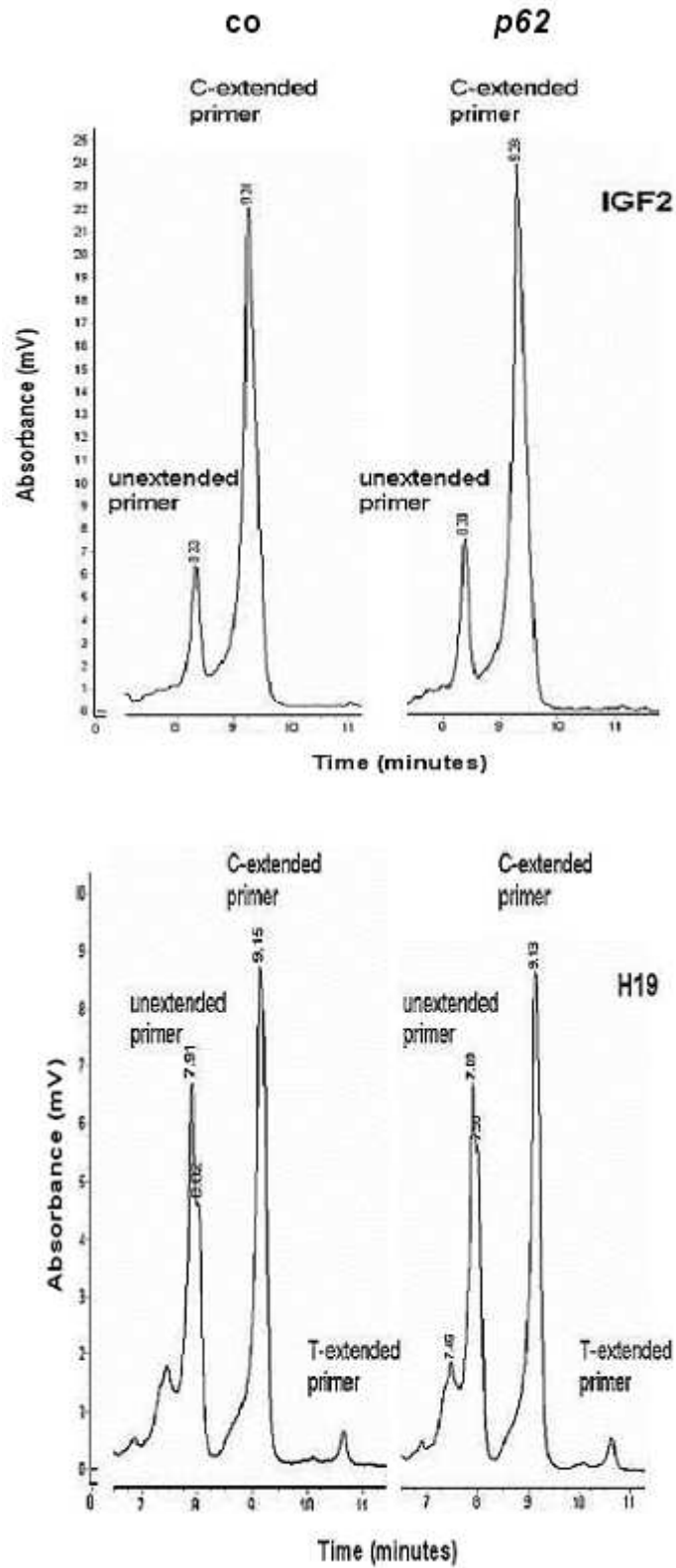


Figure 32: Allele-specific expression of IGF2 and H19.

Representative HPLC chromatograms showing amplification products for IGF2 (above) and H19 (below) in the SNuPE reaction in 2.5 week old transgenic heterozygous *p62*/SD7 mice (n=8, right) vs. controls (n=4, left).

3.10 Correlation between *p62* and IGF2 and H19 in human hepatoma cells

The relationship between *p62* and IGF2/H19 observed in *p62* transgenic mice was investigated also in human cells by knocking down *p62* by siRNA and determine IGF2 and H19 expression.

We decided to use different hepatoma cell lines due to variations in basal expression levels of *p62*. In contrast to Alexander cells, HepG2 and HUH7 express more *p62* protein (Figure 33).

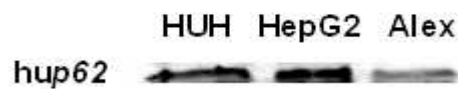


Figure 33: *p62* protein expression in three different human hepatoma cell lines. Protein expression was determined by Western Blot with 3.5 μ g whole protein lysate loaded onto an 8% SDS gel.

For each experiment, cells were treated with a random siRNA to exclude unspecific gene knockdown. Western Blot experiments underline the specificity of the *p62* siRNA. As Figure 34 points out, random siRNA did not lead to alterations in the protein expression of *p62*.

The effect of siRNA-mediated knockdown of *p62* was observed on the protein level after 48 h and 72 h (Figure 34), whereas no effect was observed 24 h after cell transfection (data not shown).

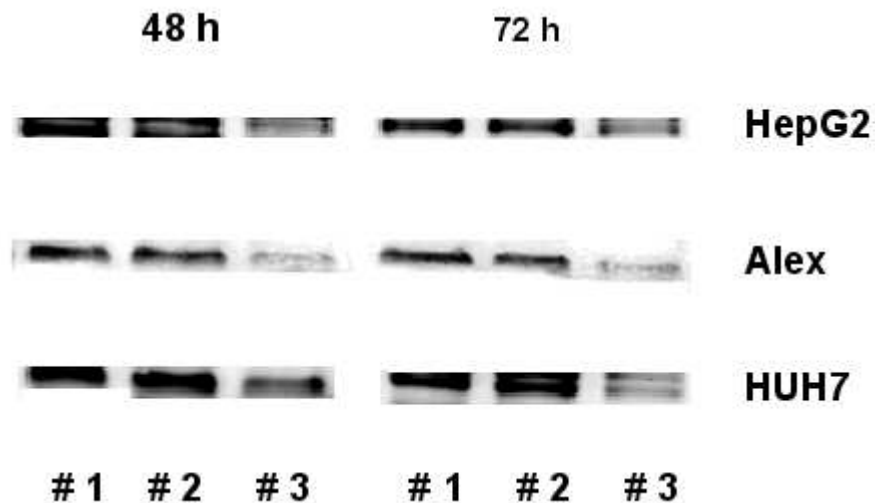


Figure 34: *p62* protein in human hepatoma cells after RNAi transfection.

The 62kDa band of *p62* was determined by Western Blot. The difference in protein expression is shown after 48 h and 72 h after siRNA-mediated gene knockdown of *p62* (lane #3) in comparison to Interferin™ (lane #2) and random siRNA (lane #1) treated cells. Equal concentrations of 5 μ g whole protein lysates were loaded per lane.

The observations made on the protein level could be confirmed for mRNA.

According to mRNA expression levels no significant difference for each examined cell line, time point and gene was measured for random siRNA and Interferin™ treatment (Figure 35), whereas a significant decrease of *p62* mRNA was detected, coexistent with a significantly reduced mRNA expression of IGF2 and H19 (Figure 35) after *p62*-siRNA-mediated gene-knockdown.

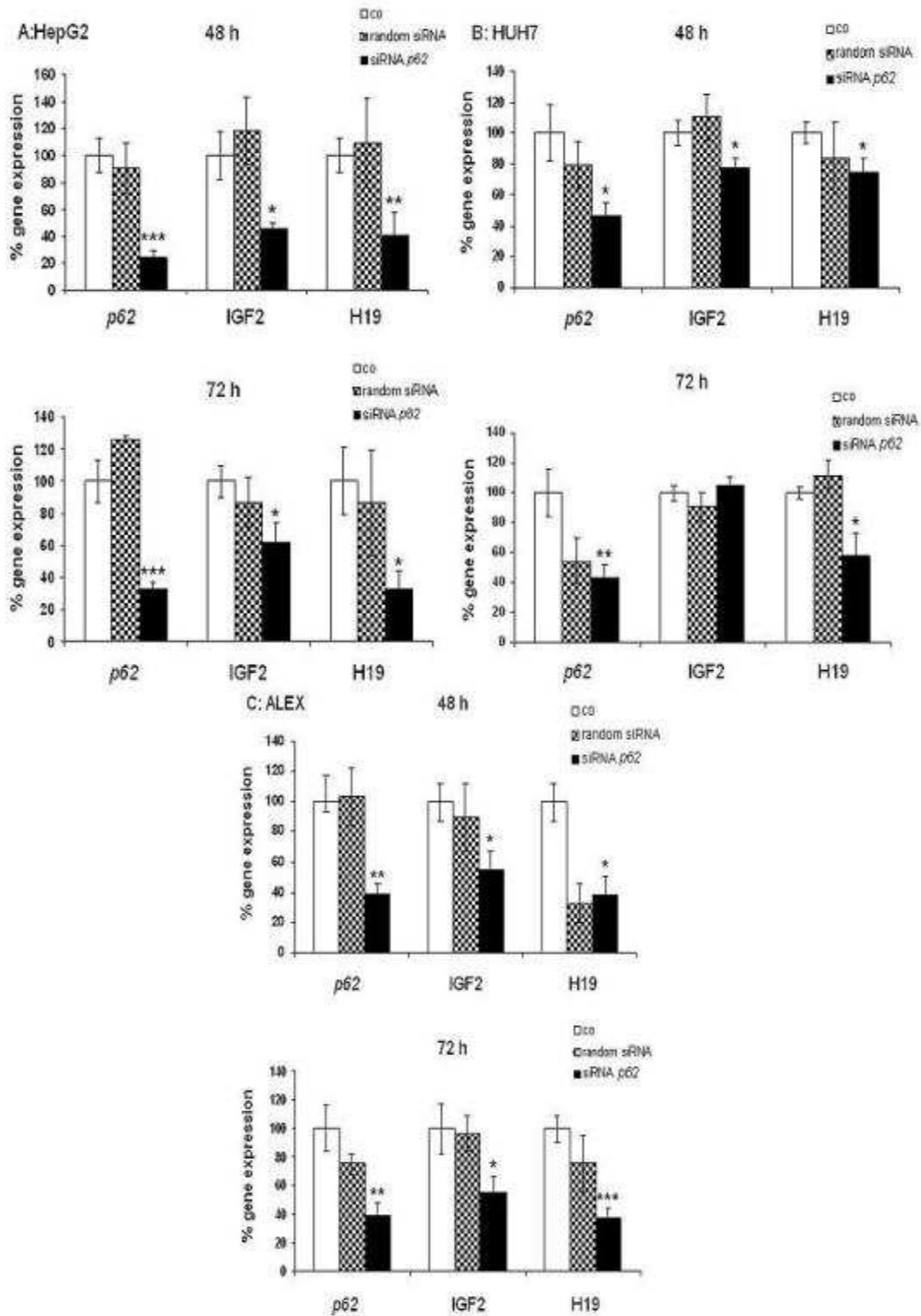


Figure 35: mRNA expression in (A) HepG2 (upper left), (B) HUH7 (upper right) and (C) Alexander cells (below) after siRNA-mediated knockdown of *p62*.

mRNA expression of *p62*, IGF2 and H19 48 h (upper) and 72 h (lower). Gene expression is shown in % relative to controls (Interferin/mock treatment), representing the mean \pm S.E.M. A value of $p < 0.05$ (*), of $p < 0.005$ (**) and of $p < 0.0005$ (***) was considered statistically different using student's t-test, whereas no statistical significance was detected for random siRNA-treated cells.

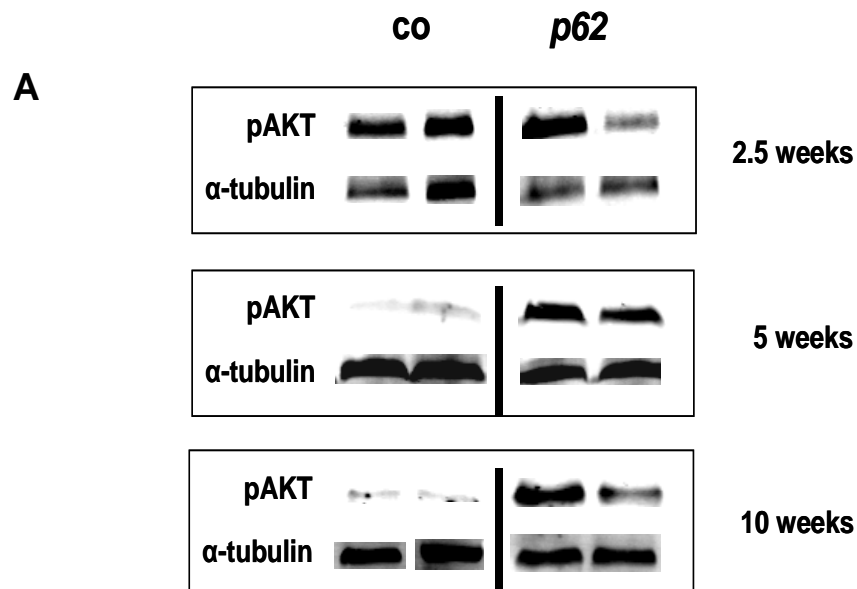
In summary, the RNA_i experiments confirmed the relation of IGF2, H19 and *p62* in human hepatoma cells.

Further experiments focussed on the question whether the influence of *p62* on IGF2 exerted functional consequences on protein kinase B/AKT and the inversely correlated PTEN pathway in *p62* transgenic mice.

3.11 Increased phosphorylation of the protein kinase AKT

IGF2 dependent downstream signalling is known to exert anti-apoptotic effects *via* AKT to counteract programmed cell death while at the same time supporting cell proliferation (Cory, Vaux et al. 1999).

AKT phosphorylation at Ser473 was examined in liver protein extracts from 2.5, 5 and 10 week old mice. Significantly enhanced AKT phosphorylation was observed in transgenic livers from 5 and 10 week old animals, whereas 2.5 week old animals showed no changes (Figures 36 A + B).



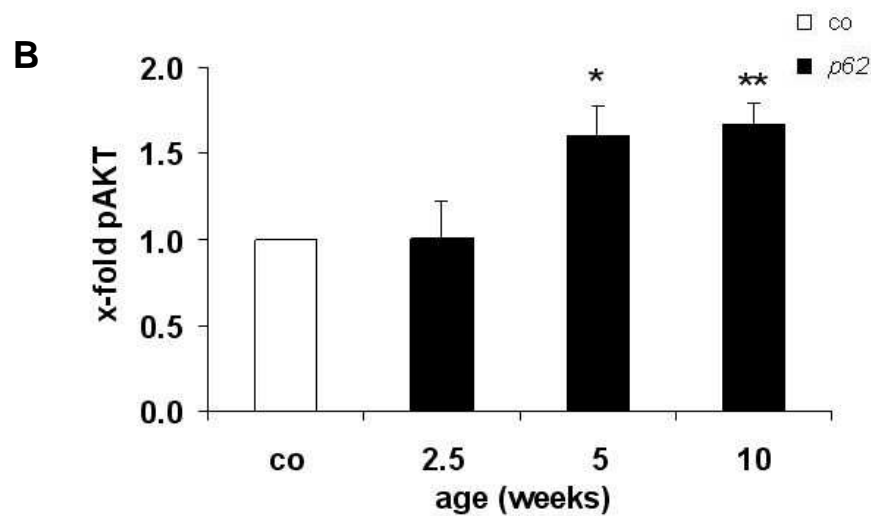


Figure 36: AKT activation.

A Western Blot experiments showing the phosphorylation of AKT in transgenic *p62* animals at the age of 2.5, 5 and 10 weeks normalized to α -tubulin.

B Quantification of (A) expressed as the mean x-fold values \pm S.E.M. Values of (*) $p < 0.05$ and (**) $p < 0.01$ were considered statistically different compared to values of control animals of the respective age using student's t-test. (2.5 weeks co: n=6, tr: n=7; 5 weeks co: n=4, tr: n=5; 10 weeks co: n=7, tr: n=6).

3.12 ActD/TNF- α -induced apoptosis protection

The observation of activated AKT in *p62* transgenic animals suggested a potential anti-apoptotic phenotype since pAKT can prevent cells from undergoing apoptosis. This is why the extent of apoptosis induction was assayed using hepatocytes derived from control as well as from *p62* transgenic mice.

Figure 37 A shows that hepatocytes from *p62* transgenic mice displayed significantly lower caspase-3-like activity upon apoptosis induction by Act D/TNF- α when compared to control hepatocytes.

In order to investigate whether programmed cell death was detected in *p62* transgenic livers *in vivo*, caspase activities in whole liver lysates were examined. However, *p62* transgenic animals showed no significant differences to controls

(Figure 37 B). These results suggested a prominent apoptosis protection of hepatocytes in the presence of the *p62* transgene.

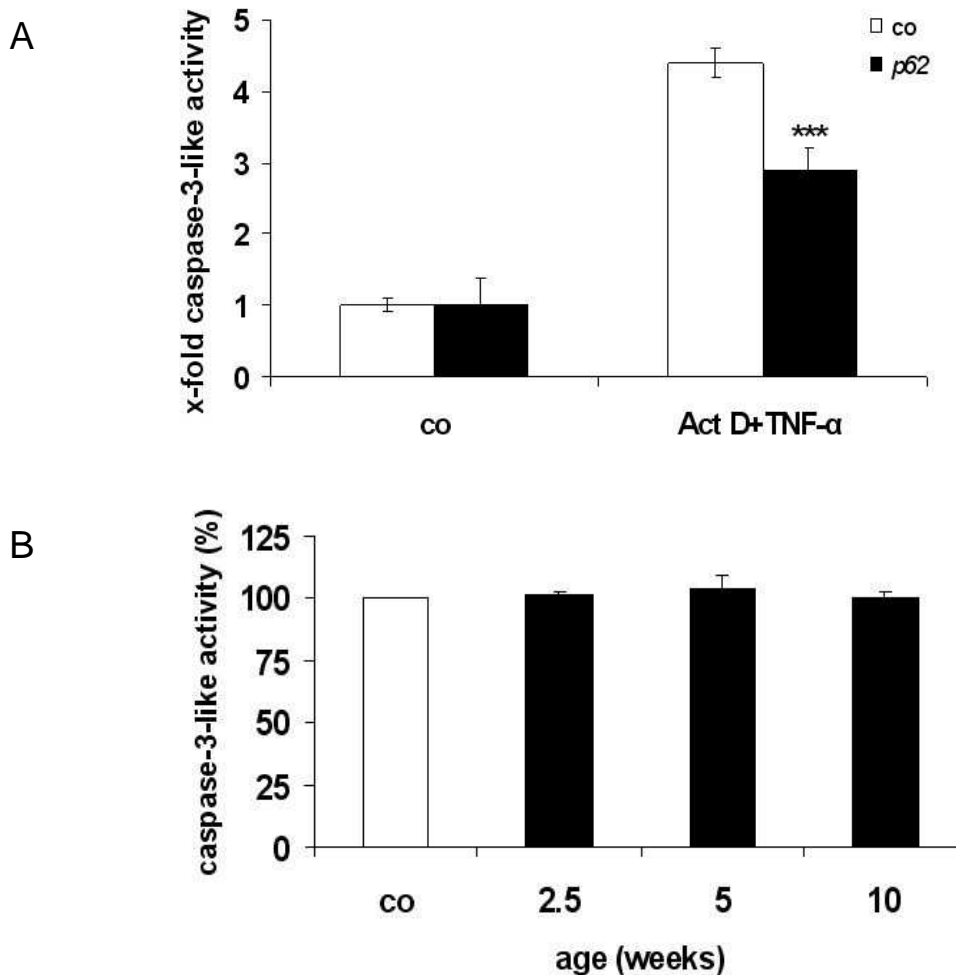


Figure 37:

A Caspase-3-like activity in isolated hepatocytes.

Hepatocytes were left untreated (co) or were treated with ActD for 15 min followed by TNF- α -incubation for 20 h (ActD + TNF- α). Data are expressed as x-fold enzyme activity with control cells set as 1 expressed as the mean \pm S.E.M. (performed in triplicate). White columns show control mice (n=3), black columns show *p62* transgenic mice (n=2). A value of $p < 0.001$ (***) was considered statistically different from treated ActD/TNF- α non-transgenic hepatocytes.

B Caspase-3-activity in liver tissue.

Caspase-3-like activity in livers of 2.5, 5 and 10 week old *p62* transgenic animals is expressed in comparison to controls of the respective age set equal to 100%. The white column shows control mice (n=3 per age), black columns show *p62* transgenic mice (n=3 per age), expressed as the mean \pm S.E.M. (performed in triplicate).

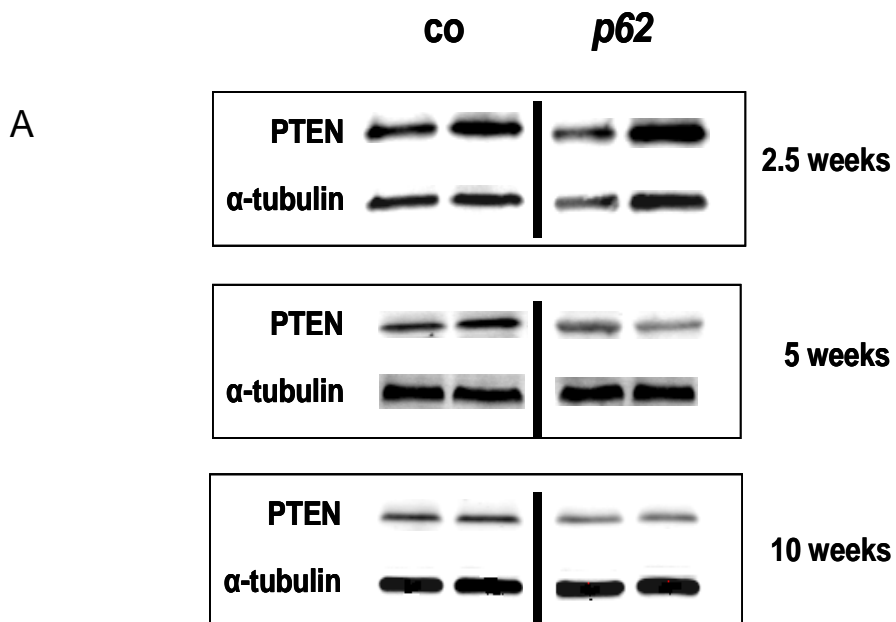
3.13 Decreased PTEN expression

3.13.1 PTEN in *p62* transgenic mice

IGF2 is known to influence PTEN expression, which inversely correlates with the phosphorylation of AKT. As the Western Blot experiments revealed an increase in pAKT, PTEN expression levels in *p62* transgenic mice were hypothesized to be altered, too. This was examined by Western Blot and real time PCR experiments.

In *p62* transgenic livers, a significant downregulation of the PTEN protein could be detected in liver extracts derived from 5 and from 10 week old transgenic mice. The tendency was the same for 2.5 week old mice, but could not be considered significant (Figures 38 A + B).

A significant reduction in PTEN mRNA expression levels could be shown for 2.5 as well as for 10 week old *p62* transgenic mice. The same tendency was measured for 5 week old mice, but could not be considered significant (Figure 38 C).



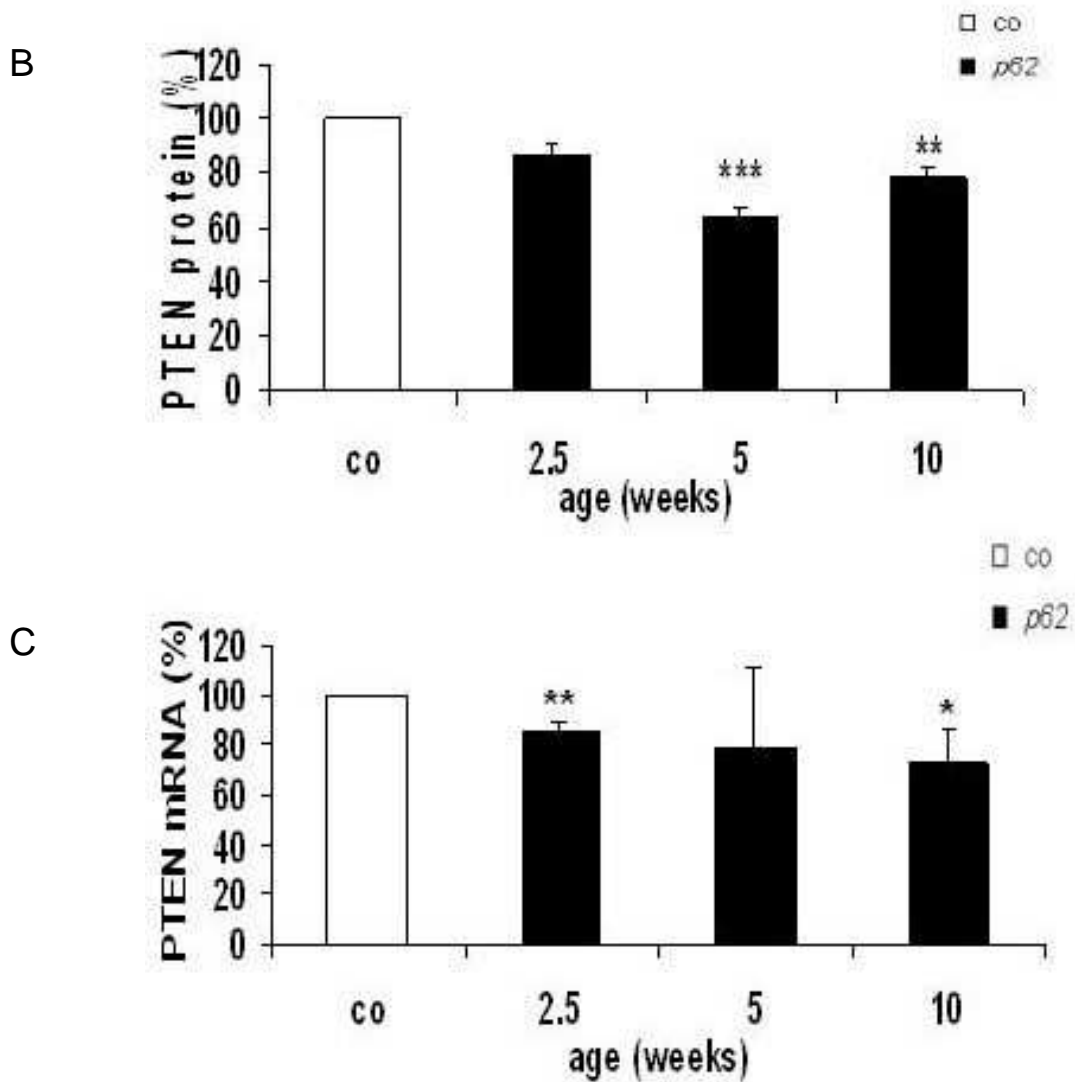


Figure 38: PTEN expression.

- A** PTEN protein in *p62* mice at the age of 2.5, 5 and 10 weeks normalized to α -tubulin.
- B** Quantification of (A) expressed as the mean x-fold values \pm S.E.M. Values of $p < 0.05$ (*) and of $p < 0.01$ (**) were considered statistically different from control animals of the respective age using student's t-test. (2.5 weeks co: n=6, tr: n=7; 5 weeks co: n=4, tr: n=5; 10 weeks co: n=7, tr: n=6)
- C** PTEN mRNA expression (%), representing the mean \pm S.E.M. compared to control animals. Values of $p < 0.05$ (*) and $p < 0.01$ (**) were considered statistically significant in comparison to control animals of the respective age using student's t-test. (2.5 weeks co: n=8, tr: n=13; 5 weeks co: n=4, tr: n=6; 10 week co: n=8, tr: n=12)

3.13.2 PTEN in HepG2 cells

p62 expression was knocked down by siRNA followed by determination of PTEN expression. In fact, 72 h after *p62* siRNA-transfection of HepG2 cells, we measured a significant downregulation of PTEN, suggesting a causal effect of *p62* on PTEN expression. This effect was not seen 48 h hours after *p62* siRNA-transfection (Figure 39).

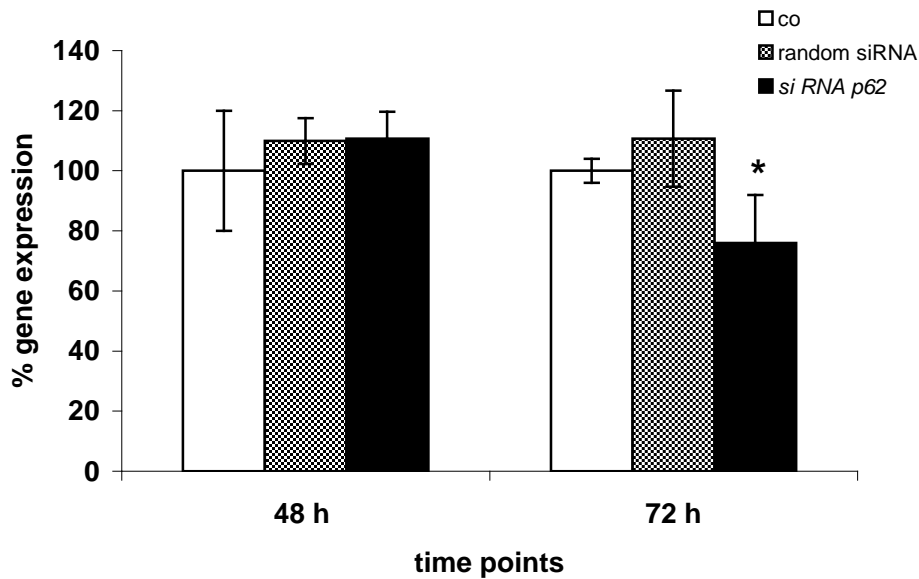


Figure 39: PTEN expression in HepG2 cells after *p62* knockdown.

mRNA expression of PTEN (%) in HepG2 cells 48 h and 72 h after *p62* siRNA-mediated knockdown. Data represents the mean \pm S.E.M. A value of $p < 0.05$ (*) was considered statistically different from controls (= cells treated with Interferin™ transfection reagent only) using student's t-test. No statistically significant changes were detected for random siRNA-treated cells.

3.14 Improved glucose tolerance

Since histological analyses suggested metabolic changes in *p62* transgenic animals at the age of 2.5 weeks, an intraperitoneal glucose tolerance test (IP-GTT) was performed at that age.

Fasting levels of glucose were similar in control and *p62* transgenic animals; also the end point values corresponded to the normoglycemic controls. The time course revealed a slight but not significantly improved glucose clearance of *p62* transgenic animals at 30 min after glucose administration (Figure 40).

Since the observation was made that female mice display higher IGF2 levels and develop fatty livers to a higher extent than their male littermates, potential gender-specific differences were assessed.

Whereas the glucose tolerance distribution curve in male *p62* transgenic mice did not reveal any significant differences in neither glucose uptake nor clearance (data not shown), in female *p62* transgenic mice, however, a significant reduction of glucose levels at 30 min (69.5 ± 10.8 %) and at 75 min (75.2 ± 15.1 %) (both: $p < 0.05$) in comparison to normoglycemic controls could be revealed.

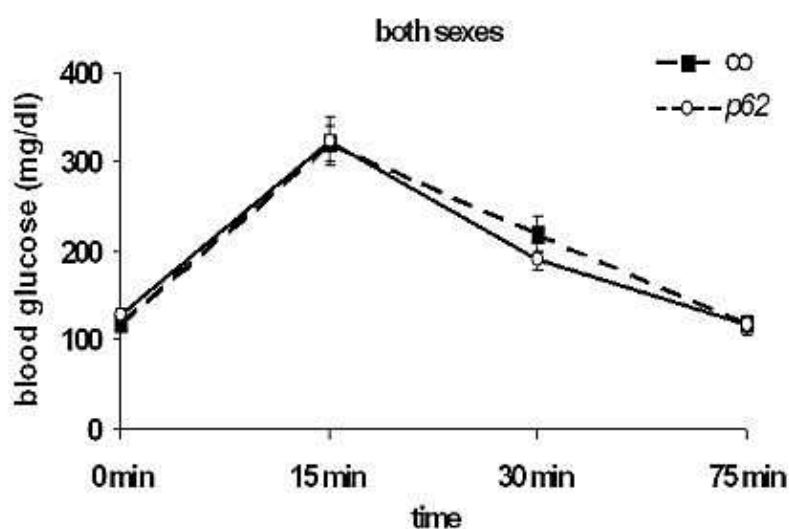


Figure 40: Glucose tolerance test.

Blood glucose values of 2.5 week old *p62* transgenic mice after i.p. injection of 10 μ l/g body weight glucose (20%). Blood glucose values are expressed as mg/dl, representing the mean \pm S.E.M. (control: $n=17$, transgenic: $n=11$).

The area under the concentration time curve (AUC) is useful for calculating the relative efficiency of the elimination of substances from the body (Current Protocols in Molecular Biology, unit 29 B.3.10 (Heikkinen 2007)).

The AUC for both genders revealed trends towards a slight but not significant reduction in glucose metabolism (Figure 41). However, in *p62* transgenic females the AUC was significantly lower compared to controls, meaning that blood glucose clearance is increased (Figure 41).

In summary, the results indicate enhanced glucose clearance, i. e. enhanced responsiveness to glucose in the presence of *p62* in females.

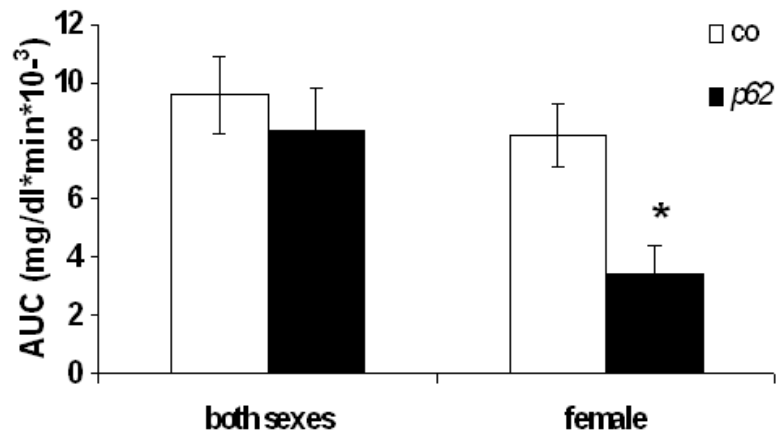


Figure 41: AUC of glucose levels.

Values represent means \pm S.E.M. integrated over 75 min. A value of $p < 0.05$ (*) was considered statistically different from gender-specific controls using student's t-test.

4. Discussion

4.1 The *p62* protein and HCC

HCC is the primary malignant liver cancer and has a very poor prognosis of survival after diagnosis. In order to improve therapy and to prevent carcinogenesis, it is important to gain knowledge of the complex pathways involved in tumor development. These very complex mechanisms result from multiple aberrations in cell proliferation, apoptosis, cell metabolism, chronic inflammatory processes and genetic alterations (Ito, Urabe et al. 1995; Piao, Kim et al. 1997; Thorgeirsson and Grisham 2002; Koike 2007). Multiple epidemiological risk factors are known from the literature, which contribute to HCC development, among which hepatitis B and C virus infection as well as metabolic diseases like obesity and diabetes mellitus are the most important ones (Wong, Limm et al. 2000; Davies, Mason et al. 2004; Ruhl and Everhart 2004; Younossi, McCullough et al. 2004).

4.1.1 *p62* transgenic mice

The *p62* protein was originally isolated from patients suffering from HCC, where it was exclusively expressed in cancer nodules (Zhang, Chan et al. 1999). This exclusive expression of *p62* in malignant tissue together with its appearance in fetal liver make it an oncofetal protein (Lu, Nakamura et al. 2001). Functional implications of the protein have as yet been completely unknown.

Transgenic mice provide a powerful tool to study specific genes enabling to see what consequences result from gene silencing or overexpression. This is why *p62* transgenic mice were generated to examine the consequences of *p62* overexpression in the liver. This thesis comprises the first phenotypic characterization of these animals.

Three different ages (2.5, 5 and 10 weeks of age) were analysed to examine a potential age-dependent expression rate of the *p62* transgene. Indeed, with the *p62* mouse lineage, which was used to perform all experiments described in this work, an

impact of the strength of the *p62* overexpression on the extent of the examined alterations could be confirmed.

As seen in *p62* transgenic animals, variegation of transgene expression, a heterocellular or mosaic expression pattern seen in all mice in a given transgenic line, is a frequently observed but unexplained phenomenon (Dobie, Mehtali et al. 1997) so far. Although the integration site of the *p62* transgene was not determined, it is known that the degree of heterocellular expression is determined at least in part of the site of integration. A respective position-effect variation (PEV) was seen in mice with X-chromosome translocation (Henikoff 1992).

Gene inactivation is associated with proximity to heterochromatic regions, which may spread along the chromosome and exert a repressive effect on the expression of flanking genes, and is also influenced by the cis-acting elements flanking the gene (Walters, Magis et al. 1996) and the presence of multiple copies of the transgene (Dorer and Henikoff 1997).

Tetracycline controlled transcriptional regulation describes a reversible process of inducible activation (*Tet-on*) or silencing (*Tet-off*) of genes through administration of tetracycline and its derivatives, e. g. doxycycline (Hillen and Berens 1994) in the drinking water. In *p62* transgenic mice, the *tTA* protein binds as a 'tet' operator to the HRP-CMV_{min} promoter, initializing mRNA expression of *p62* exclusively in the liver, which is realized upon the liver enriched activator protein (LAP).

To exclude that the induction of the *p62* transgene occurred due to genetic predisposition, doxycycline was administered to *p62* transgenic mice, which abrogated the expression of the transgene. As a consequence of the knockdown of *p62* expression, IGF2 and H19 mRNA levels in fact decreased. These findings confirm the causal relation between *p62* overexpression and IGF2 and H19 induction.

In general, correlation graphics showed that the increase in *p62* expression resulted in higher IGF2 and/ or H19 levels. Moreover, correlation between the expression levels of IGF2 and H19 displayed that the increase of one gene is accompanied by

the increase of the other gene. Worth mentioning was that females expressed higher levels of the *p62* transgene than their male littermates. Since also the metabolic growth factor IGF2 was expressed highest in females, a causal interaction can be suggested from this observation.

Since immunostaining of *p62* and IGF2 performed on serial sections of *p62* transgenic liver tissues confirmed the co-localization of both proteins in the cytoplasm of hepatocytes, a correlation on the protein level could be suggested.

The experiments described in this work focus on the phenotypic characterization of liver-specific *p62* overexpression in *p62* transgenic mice.

4.2 Phenotypic alterations

4.2.1 Appearance of basophilic cell foci

HE is a routine staining, giving a general overview of the cell morphology. Foci of cellular alterations can be classified as eosinophilic, basophilic, vacuolated, clear cell or mixed. Foci might progress to preneoplastic lesions and to carcinomas (Frith, Boothe et al. 1980; Ward and Lynch 1984).

A first hint on a pathophysiological impact of *p62* was given by the HE-stained sections as eosinophilic and basophilic foci appeared in the livers of *p62* transgenic mice, whereas in controls eosinophilic cells predominated. Basophilic cell foci are considered to be one criterion required to diagnose cell malignancy, as this phenotype suggests a progressive cellular dedifferentiation (Su, Benner et al. 1997). The occurrence of basophilic cell foci in *p62* transgenic mice might give a first hint on the implication of *p62* in tumorigenesis.

Concomitant with the HE staining results was the observation of Horie et al. in mice with a hepatocyte-specific PTEN null mutation (Horie, Suzuki et al. 2004): *p62* transgenic mice also demonstrated a central location of cell nuclei and a weakly eosinophilic staining of the cytoplasm of hepatocytes.

Liver architecture gave hints on an accumulation of neutral lipids as presumed from the occurrence of empty vacuoles in paraffin-embedded liver tissue of *p62* transgenic mice. The evidence of a fatty liver phenotype was indicated by pale liver colour in other mouse models of NAFLD (Takahashi, Qi et al. 2004; Matsuzawa, Takamura et al. 2007), an observation also made in *p62* transgenic animals.

4.2.2 Fatty liver phenotype

Changes in liver structure due to lipid accumulation have deleterious effects as they increase the risk of the development of diseases (Bugianesi, Leone et al. 2002). Metabolic disorders, such as obesity, lead to non-alcoholic fatty liver disease (NAFLD) resulting from enhanced accumulation of fat droplets in the liver (Polesel, Zucchetto et al. 2009). After a “second hit”, steatohepatitis is induced by inflammatory processes, then called NASH, which is followed by liver cirrhosis, possibly ending in HCC (Wasmuth 2007). Since a first hint on a pathophysiological impact of *p62* was given by the HE-stained tissue sections, the presumed role of *p62* on the accumulation of fat droplets in hepatocytes was examined.

Specific fat staining impressively revealed the phenotype of a fatty liver in a high proportion of 2.5 week old *p62* transgenic animals, with females displaying more frequent accumulation of fat droplets than males. Accumulation of fat droplets within hepatocytes of *p62* transgenic mice was finely dispersed; i. e. hepatocytes were not ballooned by the insertion of fat into the cytoplasm as found mostly in other genetic mouse models and in most cases of NAFLD (Burt, Mutton et al. 1998; Valls, Iannaccone et al. 2006).

Two distinct patterns of fat droplets can be distinguished: macro- and microvesicular. The large droplet type (macrovesicular) is hallmarked by a single fat droplet, which displaces the nucleus (Burt, Mutton et al. 1998), whereas the small droplet type (microvesicular) shows a finely dispersed accumulation of fat droplets with no displacement of the nucleus. The microvesicular type is associated with hepatic dysfunction (Sherlock 1983), e. g. defects in β -oxidation and might therefore represent a ‘first hit’ in subsequent malignant liver transformation.

Although during liver preparation single fatty livers were also noticed in older mice, this phenotype could only be proven as being significant in the youngest examined group of transgenic mice (2.5 weeks of age). This is on the one hand quite remarkable due to its early appearance during life. On the other hand, the fatty liver phenotype could be explained by the fact that 2.5 week old *p62* transgenic animals express the highest IGF2 levels in comparison to their older siblings. Such an increase in IGF2 protein was also observed in fatty liver disease (FLD) in steatotic livers in humans (Chiappini, Barrier et al. 2006).

The phenotype of a fatty liver clearly demonstrates the impact of *p62* on changes in lipid metabolism. This can represent a 'first hit' in the initiation of a progressive liver disease, thereby contributing to HCC development.

4.2.3 Disturbance in glycogen storage

Glycogen is a polysaccharide consisting of several glucose molecules serving as a glucose reservoir within the body. Glycogen synthesis is located in the liver and changes in glycogen levels indicate metabolic disorders. From glycogen storage disease (GSD) it is known that a deficiency in the enzyme glucose-6-phosphatase impairs the ability of the liver to produce free glucose from glycogen and gluconeogenesis, resulting in hypoglycemia and hyperlipidemia, accompanied by an accumulation of glycogen and fat droplets in the liver (Burchell 1998).

In rats with chemically induced liver cirrhosis a decrease in hepatic glycogen content was observed (Krähenbühl, Talos et al. 1996) and also in humans with alcohol-induced liver cirrhosis reduced hepatic glycogen stores have been described (Owen, Reichle et al. 1981). Krähenbühl et al. could show that this is due to an impaired hepatocellular glycogen metabolism (Krähenbühl, Lang et al. 2003).

The observed decrease of glycogen detected in 2.5 week old *p62* transgenic livers might therefore represent an early stage of liver dysfunction. In this context, it is interesting to note that an inhomogenic distribution of glycogen was detected. Glycogen accumulation occurred around the central veins, whereas Rappaport zone 2 contained less glycogen. Similarly, rats display glycogen appearance in Rappaport

zone 1 after a fat-rich diet due to a disappearance of glycogen-synthesizing enzymes in Rappaport zone 2 (Chen and Katz 1988). This finding might suggest a link between glycogen and lipid changes evoked by *p62* overexpression.

The noticed decrease in glycogen storage is contradictory to the increased glycogen storage observed in mice with a liver-specific PTEN deletion (Stiles, Wang et al. 2004). Interestingly, however, despite the fact that in *p62* transgenic animals the PTEN gene was reduced at the age of 2.5 weeks, no change in AKT phosphorylation was detected. Since glycogen is synthesized in a pAKT-dependent fashion an increase of glycogen is not to be expected.

A reexpression of IGF2 is associated with GSK-3 hyperphosphorylation in an *in vivo* mouse model of hepatocarcinogenesis (Desbois-Mouthon, Wendum et al. 2006), followed by inhibition of glycogen synthase. Thus, preneoplastic liver lesions involve focal lack of glycogen storage (Bannasch, Klimek et al. 1997). Such a decrease in glycogen concomitant with an induction of IGF2 was also noticed in *p62* transgenic animals, leading to the proposal that *p62*-mediated IGF2 overexpression results in changes in energy metabolism, which support the progression of malignant liver diseases.

Moreover, the reduction of endogenous hepatic glycogen induced by *p62* overexpression could be a consequence of the accumulation of fat droplets within hepatocytes, which would disturb glycogen synthesis, as known from GSD (Bandsma, Smit et al. 2002).

4.2.4 Metabolic alterations

The interplay between glucose and lipid metabolism is triggered by the substrate uptake and distribution between peripheral tissues and the liver, as it was shown in several mouse models (Bruning, Michael et al. 1998; Abel, Smuts et al. 2001).

4.2.4.1 Increased liver to body weight ratio

Association of the incidence and mortality of liver cancers with obesity was revealed in several studies, which showed a relationship between the high incidence of HCC in obese patients (Nair, Mason et al. 2002). Obesity is associated with decreased IGF2, which is a mitogen that stimulated cell growth (Gaunt, Cooper et al. 2001).

The liver weight to body weight ratio displayed a significant increase in 2.5 week old *p62* transgenic animals. This result corresponds to observations made in fatty livers developing in animals after feeding a high-fat diet (Otogawa, Kinoshita et al. 2007) or upon genetic manipulations (Wagener, Schmitt et al. 2006). Positive effects for IGF2 on body and organ weights are reported (Zaina, Pettersson et al. 2003).

4.2.4.2 Alteration of serum levels

Regarding alterations in serum parameters, an increase in serum triglycerides (TG) in male *p62* transgenic animals was detected, which was also found in mice with a liver-specific nuclear respiratory factor 1 (NRF-1) deletion, although gender-specific differences were not considered in this study (Xu, Chen et al. 2005). In contrast, female serum TG levels were lower as it was also shown in a work by Anezaki et al. working on PTEN k. o. mice (Anezaki, Ohshima et al. 2009). These results suggest that in *p62* transgenic males, the redistribution of fat from other tissues to the liver and/ or an enhanced fat synthesis, or decreased lipolysis, might be changed upon *p62* overexpression.

The accumulation of TGs in *p62* transgenic males could also be secondary to the reduction in glycogen storage. An increase in glycolysis leads to an enforced production of acetyl-CoA, which in turn stimulates lipogenesis, while at the same time inhibiting fatty acid oxidation in the liver. Fatty acids released after lipolysis are transported to the liver where they are used for triglyceride synthesis. This finally ends in steatosis due to the discrepancy between fatty acid uptake and synthesis on the one hand and fatty acid oxidation and release on the other hand (Bandsma, Smit et al. 2002). Furthermore, an impact on the rate of the synthesis of fatty acids and their secretion could probably be amplified through the *p62*-caused downregulation of

PTEN in *p62* transgenic mice, as it was shown by Stiles after liver-specific PTEN deletion in mice (Stiles, Wang et al. 2004).

4.2.5 Non-inflammatory phenotype

The observations on changes in lipid and glucose metabolism arose the question whether *p62* might not solely contribute to the 'first hit', i. e. fat accumulation, but also to the 'second hit', i. e. inflammation, thereby supporting the progression of a steatohepatitis. In addition to the investigation of metabolic alterations in *p62* transgenic animals, experiments were performed to elucidate whether the fatty liver phenotype is accompanied by NASH, i. e. the simultaneous occurrence of inflammation besides fat accumulation.

4.2.5.1 Absence of inflammatory parameters

Acute inflammation is a necessary response to tissue injury, directed towards the restoration of normal tissue structure and/ or function. The dysregulation of inflammatory processes is involved in the pathogenesis of diseases.

Elevated transaminase levels are parameters, which indicate inflammatory processes in the body. Both genders revealed a lack of transaminase increases, also observed in a genetic mouse model of NAFLD (Xu, Chen et al. 2005) suggesting a non-inflammatory phenotype. Noteworthy in this context is the observation made by Hashimoto et al., which could reveal low levels of AST and ALT as independent predictors of HCC development in humans (Hashimoto, Yatsuji et al. 2009). To transcribe this result onto *p62* transgenic mice would lead to the conclusion that the decrease in serum transaminase levels in the presence of the *p62* transgene might contribute to the onset of HCC.

On the other hand, Horie et al. demonstrated increased transaminase levels in hepatocyte-specific PTEN-deficient mice (Horie, Suzuki et al. 2004). This result is in contrast to the observation made in *p62* transgenic mice. On the other hand, neither an increased in serum transaminase levels nor an accumulation of leukocytes could be revealed in 2.5 week old *p62* transgenic livers.

4.2.5.2 Absence of NF- κ B translocation

NF- κ B is a pivotal transcription factor involved in inflammatory processes. Upon activation, it translocates into the nucleus where it supports transcription of pro-inflammatory proteins (Sen and Baltimore 1986). One step in the manifestation of a steatohepatitis is the support of inflammation besides fat accumulation. After translocation into the nucleus, NF- κ B plays an important role in the initiation of a cascade leading to liver injury. It mediates the inductions of adhesion molecules and chemokines and thereby the recruitment of neutrophilic cells into the liver. Sequestered neutrophils release proteases and reactive oxygen species, which directly damage hepatocytes and endothelial cells causing hepatic hypoperfusion (Jaeschke 1996; Vollmar, Schmidt et al. 1996).

Several studies revealed the significance of the NF- κ B p65 subunit in hepatocytes, which directly acts to promote cell survival (Verma, Stevenson et al. 1995; Bellas, FitzGerald et al. 1997). Schoemaker et al. showed that NF- κ B regulates members of the inhibitor of apoptosis protein family (IAP) in hepatocytes, leading to an inhibition of caspase activity, thereby preventing apoptosis (Schoemaker, Ros et al. 2002). Moreover, studies revealed the implication of NF- κ B activation in the progression of NASH (Luedde, Beraza et al. 2006; Luedde, Beraza et al. 2007).

Interestingly, a high proportion of p62 transgenic hepatocytes showed a distinct increase in cytoplasmic NF- κ B p65.

Constitutive overexpression of the p65 protein has previously been shown in thyroid carcinoma cells (Visconti, Cerutti et al. 1997) and an increased cytoplasmic staining of the NF- κ B subunit p65 has also been demonstrated in malignant epithelial cells from colorectal tissue compared to normal epithelium (Charalambous, Lightfoot et al. 2009). Moreover, it has been demonstrated that the oncogene MDM2 induces protein expression of the NF- κ B p65 subunit in acute lymphoblastic leukemia (Gu, Findley et al. 2002). From carcinoma cells it has been reported that NF- κ B and I κ K are linked in an autoregulatory loop, i. e. the p65 subunit itself stimulates I κ K expression, which in turn results in self-inactivation (Scott, Fujita et al. 1993; Sun, Ganchi et al. 1994).

This observation could explain an enhanced cytoplasmic staining in the absence of a translocation into the nucleus in *p62* transgenic hepatocytes.

Although functional implications of increased levels of the regulatory NF- κ B p65 subunit in cancerogenesis are as yet largely unknown, they might enhance an inflammatory response upon respective stimuli. Whereas fat accumulation as coalesced lipid droplets in hepatocytes of *p62* transgenic animals forms the borderline from a benign to a morbid condition (Neuschwander-Tetri 2005), the results from the investigations within this thesis confirm a non-inflammatory phenotype, i. e. the 'second hit' towards the progression of NASH, resulting from inflammation, is missing.

4.3 Increased IGF2 and H19 expression

The interaction of *p62* with tumor-related factors was suggested due to the upregulation of IGF2 and H19 expression (Leighton, Saam et al. 1995) The use of doxycycline excluded that the overexpression of the three genes occurred due to genetic predisposition. Within one age group the extent of *p62* correlated with the expression of IGF2 and H19.

In order to address the question which steps in gene expression of IGF2 and H19 are modulated by *p62*, a set of experiments was performed, elucidating the possible impact on mRNA stability and on chromosomal changes.

4.3.1 Absence of transcriptional stability changes

Regulation of gene expression is used to turn the information of genes into gene products, either protein or RNA. The regulatory steps are versatile, reaching from chromatin domains, transcription, post-transcriptional modification, RNA transport, translation, mRNA degradation up to post-translational modification. Any step in gene expression can be modulated (Alberts 1992). The regulation of mRNA decay is a major control point in gene expression. Regulated mRNA stability is achieved either through *cis*-acting elements within mRNA (poly (A) tail, 3'- and 5'-untranslated regions, mRNA coding region) or by *trans*-acting regulatory factors (Ross 1995). One

way that dictates mRNA stability is mediated by mRNA binding proteins. Since *p62* was shown to belong to the family of IGF2 mRNA-binding proteins (IMPs) (Lu, Nakamura et al. 2001) and IMPs have been regarded to bind to H19 (Runge, Nielsen et al. 2000), IMPs are potential candidates to influence mRNA stability.

Since the causal relationship of the upregulation of IGF2 and H19 in *p62* transgenic mice still remained ambiguous, experiments to elucidate a regulation on the transcript level were performed on isolated hepatocytes. However, the results revealed no influence of *p62* on mRNA stability of IGF2 and H19.

Since both mRNAs turned out to be a rather stable mRNA ($t_{1/2} > 10$ h) the regulation *via* stabilizing mechanisms would be rather unexpected since stability-regulatory genes mostly regulate short-lived mRNAs (Eberhardt, Doller et al. 2007)

Further transcriptional mechanisms of *p62*-evoked IGF2 upregulation are conceivable, as IGF2 is subjected to differential polyadenylation, alternative splicing, site-specific endonucleolytic cleavage, and postsecretory attenuation of IGF2 function by IMPs (Sussenbach, Steenbergh et al. 1992; Stewart and Rotwein 1996).

The similar spatiotemporal expressions of the IGF2 and H19 mRNAs as well as their complex counter-regulatory actions (Brannan, Dees et al. 1990) are characteristics that show the functional coupling of both genes. The putative role of the IMP-family member *p62* in the upregulation of IGF2 and H19 mRNA levels could therefore result from IGF2-mediated induction of H19 mRNA, implicating a *trans* effect of H19 caused by *p62* overexpression, as it was shown by Li et al. (Li, Franklin et al. 1998).

Moreover, the maintenance of elevated IGF2 mRNA levels could be explained by the fact that H19 mRNA can bind four molecules of IMP1, which in turn binds to the 5' UTR of IGF2 mRNA, thereby promoting post-transcriptional or translational IGF2 expression (Runge, Nielsen et al. 2000).

Mice with a targeted deletion of IMP1 display growth retardation accompanied by IGF2 downregulation (Hansen, Hammer et al. 2004). This suggests a general IGF2-elevating action of IMPs. In fact, the expression patterns of IMPs and IGF2 overlap in

many tissues suggesting a controlling function on the production of IGF2 mRNA (Hansen, Hammer et al. 2004)

4.3.2 Monoallelic expression of IGF2 and H19

Both transcriptional as well as chromosomal changes could account for the upregulation. As no effects on mRNA turnover of IGF2 and H19 were detected in *p62* transgenic animals, implications on possible genetic alterations of the chromosomal expression of IGF2 and H19 evoked by *p62* were examined.

The oppositely imprinted genes IGF2 and H19 often show coordinate, reciprocal regulation (Ohlsson, Hedborg et al. 1994; Liu, Kahri et al. 1995). Imprinted expression is reciprocally controlled by a common CpG island located upstream of H19, which shows parent-specific methylation. Methylation alterations at this site are correlated with abnormal IGF2 and H19 expression and are linked to many tumors (Cui, Niemitz et al. 2001; Takai, Gonzales et al. 2001).

Li et al. found parallel expression of IGF2 and H19 in HCC (Li, Nong et al. 1997). The overexpression of IGF2 was not only demonstrated in about 20% of human HCC (Cariani, Lasserre et al. 1988) but has also been detected in HCCs in transgenic mice (Schirmacher, Held et al. 1992).

IGF2 is a growth factor, which is known to promote tumorigenesis after switching from mono- to biallelic expression (Kim and Lee 1997). But also loss of imprinting (LOI) of IGF2 was described in tumors (Kondo, Suzuki et al. 1995; Kim, Choi et al. 1998). LOI of IGF2 in HCC is uncoupled from the downregulation of H19 expression but rather associated with coexpression for H19 and IGF2 (Ariel, Ayesch et al. 1997). Another common feature of human HCC which explains the frequent loss of biallelic IGF2 expression is explained by the disruption of the IGF2 promotor region, particularly the loss of the P1 activity (Li, Nong et al. 1997).

The role of the untranslated RNA H19 in tumorigenesis is described controversially. By now, several studies indicate a tumor suppressor activity but also the necessity of H19 in tumor growth has been shown (Matouk, DeGroot et al. 2007; Yoshimizu,

Miroglio et al. 2008). Its implication for HCC development has been underlined in a mouse model of HCC, where diethylnitrosamine, a known carcinogen of the liver, induced H19 mRNA expression (Graveel, Jatkoa et al. 2001). Moreover, H19 transcription was initiated after binding of c-myc near the imprinting control region (ICR) (Barsyte-Lovejoy, Lau et al. 2006). Consistent with the theory of H19 being a tumor suppressor gene (Yoshimizu, Miroglio et al. 2008) is the fact that tumorigenicity was ablated *in vivo* in nude mice after transfection with an H19 expression construct (Hao, Crenshaw et al. 1993).

For both examined ages, neither a change in allele-specific nor biallelic expression was detected for IGF2 and H19. This result is in concordance with the observation made by Feinberg et al. (Feinberg and Vogelstein 1983), leading to the conclusion that *p62* does not contribute to the upregulation of the both genes through genetic alterations.

One possible mechanism of *p62* might be to change the DNA methylation pattern, since it is known from the literature that parent-specific methylation patterns have been detected in endogenous imprinted genes (Sasaki, Jones et al. 1992; Ferguson-Smith, Sasaki et al. 1993; Reik and Allen 1994). The methylation of the paternal allele of IGF2 in the 3' region correlates directly with expression and might therefore be a target for *p62* (Feil, Walter et al. 1994). *p62* could contribute to high IGF2 expression levels by maintaining the methylation level high.

The observed result from this experiment that LOI of the IGF2 locus is not involved in increased IGF2 gene expression in *p62* transgenic animals has also been described in HCC (Kaneda and Feinberg 2005).

An accelerated liver tumor development was demonstrated in the absence of H19 (Yoshimizu, Miroglio et al. 2008). Upregulated H19 expression could therefore account for the prevention of liver tumor development in *p62* transgenic mice by antagonizing the tumorigenic potential of IGF2 and IGF2-induced metabolic alterations. In fact, H19 expression might also contribute to IGF2 downregulation at higher age (Leighton, Saam et al. 1995).

4.3.3 Silencing of *p62*

siRNA-mediated knockdown is a RNA-dependent gene-silencing process that is controlled by the RISC complex, initiated by short double-stranded RNA molecules (Hannon 2002).

Gene silencing by siRNA-mediated gene knockdown of *p62* in human hepatoma cells, followed by the examination of IGF2 and H19 mRNA expression, was performed in order to address the relationship between the simultaneously occurring overexpression of the three genes in a human system. Indeed, a detected reduction in *p62*, IGF2 and H19 mRNA expression levels demonstrated the direct correlation.

This experiment proved significance of the *in vivo* findings in mice also on the human level.

A conceivable therapeutic treatment with siRNA could be gene-silencing of *p62* to attenuate metabolic effects resulting from IGF2 expression.

4.4 IGF2 downstream effects

Although the detailed mechanisms how *p62* increases IGF2 expression remain to be clarified, its downstream actions lead to severe pathophysiological consequences. They are most likely exerted by IGF2. Increased IGF2 expression in the absence of macroscopic signs of inflammation has been demonstrated in human steatosis (Chiappini, Barrier et al. 2006). These findings suggest IGF2 as a pathophysiological factor in fatty liver disease. Therefore, a second set of experiments performed within this work concentrated on downstream effects exerted by IGF2.

4.4.1 Decreased PTEN expression

Since IGF2 is known to mediate cell survival signals through the PI3-kinase pathway, experiments focused on the expression of two proteins within this cascade, i. e. PTEN and pAKT (Kandel and Hay 1999). Upon activation of PI3-kinase after initial binding of IGF2 to its receptor, PIP3 is generated. This molecule leads to the

activation of AKT through phosphorylation (Franke, Hornik et al. 2003). In contrast, PTEN is able to dephosphorylate PIP3 and thereby participates in the reciprocal regulation of AKT activity (Franke, Hornik et al. 2003).

Experiments revealed attenuated PTEN expression in the presence of the *p62* transgene. This result could give a first hint on a potential participation of *p62* in the development of HCC, as PTEN is a tumor suppressor gene and deletion of the PTEN gene as well as reduced PTEN expression was shown to be implicated in diverse tumors (Di Cristofano and Pandolfi 2000).

Unsaturated fatty acids are known to downregulate PTEN expression (Terrettaz and Jeanrenaud 1983). It might therefore be possible that the reduction of PTEN expression in *p62* transgenic animals at the age of 2.5 weeks results from the increase of free fatty acids, which accumulated in hepatocytes, as it was shown in liver-specific PTEN deficient mice, which displayed NASH (Stiles, Wang et al. 2004). On the other hand, the lipid phosphatase activity of PTEN controls the intracellular triglyceride content as shown in HepG2 when PTEN depletion resulted in enhanced accumulation of triglycerides (Vinciguerra and Foti 2008). Vice versa, unsaturated fatty acids are thought to contribute to the development of liver injury through their induction of a PTEN downregulation (Vinciguerra, Sgroi et al. 2009). An impact on the rate of the synthesis of fatty acids and their secretion by *p62*-induced IGF2 might be amplified through the *p62*-caused downregulation of PTEN as shown in the past through a liver-specific PTEN deletion in mice (Stiles, Wang et al. 2004).

Since fatty acids play a role in PTEN downregulation (Vinciguerra, Carrozzino et al. 2009), one might suggest that a reduction in PTEN expression is secondary to fatty liver induction. This is further supported by the observation of liver regeneration from pathophysiological to physiological conditions with increased age concomitant with a decline in IGF2 mRNA expression. The shared regulation of IGF2 and PTEN has also been shown in several cancer cells (Perks, Vernon et al. 2007).

Moreover, results are supported by the observations made in the study of Moorehead et al. where a negative feedback loop of IGF2 on PTEN was observed, i. e. IGF2 induction itself inhibits PTEN expression (Moorehead, Hojilla et al. 2003).

To underline the relationship of *p62* overexpression and PTEN downregulation found in *p62* transgenic mice, PTEN transcript levels were determined in human hepatoma cell lines after siRNA-mediated knockdown of *p62*. The increase in PTEN mRNA levels correlated with the decrease in mRNA levels determined for *p62*, thereby underlining the theory that *p62* promotes tumorigenesis by inhibiting PTEN activity. The contradictory result 72 h after *p62* knockdown, i. e. the detection of elevated PTEN transcript levels, could be explained by a partial degradation of siRNA molecules, thereby allowing the recovery of *p62* mRNA levels.

4.4.2 Increased phosphorylation of AKT/protein kinase B

Growth promoting as well as metabolic effects of IGF2 are mediated upon binding to the IGF-1R. This follows the activation of downstream signal transduction pathways, mainly the activation of PI3-kinase. The signaling cascade following AKT activation is rather complex, not only apoptosis is inhibited but also metabolic and proliferative effects are exhibited (Cardone, Roy et al. 1998; Crowder and Freeman 1998; Diehl, Cheng et al. 1998; Gille and Downward 1999). Increased IGF2 expression thereby leads to constitutive AKT activation (Andjelkovic, Alessi et al. 1997; O'Connor 1998; O'Dell and Day 1998).

The significant increase in AKT phosphorylation in *p62* transgenic animals might therefore be explained by *p62*-mediated IGF2 induction. On the other hand, it has to be kept in mind that AKT phosphorylation culminated with increased age, while at the same time impaired IGF2 expression was detected.

PTEN and pAKT are reciprocally regulated through the ability of PTEN to dephosphorylate the AKT activator PIP-3 (Parsons and Simpson 2003). Therefore, PTEN downregulation could support the IGF2-caused induction of AKT phosphorylation observed in *p62* transgenic animals, thereby contributing to a progressive AKT activation.

AKT has also been suggested to promote tumorigenesis as it appears to be hyperactivated in the majority of human cancers (Hay 2005; Hennessy, Smith et al.

2005). *p62* overexpression might therefore contribute to tumor development as it leads to a constitutive activation of AKT.

Upon AKT phosphorylation, GSK-3 is inhibited, ending in an enhanced glycogen synthesis in the liver (Cross, Alessi et al. 1995). Nevertheless, 2.5 week old *p62* transgenic animals displayed reduced glycogen levels. Since no increase in AKT activation was detected for that age group, this result might support the conclusion that an effect of AKT on GSK-3 could be neglected at the age of 2.5 weeks.

4.4.3 Apoptosis protection

Hepatocyte apoptosis is a cardinal feature of NAFLD and NASH and emerges as a critical mechanism contributing to the progression of liver diseases (Feldstein, Canbay et al. 2003; Wieckowska, Zein et al. 2006). On the other hand, apoptosis protection has been associated with poor prognosis of HCC (Ito, Monden et al. 2000).

In contrast to necrosis, which results from acute cellular injury, apoptosis describes a process of programmed cell death. Upon release of cytochrome c, a protein complex, the apoptosome, is formed which in turn activates the caspase cascade, triggering a cascade of caspase activation events leading to apoptosis (Li, Bergeron et al. 1997; Li, Nijhawan et al. 1997).

Caspase-3 activation plays a key role in the initiation of cellular events during the early apoptotic process. After induction of apoptosis through Act D and TNF- α , detection of caspase-3 activity was measured in cellular lysates from isolated hepatocytes.

The fatty liver phenotype and the constitutive AKT activation gave hints that apoptosis might be altered under *p62* overexpression.

In fact, after induction of apoptosis through Act D and TNF- α , caspase-3 activity was significantly lower in hepatocytes from *p62* transgenic animals and can be explained

by the implication of AKT in caspases inhibition upon activation through phosphorylation (Cardone, Roy et al. 1998).

Apoptosis inhibition results in a survival advantage of malignant cells, which in second line can convert to tumor cells, promoting carcinogenesis. Several studies demonstrated that the induction of apoptosis resulted in tumor regression (Hood and Cheresch 2002; Motoki, Mori et al. 2005). The results clearly support the theory of *p62* as a promotor of tumor progression.

4.5 Improved glucose tolerance

Insulin is the primary hormone involved in glucose homeostasis and in the stimulation of glucose transport. Insulin resistance is a common pathophysiological state in which target tissues fail to respond properly to normal levels of circulating insulin. Thereafter, impaired glucose tolerance can develop. Since the levels of circulating free fatty acids are thought to play a significant role in the establishment of insulin resistance (Shulman 2000), IP-GTT was performed.

p62 transgenic mice demonstrated a non-significant decrease in the area under the curve (AUC). However, this decrease was demonstrated to be significant in *p62* transgenic females.

The gender differences might simply reflect the observation that females expressed higher levels of the *p62* transgene than their male littermates. Since also the metabolic growth factor IGF2 showed increased expression in females, a causal interaction can be suggested.

The observation is in concordance with the improved glucose tolerance measured after liver-specific PTEN deletion in mice (Stiles, Wang et al. 2004). In this study, after an i. p. glucose load, the peak glucose concentration was lower and displayed a faster decline towards the basal level indicating an enhanced glucose disposal.

The results might display an increased ability of *p62* transgenic animals to clear glucose.

5. Summary

This study represents the first phenotypic characterization of mice showing a liver-specific expression of the IGF2 mRNA-binding protein *p62*. It clearly demonstrates the interaction between *p62*/IGF2 and H19 expression in *p62* transgenic mice and in human hepatoma cell lines and elucidates several effects of *p62* on apoptosis regulation and metabolism.

Since *p62* belongs to the IGF2 mRNA binding proteins, investigations were made on the expression level of IGF2 mRNA. An increase in IGF2 as well as the reciprocally imprinted H19 mRNA could be verified. This effect did neither originate from changes in allele-specific gene expression nor from alterations in mRNA turnover.

To elucidate the downstream effects of IGF2 induction caused by *p62* overexpression, the focus concentrated on the PI3-kinase pathway, known to regulate metabolism and apoptosis. Several experiments within this work demonstrated a reduction in PTEN gene expression concomitant with an increase in AKT phosphorylation, resulting in the prevention of *p62* transgenic hepatocytes from undergoing apoptosis.

In this study, the most prominent alteration discovered was a fatty liver phenotype in *p62* transgenic mice accompanied by a decrease in glycogen storage. This indicated a rise in the usage of glucose for lipogenesis. The fatty liver phenotype displayed improved glucose tolerance, at least in female mice.

Taken together, our data provide evidence that the oncofetal tumor-associated autoantigen *p62* plays a distinct pathophysiological role in liver disease. Its overexpression induced both a fatty liver and an anti-apoptotic phenotype. These findings suggest that the observed increase of *p62* expression during transition from liver disease to cancer has a causal role in disease progression. Alterations of *p62* levels might therefore serve as both a diagnostic marker and as a pharmacological target.

6. Outlook

Further studies are necessary to elucidate the distinct pathophysiological role of the oncofetal tumor-associated autoantigen *p62* in order to use *p62* both as a diagnostic marker and as a pharmacological target.

Since the pathways involved in the progression of the fatty liver phenotype are largely unknown and due to findings that the ratio of saturated to unsaturated fatty acids contributes to metabolic changes, gas chromatography experiments could give hints into the lipid composition of *p62* transgenic livers.

By now, the molecular pathways involved in the accumulation of fat droplets under *p62* overexpression remains to be elucidated.

Since the lipogenesis-promoting gene sterol regulatory element-binding protein 1 (SREBP1) is known to play a significant role in hepatic steatosis through the regulation of the synthesis and storage of fatty acids in the liver, investigations on SREBP1 expression levels might be of interest.

Another potential candidate might be the transcription factor peroxisome proliferator-activated receptor gamma (PPAR- γ), as PPAR- γ deficient mice display massive steatosis.

7. Supplement

7.1 PCR primer

gene	forward primer sequence 5'-3'	reverse primer sequence 5'-3'	amplicon size	gene bank accession number
<i>p62</i>	CAT CAA ACA GCT GGC GAG AT	GTG CCC GAT AAT TCT GAC GA	342 bp	AF057352
<i>LT2</i>	CTT AAT GAG GTC GGA ATC GA	GCT TGT CGT AAT AAT GGC GGC ATA C	500 bp	DL242837
<i>D7 Mit140</i>	GGA AGT TGT GGG ACC TTT AGG	CCT CTT CTG GCC TGT GAG GG	137 bp/125 bp	AC133502
<i>D7 Mit12</i>	GCT GGG TTT ATT CAT TGA AA	TCC AGC TCA TGG GTA GAA GA	197 bp/220 bp	AC122001
<i>SnuPE IGF2</i>	TCA GTG AAT CAA ATT A			NM_010514.2
<i>SnuPE H19</i>	CTC AGA CCG AGA TGG A			NR_001592
<i>hu-H19</i>	TTC AAA GCC TCC ACG ACT CT	CTG AGA CTC AAG GCC GTC TC	100 bp	NR_002196
<i>hu-β-actin</i>	TGC GTG ACA TTA AGG AGA AG	GTC AGG CAG CTC GTA GCT CT	106 bp	NM_001101
<i>hu-IGF2</i>	GGA CTT GA TCC CTG AAC CA	TGA AAA TTC CCG TGA GAA GG	100 bp	NM_000612
<i>mu-β-actin</i>	GCT GTG CTA TGT TGC TCT AGA CTT C	CTC AGT AAC AGT CCG CCT AGA AGC	500 bp	NM_007393
<i>mu-H19</i>	TAA GTC GAT TGC ACT GGT TTG GAG T	TGA TGG AAC TGC TTC CAH ACT AG	188 bp	NR_001592
<i>mu-IGF2</i>	GGC CCC GGA GAG ACT CTG TGC	TGG GGG TGG GTA AGG AGA AAC CT	600 bp	NM_010514
<i>hu p62</i>	GTT CCC GCA TCA CTC TTA T	GAA TCT CGC CAG CTG TTT GA	117 bp	AF057352
<i>mu IGF2</i>	GGA AGT CGA TGT TGG TGC TTC TC	CGA ACA GAC AAA CTG AAG CGT GT	186 bp	NM_010514
<i>mu H19</i>	CAG AGG TGG ATG TGC CTG CC	CAG AGG TGG ATG TGC CTG CC	80 bp	NM_023123
<i>mu-18S</i>	GCG CTT CTC TTT CCG CCA	AGC TCT CCG ACA CCT CTC TT	149 bp	NM_003278
<i>mu-cyclophilin</i>	GGC CGA TGA CGA GCC C	TGT CTT TGG AAC TTT GTC TGC	63 bp	NM_0089707
<i>PTEN</i>	GTG AGG ATG GTA GGG GAA TC	AGA GGA CTC AAA GGG GTG ACC	133 bp	NM_008960

7.2 Taq Man probes

probe name	sequence 5'-3'
hu- <i>p62</i> -FAM-BHQ	6-FAM d(TGT GAA TCT CTT CAT CCC AAC CCA GGC T) BHQ-1
IGF2-FAM-BHQ	6-FAM d(CCT TCG CCT TGT GCT GCA TCG CTG CT) BHQ-1
H19-FAM-BHQ	6-FAM d(TCA CTG AAG GCG AGG ATG ACA GGT GTG G) BHQ-1
18S-FAM-BHQ	6-FAM d(CCA CGC CAA CCC ACC GCC CTG TG) BHQ-1
Cyclophilin-FAM-BHQ	6-FAM d(TGG GCC GCG TCT CCT TCG A) BHQ-1

7.3 Real-time PCR conditions using Taq Man probes

gene	amount of Taq Man probe	Mg ²⁺ concentration	annealing temperature	number of cycles
hu <i>p62</i>	1.5 pmol	5 mM	60°C	40
mu IGF2	1.5 pmol	4 mM	60°C	40
mu H19	2.5 pmol	3 mM	60°C	40
mu 18S	2.5 pmol	3 mM	60°C	45
cyclophilin	1.5 pmol	3 mM	60°C	45
mu <i>p62</i>	2.5 pmol	5 mM	60°C	40

7.4 Real-time PCR conditions using SYBR green

gene	Initial denaturation (94°C)	Denaturation (94°C)	annealing (60°C)	Elongation (72°C)	number of cycles
β- actin	10 min	10 sec	15 sec	15 sec	40
hu <i>p62</i>	10 min	10 sec	15 sec	15 sec	40
hu H19	5 min	30 sec	30 sec	30 sec	40
hu IGF2	5 min	30 sec	30 sec	30 sec	40
PTEN	10 min	15 sec	15 sec	15 sec	45
mu 18S	8 min	15 sec	15 sec	15 sec	40

7.5 Antibodies

antibody	isotype	Dilution
monoclonal anti- α -tubulin	mouse IgG1	1/500 in RBB
phospho-AKT (Ser 473)	rabbit IgG1	1/1000 in RBB
PTEN	rabbit IgG1	1/1000 in RBB
hu <i>p62</i> (Western Blot)	human IgG1	1/1000 in RBB
goat anti-rabbit Irdye [®] 680	rabbit IgG, whole molecule	1/5000 in RBB
goat anti-mouse Irdye [®] 800 CW	mouse IgG, whole molecule	1/5000 in RBB
hu <i>p62</i> (immunohistology)	rabbit IgG1	1/500 in DRA
IGF2 (immunohistology)	rabbit IgG1	1/100 in DRA
NF κ B (immunohistology)	rabbit IgG1	1/100 in DRA

RBB= Rockland blocking buffer (purchased from Biomol, Hamburg, Germany)

DRA= DakoREAL[™] Antibody diluent (purchased from DAKO, Hamburg, Germany)

7.6 siRNA

code	name	sequence	purchased from
hu <i>p62</i> siRNA	Hs-IMP-2_2_HP siRNA	r(GGG UAG AUA UCC AUA GAA A)dTdT	Qiagen, Hilden, Germany
random siRNA	siGENOME non-targeting siRNA #2	including non-targeting siRNAs #2-#5, targeting firefly luciferase	Dharmacon, Thermo Fisher Scientific, Bonn, Germany

7.7 Molecular weight markers

PageRuler [™] Prestained Protein Ladder (Fermentas, St.Leon- Rot, Germany)
1 kb DNA ladder (Invitrogen, Karlsruhe, Germany)
50 base-pair ladder (Amersham, GE Healthcare, Munich, Germany)

7.8 Solutions and buffers

7.8.1 Cell culture media

Cell culture medium (hepatoma cell lines)

RPMI containing

10% FCS gold

1% penicillin/streptomycin

2 mM L-glutamine stock

L-glutamine stock

200 mM L-glutamine

Cell culture medium (primary murine hepatocytes)

Gibco Williams E with GlutaMax

10% FCS

1% penicillin/streptomycin

0.1% gentamycin

7.8.2 Solutions for primary murine hepatocyte isolation

EGTA stock, pH 7.6

125 mM EGTA

Calcium chloride stock (CaCl₂)

130 mM CaCl₂*2 H₂O

Magnesium sulfate stock (MgSO₄)

100 mM MgSO₄*7 H₂O

KH-stock, pH 7.4

1 M NaCl

23 mM KCl

12 mM KH₂PO₄

HEPES (*4-(2-hydroxyethyl)-1-piperazineethanesulfonic acid*), pH 7.6 or pH 8.5

252 mM HEPES

Glucose stock

50 mM Glucose

L-glutamine stock

200 mM L-glutamine

Amino-acid solution mix, pH 7.6 (sterile filtrated, stored at -20°C)

0.27 g/l L alanine

0.14 g/l L-aspartate-acid

0.40 g/l asparagine

0.27 g/l citrulline

0.14 g/l L-cysteine

1.0 g/l L-histidine

1.0 g/l L-glutamine-acid

1.0 g/l L-glycine

0.4 g/l L-isoleucine

0.80 g/l L-leucine

1.30 g/l L-lysine

0.55 g/l L-methionine

0.65 g/l L-ornithine

0.55 g/l L-phenylalanine

0.55 g/l L-proline

0.65 g/l L-serine

1.35 g/l L-tryptophane

0.55 g /l L-tyrosine

0.80 g/l L-valine

EGTA perfusion solution

25 mM Glucose stock

20 mM HEPES, pH 8.5 stock

0.4 mM L-glutamine stock

0.4 mM EGTA stock
12% amino acid solution mix
8% KH stock

Collagenase perfusion buffer

30 mM glucose stock
9.6% KH stock
24 mM HEPES, pH 8.5 stock
15% amino acid solution mix
5 mM CaCl₂ stock
2 mM L-glutamine stock
~0.25 g/l collagenase H

Suspension buffer

31 mM glucose stock
25 mM HEPES, pH 7.6
15% amino acid solution mix
10% KH stock
1 mM CaCl₂ stock
0.4 mM MgSO₄ stock
2 mM L-glutamine
2 g/l BSA (bovine serum albumine)

7.8.3 Solutions for Western Blotting

Moini lysis buffer (proteins)

50 mM Tris-HCl, pH 7.2
150 mM NaCl
1.0% Triton X-100
0.5% sodium deoxycholat
0.1% SDS (sodium dodecyl sulphate)
1 mM EGTA
25 mM NaF

(add immediately before use):

1 mM sodium orthovanadate

1 mM PMSF

14% complete mini (7x)

Running buffer (Western Blotting)

25 mM Tris base

86 mM glycine

1% SDS (10% stock)

Transfer buffer (Western Blotting)

25 mM Tris base

86 mM glycine

0.5% SDS (10% stock)

20% methanol

Collecting gel stock, pH 6.8

0.5 M Tris base

0.4% SDS

Separating gel stock, pH 8.8

1.5 M Tris base

0.4% SDS

10 % SDS PAGE separating gel composition

25% separating gel stock

33% Rotiphorese gel 30 (Roth)

1% APS (10%)

1% SDS (10%)

0.1% TEMED

39.5% H₂O

5% collecting gel for SDS- PAGE

12% collecting gel stock

16% Rotiphorese gel 30 (Roth)

1% APS (10%)

1% SDS (10%)

0.1% TEMED

68% H₂O

PBS, pH 7.4

150 mM NaCl

3 mM KCl

10 mM Na₂HPO₄*2 H₂O

1.4 mM KH₂PO₄

PBST, pH 7.4

PBS, pH 7.4

0.05% Tween 20

7.8.4 Solutions for caspase measurements**Lysis buffer (caspase activity)**

5 mM MgCl₂

1 mM EGTA

0.1% Triton X-100

25 mM HEPES, pH 7.5

1 mM Pefabloc SC

1 µg/ml Aprotinin/ Leupeptin/Pepstatin A

Substrate buffer (caspase activity), pH 7.5, (store at 4°C)

50 mM HEPES, pH 7.5

1% sucrose

0.1% CHAPS (*3-[(3-Cholamidopropyl) dimethylammonio]-1-propanesulfonate*)

DTT stock (store at -20°C)

1 M DTT (*Dithiothreitol*)

Ac-DEVD-AFC (stock), (store at -20°C)

10 mM ac-DEVD-AFC

7.8.5 Material for SNuPE analysis

SNuPE extension mastermix

50 mM Tris-HCl, pH 9.5

2.5 mM MgCl₂

0.05 mM ddTTP

0.05 mM ddCTP

3.6 μM SNuPE primer

0.25 U Termipol [Solis BioDyne]

SNuPE buffer A

0.1 M triethylammonium acetate (TEAA)

SNuPE buffer B

0.1 M triethylammonium acetate (TEAA) and 25% acetonitrile

8. Bibliography

- Abel S, Smuts CM, de Villiers C and Gelderblom WC (2001). Changes in essential fatty acid patterns associated with normal liver regeneration and the progression of hepatocyte nodules in rat hepatocarcinogenesis. Carcinogenesis **22** (5): 795-804.
- Aden DP, Fogel A, Plotkin S, Damjanov I and Knowles BB (1979). Controlled synthesis of HBsAg in a differentiated human liver carcinoma-derived cell line. Nature **282** (5739): 615-616.
- Ahmed NN, Franke TF, Bellacosa A, Datta K, Gonzalez-Portal ME, Taguchi T, Testa JR and Tschlis PN (1993). The proteins encoded by c-akt and v-akt differ in post-translational modification, subcellular localization and oncogenic potential. Oncogene **8** (7): 1957-1963.
- Alberts B, Johnson, Alexander., Lewis,Julian., Raff,Martin., Roberts,Keith., Walter,Peter. (1992). Molecular Biology of the cell, 4th edition, Taylor & Francis.
- Alexander JJ, Bey EM, Geddes EW and Lecatsas G (1976). Establishment of a continuously growing cell line from primary carcinoma of the liver. S Afr Med J **50** (54): 2124-2128.
- Andjelkovic M, Alessi DR, Meier R, Fernandez A, Lamb NJ, Frech M, Cron P, Cohen P, Lucocq JM and Hemmings BA (1997). Role of translocation in the activation and function of protein kinase B. J Biol Chem **272** (50): 31515-31524.
- Anezaki Y, Ohshima S, Ishii H, Kinoshita N, Dohmen T, Kataoka E, Sato W, Iizuka M, Goto T, Sasaki J, Sasaki T, Suzuki A, Ohnishi H and Horie Y (2009). Sex difference in the liver of hepatocyte-specific Pten-deficient mice: A model of nonalcoholic steatohepatitis. Hepatol Res **39** (6): 609-618.
- Angulo P (2002). Nonalcoholic fatty liver disease. N Engl J Med **346** (16): 1221-1231.

- Ariel I, Ayesch S, Perlman EJ, Pizov G, Tanos V, Schneider T, Erdmann VA, Podeh D, Komitowski D, Quasem AS, de Groot N and Hochberg A (1997). The product of the imprinted H19 gene is an oncofetal RNA. Mol Pathol **50** (1): 34-44.
- Baker J, Liu JP, Robertson EJ and Efstratiadis A (1993). Role of insulin-like growth factors in embryonic and postnatal growth. Cell **75** (1): 73-82.
- Bandsma RH, Smit GP and Kuipers F (2002). Disturbed lipid metabolism in glycogen storage disease type 1. Eur J Pediatr **161 Suppl 1**: S65-69.
- Banet G, Bibi O, Matouk I, Ayesch S, Laster M, Kimber KM, Tykocinski M, de Groot N, Hochberg A and Ohana P (2000). Characterization of human and mouse H19 regulatory sequences. Mol Biol Rep **27** (3): 157-165.
- Bannasch P, Klimek F and Mayer D (1997). Early bioenergetic changes in hepatocarcinogenesis: preneoplastic phenotypes mimic responses to insulin and thyroid hormone. J Bioenerg Biomembr **29** (4): 303-313.
- Baron U and Bujard H (2000). Tet repressor-based system for regulated gene expression in eukaryotic cells: principles and advances. Methods Enzymol **327**: 401-421.
- Barsyte-Lovejoy D, Lau SK, Boutros PC, Khosravi F, Jurisica I, Andrulis IL, Tsao MS and Penn LZ (2006). The c-Myc oncogene directly induces the H19 noncoding RNA by allele-specific binding to potentiate tumorigenesis. Cancer Res **66** (10): 5330-5337.
- Barthel A, Okino ST, Liao J, Nakatani K, Li J, Whitlock JP, Jr. and Roth RA (1999). Regulation of GLUT1 gene transcription by the serine/threonine kinase Akt1. J Biol Chem **274** (29): 20281-20286.
- Bellas RE, FitzGerald MJ, Fausto N and Sonenshein GE (1997). Inhibition of NF-kappa B activity induces apoptosis in murine hepatocytes. Am J Pathol **151** (4): 891-896.

- Bernstein E, Caudy AA, Hammond SM and Hannon GJ (2001). Role for a bidentate ribonuclease in the initiation step of RNA interference. Nature **409** (6818): 363-366.
- Bestor TH (2000). The DNA methyltransferases of mammals. Hum Mol Genet **9** (16): 2395-2402.
- Bhattacharya SK, Ramchandani S, Cervoni N and Szyf M (1999). A mammalian protein with specific demethylase activity for mCpG DNA. Nature **397** (6720): 579-583.
- Boshart M, Weber F, Jahn G, Dorsch-Hasler K, Fleckenstein B and Schaffner W (1985). A very strong enhancer is located upstream of an immediate early gene of human cytomegalovirus. Cell **41** (2): 521-530.
- Brannan CI, Dees EC, Ingram RS and Tilghman SM (1990). The product of the H19 gene may function as an RNA. Mol Cell Biol **10** (1): 28-36.
- Brazil DP, Yang ZZ and Hemmings BA (2004). Advances in protein kinase B signalling: AKTion on multiple fronts. Trends Biochem Sci **29** (5): 233-242.
- Bressac B, Galvin KM, Liang TJ, Isselbacher KJ, Wands JR and Ozturk M (1990). Abnormal structure and expression of p53 gene in human hepatocellular carcinoma. Proceedings of the National Academy of Sciences of the United States of America **87** (5): 1973-1977.
- Bruning JC, Michael MD, Winnay JN, Hayashi T, Horsch D, Accili D, Goodyear LJ and Kahn CR (1998). A muscle-specific insulin receptor knockout exhibits features of the metabolic syndrome of NIDDM without altering glucose tolerance. Mol Cell **2** (5): 559-569.
- Brunkow ME and Tilghman SM (1991). Ectopic expression of the H19 gene in mice causes prenatal lethality. Genes Dev **5** (6): 1092-1101.
- Bugianesi E, Leone N, Vanni E, Marchesini G, Brunello F, Carucci P, Musso A, De Paolis P, Capussotti L, Salizzoni M and Rizzetto M (2002). Expanding the

- natural history of nonalcoholic steatohepatitis: from cryptogenic cirrhosis to hepatocellular carcinoma. Gastroenterology **123** (1): 134-140.
- Burchell A (1998). Glycogen storage diseases and the liver. Baillieres Clin Gastroenterol **12** (2): 337-354.
- Burt AD, Mutton A and Day CP (1998). Diagnosis and interpretation of steatosis and steatohepatitis. Semin Diagn Pathol **15** (4): 246-258.
- Bustin SA (2000). Absolute quantification of mRNA using real-time reverse transcription polymerase chain reaction assays. J Mol Endocrinol **25** (2): 169-193.
- Butler M, McKay RA, Popoff IJ, Gaarde WA, Witchell D, Murray SF, Dean NM, Bhanot S and Monia BP (2002). Specific inhibition of PTEN expression reverses hyperglycemia in diabetic mice. Diabetes **51** (4): 1028-1034.
- Cantley LC and Neel BG (1999). New insights into tumor suppression: PTEN suppresses tumor formation by restraining the phosphoinositide 3-kinase/AKT pathway. Proc Natl Acad Sci U S A **96** (8): 4240-4245.
- Cardone MH, Roy N, Stennicke HR, Salvesen GS, Franke TF, Stanbridge E, Frisch S and Reed JC (1998). Regulation of cell death protease caspase-9 by phosphorylation. Science **282** (5392): 1318-1321.
- Cariani E, Lasserre C, Seurin D, Hamelin B, Kemeny F, Franco D, Czech MP, Ullrich A and Brechot C (1988). Differential expression of insulin-like growth factor II mRNA in human primary liver cancers, benign liver tumors, and liver cirrhosis. Cancer Res **48** (23): 6844-6849.
- Casola S, Ungaro P, Pedone PV, Lazzaro D, Fattori E, Ciliberto G, Zarrilli R, Bruni CB and Riccio A (1995). Loss of heterozygosity of imprinted genes in SV40 t/T antigen-induced hepatocellular carcinomas. Oncogene **11** (4): 711-721.

- Chan TO, Rittenhouse SE and Tsichlis PN (1999). AKT/PKB and other D3 phosphoinositide-regulated kinases: kinase activation by phosphoinositide-dependent phosphorylation. Annu Rev Biochem **68**: 965-1014.
- Charalambous MP, Lightfoot T, Speirs V, Horgan K and Gooderham NJ (2009). Expression of COX-2, NF-kappaB-p65, NF-kappaB-p50 and IKKalpha in malignant and adjacent normal human colorectal tissue. Br J Cancer **101** (1): 106-115.
- Chen KS and Katz J (1988). Zonation of glycogen and glucose syntheses, but not glycolysis, in rat liver. Biochem J **255** (1): 99-104.
- Chen R, Kim O, Yang J, Sato K, Eisenmann KM, McCarthy J, Chen H and Qiu Y (2001). Regulation of Akt/PKB activation by tyrosine phosphorylation. J Biol Chem **276** (34): 31858-31862.
- Chiappini F, Barrier A, Saffroy R, Domart MC, Dagues N, Azoulay D, Sebah M, Franc B, Chevalier S, Debuire B, Dudoit S and Lemoine A (2006). Exploration of global gene expression in human liver steatosis by high-density oligonucleotide microarray. Lab Invest **86** (2): 154-165.
- Cho H, Thorvaldsen JL, Chu Q, Feng F and Birnbaum MJ (2001). Akt1/PKBalpha is required for normal growth but dispensable for maintenance of glucose homeostasis in mice. J Biol Chem **276** (42): 38349-38352.
- Chomczynski P and Sacchi N (1987). Single-step method of RNA isolation by acid guanidinium thiocyanate-phenol-chloroform extraction. Anal Biochem **162** (1): 156-159.
- Christofori G, Naik P and Hanahan D (1994). A second signal supplied by insulin-like growth factor II in oncogene-induced tumorigenesis. Nature **369** (6479): 414-418.

- Christofori G, Naik P and Hanahan D (1995). Deregulation of both imprinted and expressed alleles of the insulin-like growth factor 2 gene during beta-cell tumorigenesis. Nat Genet **10** (2): 196-201.
- Clark JM, Brancati FL and Diehl AM (2002). Nonalcoholic fatty liver disease. Gastroenterology **122** (6): 1649-1657.
- Cong LN, Chen H, Li Y, Zhou L, McGibbon MA, Taylor SI and Quon MJ (1997). Physiological role of Akt in insulin-stimulated translocation of GLUT4 in transfected rat adipose cells. Mol Endocrinol **11** (13): 1881-1890.
- Constancia M, Dean W, Lopes S, Moore T, Kelsey G and Reik W (2000). Deletion of a silencer element in Igf2 results in loss of imprinting independent of H19. Nat Genet **26** (2): 203-206.
- Cornel M (2008). Der Experimentator: Molekularbiologie/Genomics, Spektrum Akademischer Verlag.
- Cory S, Vaux DL, Strasser A, Harris AW and Adams JM (1999). Insights from Bcl-2 and Myc: malignancy involves abrogation of apoptosis as well as sustained proliferation. Cancer Res **59** (7 Suppl): 1685s-1692s.
- Coulouarn C, Gomez-Quiroz LE, Lee JS, Kaposi-Novak P, Conner EA, Goldina TA, Onishchenko GE, Factor VM and Thorgeirsson SS (2006). Oncogene-specific gene expression signatures at preneoplastic stage in mice define distinct mechanisms of hepatocarcinogenesis. Hepatology **44** (4): 1003-1011.
- Cross DA, Alessi DR, Cohen P, Andjelkovich M and Hemmings BA (1995). Inhibition of glycogen synthase kinase-3 by insulin mediated by protein kinase B. Nature **378** (6559): 785-789.
- Crowder RJ and Freeman RS (1998). Phosphatidylinositol 3-kinase and Akt protein kinase are necessary and sufficient for the survival of nerve growth factor-dependent sympathetic neurons. J Neurosci **18** (8): 2933-2943.

- Cui H, Niemitz EL, Ravenel JD, Onyango P, Brandenburg SA, Lobanenko VV and Feinberg AP (2001). Loss of imprinting of insulin-like growth factor-II in Wilms' tumor commonly involves altered methylation but not mutations of CTCF or its binding site. Cancer Res **61** (13): 4947-4950.
- Datta SR, Dudek H, Tao X, Masters S, Fu H, Gotoh Y and Greenberg ME (1997). Akt phosphorylation of BAD couples survival signals to the cell-intrinsic death machinery. Cell **91** (2): 231-241.
- Davies CC, Mason J, Wakelam MJ, Young LS and Eliopoulos AG (2004). Inhibition of phosphatidylinositol 3-kinase- and ERK MAPK-regulated protein synthesis reveals the pro-apoptotic properties of CD40 ligation in carcinoma cells. J Biol Chem **279** (2): 1010-1019.
- Davies SM (1994). Developmental regulation of genomic imprinting of the IGF2 gene in human liver. Cancer Res **54** (10): 2560-2562.
- Day CP and James OF (1998). Steatohepatitis: a tale of two "hits"? Gastroenterology **114** (4): 842-845.
- DeChiara TM, Efstratiadis A and Robertson EJ (1990). A growth-deficiency phenotype in heterozygous mice carrying an insulin-like growth factor II gene disrupted by targeting. Nature **345** (6270): 78-80.
- DeChiara TM, Robertson EJ and Efstratiadis A (1991). Parental imprinting of the mouse insulin-like growth factor II gene. Cell **64** (4): 849-859.
- Desbois-Mouthon C, Baron A, Blivet-Van Eggelpoel MJ, Fartoux L, Venot C, Bladt F, Housset C and Rosmorduc O (2009). Insulin-like growth factor-1 receptor inhibition induces a resistance mechanism via the epidermal growth factor receptor/HER3/AKT signaling pathway: rational basis for cotargeting insulin-like growth factor-1 receptor and epidermal growth factor receptor in hepatocellular carcinoma. Clin Cancer Res **15** (17): 5445-5456.

- Desbois-Mouthon C, Wendum D, Cadoret A, Rey C, Leneuve P, Blaise A, Housset C, Tronche F, Le Bouc Y and Holzenberger M (2006). Hepatocyte proliferation during liver regeneration is impaired in mice with liver-specific IGF-1R knockout. Faseb J **20** (6): 773-775.
- Di Cristofano A, Kotsi P, Peng YF, Cordon-Cardo C, Elkon KB and Pandolfi PP (1999). Impaired Fas response and autoimmunity in Pten^{+/-} mice. Science **285** (5436): 2122-2125.
- Di Cristofano A and Pandolfi PP (2000). The multiple roles of PTEN in tumor suppression. Cell **100** (4): 387-390.
- Di Cristofano A, Pesce B, Cordon-Cardo C and Pandolfi PP (1998). Pten is essential for embryonic development and tumour suppression. Nat Genet **19** (4): 348-355.
- Diehl JA, Cheng M, Roussel MF and Sherr CJ (1998). Glycogen synthase kinase-3beta regulates cyclin D1 proteolysis and subcellular localization. Genes Dev **12** (22): 3499-3511.
- Divecha N and Irvine RF (1995). Phospholipid signaling. Cell **80** (2): 269-278.
- Dobie K, Mehtali M, McClenaghan M and Lathe R (1997). Variegated gene expression in mice. Trends in Genetics **13** (4): 127.
- Dorer DR and Henikoff S (1997). Transgene repeat arrays interact with distant heterochromatin and cause silencing in cis and trans. Genetics **147** (3): 1181-1190.
- Eberhardt W, Doller A, Akool el S and Pfeilschifter J (2007). Modulation of mRNA stability as a novel therapeutic approach. Pharmacol Ther **114** (1): 56-73.
- Ekström TJ, Cui H, Nystrom A, Rutanen EM and Ohlsson R (1995). Monoallelic expression of IGF2 at the human fetal/maternal boundary. Mol Reprod Dev **41** (2): 177-183.

- Feil R, Walter J, Allen ND and Reik W (1994). Developmental control of allelic methylation in the imprinted mouse Igf2 and H19 genes. Development **120** (10): 2933-2943.
- Feinberg AP and Vogelstein B (1983). Hypomethylation of ras oncogenes in primary human cancers. Biochem Biophys Res Commun **111** (1): 47-54.
- Feldstein AE, Canbay A, Angulo P, Tanai M, Burgart LJ, Lindor KD and Gores GJ (2003). Hepatocyte apoptosis and fas expression are prominent features of human nonalcoholic steatohepatitis. Gastroenterology **125** (2): 437-443.
- Ferguson-Smith AC, Sasaki H, Cattanach BM and Surani MA (1993). Parental-origin-specific epigenetic modification of the mouse H19 gene. Nature **362** (6422): 751-755.
- Fire A, Xu S, Montgomery MK, Kostas SA, Driver SE and Mello CC (1998). Potent and specific genetic interference by double-stranded RNA in *Caenorhabditis elegans*. Nature **391** (6669): 806-811.
- Foster LJ, Li D, Randhawa VK and Klip A (2001). Insulin accelerates inter-endosomal GLUT4 traffic via phosphatidylinositol 3-kinase and protein kinase B. J Biol Chem **276** (47): 44212-44221.
- Franke TF (2000). Assays for Akt. Methods Enzymol **322**: 400-410.
- Franke TF, Hornik CP, Segev L, Shostak GA and Sugimoto C (2003). PI3K/Akt and apoptosis: size matters. Oncogene **22** (56): 8983-8998.
- Franke TF, Tartof KD and Tschlis PN (1994). The SH2-like Akt homology (AH) domain of c-akt is present in multiple copies in the genome of vertebrate and invertebrate eucaryotes. Cloning and characterization of the *Drosophila melanogaster* c-akt homolog Dakt1. Oncogene **9** (1): 141-148.
- Frith CH, Boothe AD, Greenman DL and Farmer JH (1980). Correlations between gross and microscopic lesions in carcinogenic studies in mice. J Environ Pathol Toxicol **3** (3 Spec No): 139-153.

- Fujiwara Y, Hoon DS, Yamada T, Umeshita K, Gotoh M, Sakon M, Nishisho I and Monden M (2000). PTEN / MMAC1 mutation and frequent loss of heterozygosity identified in chromosome 10q in a subset of hepatocellular carcinomas. Jpn J Cancer Res **91** (3): 287-292.
- Gaunt TR, Cooper JA, Miller GJ, Day INM and O'Dell SD (2001). Positive associations between single nucleotide polymorphisms in the IGF2 gene region and body mass index in adult males. Hum. Mol. Genet. **10** (14): 1491-1501.
- Gille H and Downward J (1999). Multiple ras effector pathways contribute to G(1) cell cycle progression. J Biol Chem **274** (31): 22033-22040.
- Glassman ML, de Groot N and Hochberg A (1996). Relaxation of imprinting in carcinogenesis. Cancer Genet Cytogenet **89** (1): 69-73.
- Goll MG, Kirpekar F, Maggert KA, Yoder JA, Hsieh CL, Zhang X, Golic KG, Jacobsen SE and Bestor TH (2006). Methylation of tRNA^{Asp} by the DNA methyltransferase homolog Dnmt2. Science **311** (5759): 395-398.
- Gossen M and Bujard H (1992). Tight control of gene expression in mammalian cells by tetracycline-responsive promoters. Proc Natl Acad Sci U S A **89** (12): 5547-5551.
- Graveel CR, Jatkoa T, Madore SJ, Holt AL and Farnham PJ (2001). Expression profiling and identification of novel genes in hepatocellular carcinomas. Oncogene **20** (21): 2704-2712.
- Gu L, Findley HW and Zhou M (2002). MDM2 induces NF-kappaB/p65 expression transcriptionally through Sp1-binding sites: a novel, p53-independent role of MDM2 in doxorubicin resistance in acute lymphoblastic leukemia. Blood **99** (9): 3367-3375.
- Guenet JL, Nagamine C, Simon-Chazottes D, Montagutelli X and Bonhomme F (1990). Hst-3: an X-linked hybrid sterility gene. Genet Res **56** (2-3): 163-165.

- Hancock JM, Worthey EA and Santibanez-Koref MF (2001). A role for selection in regulating the evolutionary emergence of disease-causing and other coding CAG repeats in humans and mice. Mol Biol Evol **18** (6): 1014-1023.
- Hannon GJ (2002). RNA interference. Nature **418** (6894): 244-251.
- Hansen TV, Hammer NA, Nielsen J, Madsen M, Dalbaeck C, Wewer UM, Christiansen J and Nielsen FC (2004). Dwarfism and impaired gut development in insulin-like growth factor II mRNA-binding protein 1-deficient mice. Mol Cell Biol **24** (10): 4448-4464.
- Hao Y, Crenshaw T, Moulton T, Newcomb E and Tycko B (1993). Tumour-suppressor activity of H19 RNA. Nature **365** (6448): 764-767.
- Harris TM, Rogler LE and Rogler CE (1998). Reactivation of the maternally imprinted IGF2 allele in TGFalpha induced hepatocellular carcinomas in mice. Oncogene **16** (2): 203-209.
- Hashimoto E, Yatsuji S, Tobar M, Taniai M, Torii N, Tokushige K and Shiratori K (2009). Hepatocellular carcinoma in patients with nonalcoholic steatohepatitis. J Gastroenterol **44 Suppl 19**: 89-95.
- Hay N (2005). The Akt-mTOR tango and its relevance to cancer. Cancer Cell **8** (3): 179-183.
- Heikkinen S, Argmann, C.A., Champy, M.F., Auwerx, E. (2007). Evaluation of Glucose Homeostasis.
- Hengartner MO (2000). The biochemistry of apoptosis. Nature **407** (6805): 770-776.
- Henikoff S (1992). Position effect and related phenomena. Curr Opin Genet Dev **2** (6): 907-912.
- Hennessy BT, Smith DL, Ram PT, Lu Y and Mills GB (2005). Exploiting the PI3K/AKT pathway for cancer drug discovery. Nat Rev Drug Discov **4** (12): 988-1004.

- Hillen W and Berens C (1994). Mechanisms underlying expression of Tn10 encoded tetracycline resistance. Annu Rev Microbiol **48**: 345-369.
- Hood JD and Cheresh DA (2002). Targeted delivery of mutant Raf kinase to neovessels causes tumor regression. Cold Spring Harb Symp Quant Biol **67**: 285-291.
- Horie Y, Suzuki A, Kataoka E, Sasaki T, Hamada K, Sasaki J, Mizuno K, Hasegawa G, Kishimoto H, Iizuka M, Naito M, Enomoto K, Watanabe S, Mak TW and Nakano T (2004). Hepatocyte-specific Pten deficiency results in steatohepatitis and hepatocellular carcinomas. J Clin Invest **113** (12): 1774-1783.
- Hutchinson J, Jin J, Cardiff RD, Woodgett JR and Muller WJ (2001). Activation of Akt (protein kinase B) in mammary epithelium provides a critical cell survival signal required for tumor progression. Mol Cell Biol **21** (6): 2203-2212.
- Iizuka N, Oka M, Yamada-Okabe H, Mori N, Tamesa T, Okada T, Takemoto N, Tangoku A, Hamada K, Nakayama H, Miyamoto T, Uchimura S and Hamamoto Y (2002). Comparison of gene expression profiles between hepatitis B virus- and hepatitis C virus-infected hepatocellular carcinoma by oligonucleotide microarray data on the basis of a supervised learning method. Cancer Res **62** (14): 3939-3944.
- Ito T, Urabe Y, Shiraga K, Sakaguchi K, Higashi T, Hino N and Tsuji T (1995). Retrospective analysis of the multidisciplinary treatment for 534 hepatocellular carcinoma patients over a 12-year period. Intern Med **34** (7): 623-627.
- Ito Y, Monden M, Takeda T, Eguchi H, Umeshita K, Nagano H, Nakamori S, Dono K, Sakon M, Nakamura M, Tsujimoto M, Nakahara M, Nakao K, Yokosaki Y and Matsuura N (2000). The status of Fas and Fas ligand expression can predict recurrence of hepatocellular carcinoma. Br J Cancer **82** (6): 1211-1217.
- Jaeschke H (1996). Chemokines, neutrophils, and inflammatory liver injury. Shock **6** (6): 403-404.

- Jirtle RL (1999). Genomic imprinting and cancer. Exp Cell Res **248** (1): 18-24.
- Kandel ES and Hay N (1999). The regulation and activities of the multifunctional serine/threonine kinase Akt/PKB. Exp Cell Res **253** (1): 210-229.
- Kaneda A and Feinberg AP (2005). Loss of imprinting of IGF2: a common epigenetic modifier of intestinal tumor risk. Cancer Res **65** (24): 11236-11240.
- Kapeller R and Cantley LC (1994). Phosphatidylinositol 3-kinase. Bioessays **16** (8): 565-576.
- Kawamura N, Nagai H, Bando K, Koyama M, Matsumoto S, Tajiri T, Onda M, Fujimoto J, Ueki T, Konishi N, Shiba T and Emi M (1999). PTEN/MMAC1 mutations in hepatocellular carcinomas: somatic inactivation of both alleles in tumors. Jpn J Cancer Res **90** (4): 413-418.
- Kim HT, Choi BH, Niikawa N, Lee TS and Chang SI (1998). Frequent loss of imprinting of the H19 and IGF-II genes in ovarian tumors. Am J Med Genet **80** (4): 391-395.
- Kim KS and Lee YI (1997). Biallelic expression of the H19 and IGF2 genes in hepatocellular carcinoma. Cancer Lett **119** (2): 143-148.
- Kishimoto H, Hamada K, Saunders M, Backman S, Sasaki T, Nakano T, Mak TW and Suzuki A (2003). Physiological functions of Pten in mouse tissues. Cell Struct Funct **28** (1): 11-21.
- Kistner A, Gossen M, Zimmermann F, Jurecic J, Ullmer C, Lubbert H and Bujard H (1996). Doxycycline-mediated quantitative and tissue-specific control of gene expression in transgenic mice. Proc Natl Acad Sci U S A **93** (20): 10933-10938.
- Koike K (2007). Hepatitis C virus contributes to hepatocarcinogenesis by modulating metabolic and intracellular signaling pathways. J Gastroenterol Hepatol **22 Suppl 1**: S108-111.

- Kondo M, Suzuki H, Ueda R, Osada H, Takagi K, Takahashi T and Takahashi T (1995). Frequent loss of imprinting of the H19 gene is often associated with its overexpression in human lung cancers. Oncogene **10** (6): 1193-1198.
- Koufos A, Hansen MF, Copeland NG, Jenkins NA, Lampkin BC and Cavenee WK (1985). Loss of heterozygosity in three embryonal tumours suggests a common pathogenetic mechanism. Nature **316** (6026): 330.
- Krähenbühl L, Lang C, Ludes S, Seiler C, Schafer M, Zimmermann A and Krahenbuhl S (2003). Reduced hepatic glycogen stores in patients with liver cirrhosis. Liver Int **23** (2): 101-109.
- Krähenbühl L, Talos C, Reichen J and Krahenbuhl S (1996). Progressive decrease in tissue glycogen content in rats with long-term cholestasis. Hepatology **24** (4): 902-907.
- Kuroiwa M, Sakamoto J, Shimada A, Suzuki N, Hirato J, Park MJ, Sotomatsu M and Hayashi Y (2009). Manifestation of alveolar rhabdomyosarcoma as primary cutaneous lesions in a neonate with Beckwith-Wiedemann syndrome. J Pediatr Surg **44** (3): e31-35.
- Leevers SJ, Vanhaesebroeck B and Waterfield MD (1999). Signalling through phosphoinositide 3-kinases: the lipids take centre stage. Curr Opin Cell Biol **11** (2): 219-225.
- Leighton PA, Saam JR, Ingram RS, Stewart CL and Tilghman SM (1995). An enhancer deletion affects both H19 and Igf2 expression. Genes Dev **9** (17): 2079-2089.
- Leighton PA, Saam JR, Ingram RS and Tilghman SM (1996). Genomic imprinting in mice: its function and mechanism. Biol Reprod **54** (2): 273-278.
- Li E, Beard C, Forster AC, Bestor TH and Jaenisch R (1993). DNA methylation, genomic imprinting, and mammalian development. Cold Spring Harb Symp Quant Biol **58**: 297-305.

- Li H, Bergeron L, Cryns V, Pasternack MS, Zhu H, Shi L, Greenberg A and Yuan J (1997). Activation of caspase-2 in apoptosis. J Biol Chem **272** (34): 21010-21017.
- Li P, Nijhawan D, Budihardjo I, Srinivasula SM, Ahmad M, Alnemri ES and Wang X (1997). Cytochrome c and dATP-dependent formation of Apaf-1/caspase-9 complex initiates an apoptotic protease cascade. Cell **91** (4): 479-489.
- Li X, Nong Z, Ekstrom C, Larsson E, Nordlinder H, Hofmann WJ, Trautwein C, Odenthal M, Dienes HP, Ekstrom TJ and Schirmacher P (1997). Disrupted IGF2 promoter control by silencing of promoter P1 in human hepatocellular carcinoma. Cancer Res **57** (10): 2048-2054.
- Li YM, Franklin G, Cui HM, Svensson K, He XB, Adam G, Ohlsson R and Pfeifer S (1998). The H19 transcript is associated with polysomes and may regulate IGF2 expression in trans. J Biol Chem **273** (43): 28247-28252.
- Liu J, Kahri AI, Heikkila P, Ilvesmaki V and Voutilainen R (1995). H19 and insulin-like growth factor-II gene expression in adrenal tumors and cultured adrenal cells. J Clin Endocrinol Metab **80** (2): 492-496.
- Lu M, Nakamura RM, Dent ED, Zhang JY, Nielsen FC, Christiansen J, Chan EK and Tan EM (2001). Aberrant expression of fetal RNA-binding protein p62 in liver cancer and liver cirrhosis. Am J Pathol **159** (3): 945-953.
- Luedde T, Beraza N, Kotsikoris V, van Loo G, Nenci A, De Vos R, Roskams T, Trautwein C and Pasparakis M (2007). Deletion of NEMO/IKKgamma in liver parenchymal cells causes steatohepatitis and hepatocellular carcinoma. Cancer Cell **11** (2): 119-132.
- Luedde T, Beraza N and Trautwein C (2006). Evaluation of the role of nuclear factor-kappaB signaling in liver injury using genetic animal models. J Gastroenterol Hepatol **21 Suppl 3**: S43-46.

- Luedi PP, Dietrich FS, Weidman JR, Bosko JM, Jirtle RL and Hartemink AJ (2007). Computational and experimental identification of novel human imprinted genes. Genome Res **17** (12): 1723-1730.
- Maehama T and Dixon JE (1998). The tumor suppressor, PTEN/MMAC1, dephosphorylates the lipid second messenger, phosphatidylinositol 3,4,5-trisphosphate. J Biol Chem **273** (22): 13375-13378.
- Matouk IJ, DeGroot N, Mezan S, Ayeshe S, Abu-lail R, Hochberg A and Galun E (2007). The H19 non-coding RNA is essential for human tumor growth. PLoS One **2** (9): e845.
- Matsuzawa N, Takamura T, Kurita S, Misu H, Ota T, Ando H, Yokoyama M, Honda M, Zen Y, Nakanuma Y, Miyamoto K and Kaneko S (2007). Lipid-induced oxidative stress causes steatohepatitis in mice fed an atherogenic diet. Hepatology **46** (5): 1392-1403.
- Milner RD and Hill DJ (1984). Fetal growth control: the role of insulin and related peptides. Clin Endocrinol (Oxf) **21** (4): 415-433.
- Minokoshi Y, Kahn CR and Kahn BB (2003). Tissue-specific ablation of the GLUT4 glucose transporter or the insulin receptor challenges assumptions about insulin action and glucose homeostasis. J Biol Chem **278** (36): 33609-33612.
- Moore T, Constancia M, Zubair M, Bailleul B, Feil R, Sasaki H and Reik W (1997). Multiple imprinted sense and antisense transcripts, differential methylation and tandem repeats in a putative imprinting control region upstream of mouse Igf2. Proc Natl Acad Sci U S A **94** (23): 12509-12514.
- Moorehead RA, Fata JE, Johnson MB and Khokha R (2001). Inhibition of mammary epithelial apoptosis and sustained phosphorylation of Akt/PKB in MMTV-IGF-II transgenic mice. Cell Death Differ **8** (1): 16-29.

- Moorehead RA, Hojilla CV, De Belle I, Wood GA, Fata JE, Adamson ED, Watson KL, Edwards DR and Khokha R (2003). Insulin-like growth factor-II regulates PTEN expression in the mammary gland. J Biol Chem **278** (50): 50422-50427.
- Moses AC, Nissley SP, Short PA, Rechler MM, White RM, Knight AB and Higa OZ (1980). Increased levels of multiplication-stimulating activity, an insulin-like growth factor, in fetal rat serum. Proc Natl Acad Sci U S A **77** (6): 3649-3653.
- Mosmann T (1983). Rapid colorimetric assay for cellular growth and survival: application to proliferation and cytotoxicity assays. J Immunol Methods **65** (1-2): 55-63.
- Motoki K, Mori E, Matsumoto A, Thomas M, Tomura T, Humphreys R, Albert V, Muto M, Yoshida H, Aoki M, Tamada T, Kuroki R, Yoshida H, Ishida I, Ware CF and Kataoka S (2005). Enhanced apoptosis and tumor regression induced by a direct agonist antibody to tumor necrosis factor-related apoptosis-inducing ligand receptor 2. Clin Cancer Res **11** (8): 3126-3135.
- Mulisch M, Welsch, U. (1989). Romeis-Mikroskopische Technik, Spektrum Akademischer Verlag.
- Mullis KB and Faloona FA (1987). Specific synthesis of DNA in vitro via a polymerase-catalyzed chain reaction. Methods Enzymol **155**: 335-350.
- Murrell A, Heeson S, Bowden L, Constancia M, Dean W, Kelsey G and Reik W (2001). An intragenic methylated region in the imprinted Igf2 gene augments transcription. EMBO Rep **2** (12): 1101-1106.
- Nair S, Mason A, Eason J, Loss G and Perrillo RP (2002). Is obesity an independent risk factor for hepatocellular carcinoma in cirrhosis? Hepatology **36** (1): 150-155.
- Nakabayashi H, Taketa K, Miyano K, Yamane T and Sato J (1982). Growth of human hepatoma cells lines with differentiated functions in chemically defined medium. Cancer Res **42** (9): 3858-3863.

- Nakagawa H, Chadwick RB, Peltomaki P, Plass C, Nakamura Y and de La Chapelle A (2001). Loss of imprinting of the insulin-like growth factor II gene occurs by biallelic methylation in a core region of H19-associated CTCF-binding sites in colorectal cancer. Proc Natl Acad Sci U S A **98** (2): 591-596.
- Neuschwander-Tetri BA (2005). Nonalcoholic Steatohepatitis and the Metabolic Syndrome. The American Journal of the Medical Sciences **330** (6): 326-335.
- Neuschwander-Tetri BA and Caldwell SH (2003). Nonalcoholic steatohepatitis: summary of an AASLD Single Topic Conference. Hepatology **37** (5): 1202-1219.
- Nielsen FC (1992). The molecular and cellular biology of insulin-like growth factor II. Prog Growth Factor Res **4** (3): 257-290.
- Nielsen J, Christiansen J, Lykke-Andersen J, Johnsen AH, Wewer UM and Nielsen FC (1999). A family of insulin-like growth factor II mRNA-binding proteins represses translation in late development. Mol Cell Biol **19** (2): 1262-1270.
- O'Connor R (1998). Survival factors and apoptosis. Adv Biochem Eng Biotechnol **62**: 137-166.
- O'Dell SD and Day IN (1998). Insulin-like growth factor II (IGF-II). Int J Biochem Cell Biol **30** (7): 767-771.
- Ohlsson R, Hedborg F, Holmgren L, Walsh C and Ekstrom TJ (1994). Overlapping patterns of IGF2 and H19 expression during human development: biallelic IGF2 expression correlates with a lack of H19 expression. Development **120** (2): 361-368.
- Ohlsson R, Nystrom A, Pfeifer-Ohlsson S, Tohonen V, Hedborg F, Schofield P, Flam F and Ekstrom TJ (1993). IGF2 is parentally imprinted during human embryogenesis and in the Beckwith-Wiedemann syndrome. Nat Genet **4** (1): 94-97.

- Oka Y, Rozek LM and Czech MP (1985). Direct demonstration of rapid insulin-like growth factor II Receptor internalization and recycling in rat adipocytes. Insulin stimulates ¹²⁵I-insulin-like growth factor II degradation by modulating the IGF-II receptor recycling process. J Biol Chem **260** (16): 9435-9442.
- Otogawa K, Kinoshita K, Fujii H, Sakabe M, Shiga R, Nakatani K, Ikeda K, Nakajima Y, Ikura Y, Ueda M, Arakawa T, Hato F and Kawada N (2007). Erythrophagocytosis by liver macrophages (Kupffer cells) promotes oxidative stress, inflammation, and fibrosis in a rabbit model of steatohepatitis: implications for the pathogenesis of human nonalcoholic steatohepatitis. Am J Pathol **170** (3): 967-980.
- Owen OE, Reichle FA, Mozzoli MA, Kreulen T, Patel MS, Effenbein IB, Golsorkhi M, Chang KH, Rao NS, Sue HS and Boden G (1981). Hepatic, gut, and renal substrate flux rates in patients with hepatic cirrhosis. J Clin Invest **68** (1): 240-252.
- Pachnis V, Belayew A and Tilghman SM (1984). Locus unlinked to alpha-fetoprotein under the control of the murine raf and Rif genes. Proc Natl Acad Sci U S A **81** (17): 5523-5527.
- Pachnis V, Brannan CI and Tilghman SM (1988). The structure and expression of a novel gene activated in early mouse embryogenesis. Embo J **7** (3): 673-681.
- Paramio JM, Navarro M, Segrelles C, Gomez-Casero E and Jorcano JL (1999). PTEN tumour suppressor is linked to the cell cycle control through the retinoblastoma protein. Oncogene **18** (52): 7462-7468.
- Parkin DM, Bray F, Ferlay J and Pisani P (2005). Global cancer statistics, 2002. CA Cancer J Clin **55** (2): 74-108.
- Parsons R and Simpson L (2003). PTEN and cancer. Methods Mol Biol **222**: 147-166.

- Patra SK, Patra A, Zhao H and Dahiya R (2002). DNA methyltransferase and demethylase in human prostate cancer. Mol Carcinog **33** (3): 163-171.
- Pavelic K, Bukovic D and Pavelic J (2002). The role of insulin-like growth factor 2 and its receptors in human tumors. Mol Med **8** (12): 771-780.
- Pellino JL and Sontheimer EJ (2003). R2D2 leads the silencing trigger to mRNA's death star. Cell **115** (2): 132-133.
- Perks CM, Vernon EG, Rosendahl AH, Tonge D and Holly JM (2007). IGF-II and IGFBP-2 differentially regulate PTEN in human breast cancer cells. Oncogene **26** (40): 5966-5972.
- Persad S, Attwell S, Gray V, Mawji N, Deng JT, Leung D, Yan J, Sanghera J, Walsh MP and Dedhar S (2001). Regulation of protein kinase B/Akt-serine 473 phosphorylation by integrin-linked kinase: critical roles for kinase activity and amino acids arginine 211 and serine 343. J Biol Chem **276** (29): 27462-27469.
- Piao Z, Kim H, Jeon BK, Lee WJ and Park C (1997). Relationship between loss of heterozygosity of tumor suppressor genes and histologic differentiation in hepatocellular carcinoma. Cancer **80** (5): 865-872.
- Polesel J, Zucchetto A, Montella M, Dal Maso L, Crispo A, La Vecchia C, Serraino D, Franceschi S and Talamini R (2009). The impact of obesity and diabetes mellitus on the risk of hepatocellular carcinoma. Ann Oncol **20** (2): 353-357.
- Rameh LE and Cantley LC (1999). The role of phosphoinositide 3-kinase lipid products in cell function. J Biol Chem **274** (13): 8347-8350.
- Rappaport AM (1960). [Observations on the pathophysiology of liver structure.]. Klin Wochenschr **38**: 561-577.
- Rappaport AM (1976). The microcirculatory acinar concept of normal and pathological hepatic structure. Beitr Pathol **157** (3): 215-243.

- Reeve AE, Eccles MR, Wilkins RJ, Bell GI and Millow LJ (1985). Expression of insulin-like growth factor-II transcripts in Wilms' tumour. Nature **317** (6034): 258-260.
- Reik W and Allen ND (1994). Genomic imprinting. Imprinting with and without methylation. Curr Biol **4** (2): 145-147.
- Reik W and Walter J (2001). Genomic imprinting: parental influence on the genome. Nat Rev Genet **2** (1): 21-32.
- Ripoche MA, Kress C, Poirier F and Dandolo L (1997). Deletion of the H19 transcription unit reveals the existence of a putative imprinting control element. Genes Dev **11** (12): 1596-1604.
- Rodriguez-Viciano P, Marte BM, Warne PH and Downward J (1996). Phosphatidylinositol 3' kinase: one of the effectors of Ras. Philos Trans R Soc Lond B Biol Sci **351** (1336): 225-231; discussion 231-222.
- Rodriguez-Viciano P, Warne PH, Dhand R, Vanhaesebroeck B, Gout I, Fry MJ, Waterfield MD and Downward J (1994). Phosphatidylinositol-3-OH kinase as a direct target of Ras. Nature **370** (6490): 527-532.
- Romano G (2004). Systems for regulated or tissue-specific gene expression. Drug News Perspect **17** (2): 85-90.
- Ross J (1995). mRNA stability in mammalian cells. Microbiol Rev **59** (3): 423-450.
- Ross JA, Schmidt PT, Perentesis JP and Davies SM (1999). Genomic imprinting of H19 and insulin-like growth factor-2 in pediatric germ cell tumors. Cancer **85** (6): 1389-1394.
- Rotwein P and Hall LJ (1990). Evolution of insulin-like growth factor II: characterization of the mouse IGF-II gene and identification of two pseudo-exons. DNA Cell Biol **9** (10): 725-735.

- Ruhl CE and Everhart JE (2004). Epidemiology of nonalcoholic fatty liver. Clin Liver Dis **8** (3): 501-519, vii.
- Rump P, Zeegers MP and van Essen AJ (2005). Tumor risk in Beckwith-Wiedemann syndrome: A review and meta-analysis. Am J Med Genet A **136** (1): 95-104.
- Runge S, Nielsen FC, Nielsen J, Lykke-Andersen J, Wewer UM and Christiansen J (2000). H19 RNA binds four molecules of insulin-like growth factor II mRNA-binding protein. J Biol Chem **275** (38): 29562-29569.
- Russo A, Tommasi AM and Renzi L (1996). Detection of minor and major satellite DNA in cytokinesis-blocked mouse splenocytes by a PRINS tandem labelling approach. Mutagenesis **11** (6): 547-552.
- Sasaki H, Ishihara K and Kato R (2000). Mechanisms of Igf2/H19 imprinting: DNA methylation, chromatin and long-distance gene regulation. J Biochem **127** (5): 711-715.
- Sasaki H, Jones PA, Chaillet JR, Ferguson-Smith AC, Barton SC, Reik W and Surani MA (1992). Parental imprinting: potentially active chromatin of the repressed maternal allele of the mouse insulin-like growth factor II (Igf2) gene. Genes Dev **6** (10): 1843-1856.
- Scheid MP and Woodgett JR (2001). PKB/AKT: functional insights from genetic models. Nat Rev Mol Cell Biol **2** (10): 760-768.
- Schirmacher P, Held WA, Yang D, Chisari FV, Rustum Y and Rogler CE (1992). Reactivation of insulin-like growth factor II during hepatocarcinogenesis in transgenic mice suggests a role in malignant growth. Cancer Res **52** (9): 2549-2556.
- Schoemaker MH, Ros JE, Homan M, Trautwein C, Liston P, Poelstra K, van Goor H, Jansen PL and Moshage H (2002). Cytokine regulation of pro- and anti-apoptotic genes in rat hepatocytes: NF-kappaB-regulated inhibitor of apoptosis protein 2 (cIAP2) prevents apoptosis. J Hepatol **36** (6): 742-750.

- Scott ML, Fujita T, Liou HC, Nolan GP and Baltimore D (1993). The p65 subunit of NF-kappa B regulates I kappa B by two distinct mechanisms. Genes Dev **7** (7A): 1266-1276.
- Sen R and Baltimore D (1986). Inducibility of kappa immunoglobulin enhancer-binding protein Nf-kappa B by a posttranslational mechanism. Cell **47** (6): 921-928.
- Sherlock S (1983). Acute fatty liver of pregnancy and the microvesicular fat diseases. Gut **24** (4): 265-269.
- Shulman GI (2000). Cellular mechanisms of insulin resistance. J Clin Invest **106** (2): 171-176.
- Stambolic V, Suzuki A, de la Pompa JL, Brothers GM, Mirtsos C, Sasaki T, Ruland J, Penninger JM, Siderovski DP and Mak TW (1998). Negative regulation of PKB/Akt-dependent cell survival by the tumor suppressor PTEN. Cell **95** (1): 29-39.
- Steck PA, Pershouse MA, Jasser SA, Yung WK, Lin H, Ligon AH, Langford LA, Baumgard ML, Hattier T, Davis T, Frye C, Hu R, Swedlund B, Teng DH and Tavtigian SV (1997). Identification of a candidate tumour suppressor gene, MMAC1, at chromosome 10q23.3 that is mutated in multiple advanced cancers. Nat Genet **15** (4): 356-362.
- Stephens LR, Eguinoa A, Erdjument-Bromage H, Lui M, Cooke F, Coadwell J, Smrcka AS, Thelen M, Cadwallader K, Tempst P and Hawkins PT (1997). The G beta gamma sensitivity of a PI3K is dependent upon a tightly associated adaptor, p101. Cell **89** (1): 105-114.
- Stewart CE and Rotwein P (1996). Growth, differentiation, and survival: multiple physiological functions for insulin-like growth factors. Physiol Rev **76** (4): 1005-1026.

- Stiles B, Gilman V, Khanzenon N, Lesche R, Li A, Qiao R, Liu X and Wu H (2002). Essential role of AKT-1/protein kinase B alpha in PTEN-controlled tumorigenesis. Mol Cell Biol **22** (11): 3842-3851.
- Stiles B, Wang Y, Stahl A, Bassilian S, Lee WP, Kim YJ, Sherwin R, Devaskar S, Lesche R, Magnuson MA and Wu H (2004). Liver-specific deletion of negative regulator Pten results in fatty liver and insulin hypersensitivity [corrected]. Proc Natl Acad Sci U S A **101** (7): 2082-2087.
- Su Q, Benner A, Hofmann WJ, Otto G, Pichlmayr R and Bannasch P (1997). Human hepatic preneoplasia: phenotypes and proliferation kinetics of foci and nodules of altered hepatocytes and their relationship to liver cell dysplasia. Virchows Arch **431** (6): 391-406.
- Su Q, Schröder CH, Hofmann WJ, Otto G, Pichlmayr R and Bannasch P (1998). Expression of hepatitis B virus X protein in HBV-infected human livers and hepatocellular carcinomas. Hepatology **27** (4): 1109-1120.
- Sun SC, Ganchi PA, Beraud C, Ballard DW and Greene WC (1994). Autoregulation of the NF-kappa B transactivator RelA (p65) by multiple cytoplasmic inhibitors containing ankyrin motifs. Proc Natl Acad Sci U S A **91** (4): 1346-1350.
- Sussenbach JS, Steenbergh PH and Holthuizen P (1992). Structure and expression of the human insulin-like growth factor genes. Growth Regul **2** (1): 1-9.
- Suzuki A, de la Pompa JL, Stambolic V, Elia AJ, Sasaki T, del Barco Barrantes I, Ho A, Wakeham A, Itie A, Khoo W, Fukumoto M and Mak TW (1998). High cancer susceptibility and embryonic lethality associated with mutation of the PTEN tumor suppressor gene in mice. Curr Biol **8** (21): 1169-1178.
- Takahashi N, Qi Y, Patel HR and Ahima RS (2004). A novel aminosterol reverses diabetes and fatty liver disease in obese mice. J Hepatol **41** (3): 391-398.
- Takai D, Gonzales FA, Tsai YC, Thayer MJ and Jones PA (2001). Large scale mapping of methylcytosines in CTCF-binding sites in the human H19 promoter

- and aberrant hypomethylation in human bladder cancer. Hum Mol Genet **10** (23): 2619-2626.
- Teli MR, James OF, Burt AD, Bennett MK and Day CP (1995). The natural history of nonalcoholic fatty liver: a follow-up study. Hepatology **22** (6): 1714-1719.
- Teng DH, Hu R, Lin H, Davis T, Iliev D, Frye C, Swedlund B, Hansen KL, Vinson VL, Gumpfer KL, Ellis L, El-Naggar A, Frazier M, Jasser S, Langford LA, Lee J, Mills GB, Pershouse MA, Pollack RE, Tornos C, Troncoso P, Yung WK, Fujii G, Berson A, Steck PA and et al. (1997). MMAC1/PTEN mutations in primary tumor specimens and tumor cell lines. Cancer Res **57** (23): 5221-5225.
- Terrettaz J and Jeanrenaud B (1983). In vivo hepatic and peripheral insulin resistance in genetically obese (fa/fa) rats. Endocrinology **112** (4): 1346-1351.
- Thorgeirsson SS and Grisham JW (2002). Molecular pathogenesis of human hepatocellular carcinoma. Nat Genet **31** (4): 339-346.
- Thorvaldsen JL, Duran KL and Bartolomei MS (1998). Deletion of the H19 differentially methylated domain results in loss of imprinted expression of H19 and Igf2. Genes Dev **12** (23): 3693-3702.
- Valls C, Iannaccone R, Alba E, Murakami T, Hori M, Passariello R and Vilgrain V (2006). Fat in the liver: diagnosis and characterization. Eur Radiol **16** (10): 2292-2308.
- Vanhaesebroeck B, Leervers SJ, Panayotou G and Waterfield MD (1997). Phosphoinositide 3-kinases: a conserved family of signal transducers. Trends Biochem Sci **22** (7): 267-272.
- Verma IM, Stevenson JK, Schwarz EM, Van Antwerp D and Miyamoto S (1995). Rel/NF-kappa B/I kappa B family: intimate tales of association and dissociation. Genes Dev **9** (22): 2723-2735.
- Vinciguerra M, Carrozzino F, Peyrou M, Carlone S, Montesano R, Benelli R and Foti M (2009). Unsaturated fatty acids promote hepatoma proliferation and

- progression through downregulation of the tumor suppressor PTEN. J Hepatol **50** (6): 1132-1141.
- Vinciguerra M and Foti M (2008). PTEN at the crossroad of metabolic diseases and cancer in the liver. Ann Hepatol **7** (3): 192-199.
- Vinciguerra M, Sgroi A, Veyrat-Durebex C, Rubbia-Brandt L, Buhler LH and Foti M (2009). Unsaturated fatty acids inhibit the expression of tumor suppressor phosphatase and tensin homolog (PTEN) via microRNA-21 up-regulation in hepatocytes. Hepatology **49** (4): 1176-1184.
- Vinciguerra M, Veyrat-Durebex C, Moukil MA, Rubbia-Brandt L, Rohner-Jeanrenaud F and Foti M (2008). PTEN down-regulation by unsaturated fatty acids triggers hepatic steatosis via an NF-kappaBp65/mTOR-dependent mechanism. Gastroenterology **134** (1): 268-280.
- Visconti R, Cerutti J, Battista S, Fedele M, Trapasso F, Zeki K, Miano MP, de Nigris F, Casalino L, Curcio F, Santoro M and Fusco A (1997). Expression of the neoplastic phenotype by human thyroid carcinoma cell lines requires NFkappaB p65 protein expression. Oncogene **15** (16): 1987-1994.
- Vollmar AM, Schmidt KN and Schulz R (1996). Natriuretic peptide receptors on rat thymocytes: inhibition of proliferation by atrial natriuretic peptide. Endocrinology **137** (5): 1706-1713.
- Wagener A, Schmitt AO, Aksu S, Schlote W, Neuschl C and Brockmann GA (2006). Genetic, sex, and diet effects on body weight and obesity in the Berlin Fat Mouse Inbred lines. Physiol Genomics **27** (3): 264-270.
- Walters MC, Magis W, Fiering S, Eidemiller J, Scalzo D, Groudine M and Martin DI (1996). Transcriptional enhancers act in cis to suppress position-effect variegation. Genes Dev **10** (2): 185-195.
- Ward A, Fisher R, Richardson L, Pooler JA, Squire S, Bates P, Shaposhnikov R, Hayward N, Thurston M and Graham CF (1997). Genomic regions regulating

- imprinting and insulin-like growth factor-II promoter 3 activity in transgenics: novel enhancer and silencer elements. Genes Funct **1** (1): 25-36.
- Ward JM and Lynch PH (1984). Transplantability of naturally occurring benign and malignant neoplasms and age-associated nonneoplastic lesions of the aging F344 rat as biological evidence for the histological diagnosis of neoplasms. Cancer Res **44** (6): 2608-2615.
- Wasmuth H, Zaldivar, MM., Beraza, N., Trautwein, C. (2007). Of mice and NASH- from fat to inflammation and fibrosis. Elsevier: Drug discovery today: Disease models.
- Watanabe S, Horie Y, Kataoka E, Sato W, Dohmen T, Ohshima S, Goto T and Suzuki A (2007). Non-alcoholic steatohepatitis and hepatocellular carcinoma: lessons from hepatocyte-specific phosphatase and tensin homolog (PTEN)-deficient mice. J Gastroenterol Hepatol **22 Suppl 1**: S96-S100.
- Wieckowska A, Zein NN, Yerian LM, Lopez AR, McCullough AJ and Feldstein AE (2006). In vivo assessment of liver cell apoptosis as a novel biomarker of disease severity in nonalcoholic fatty liver disease. Hepatology **44** (1): 27-33.
- Winwood PJ and Arthur MJ (1993). Kupffer cells: their activation and role in animal models of liver injury and human liver disease. Semin Liver Dis **13** (1): 50-59.
- Wong LL, Limm WM, Severino R and Wong LM (2000). Improved survival with screening for hepatocellular carcinoma. Liver Transpl **6** (3): 320-325.
- Xu Z, Chen L, Leung L, Yen TS, Lee C and Chan JY (2005). Liver-specific inactivation of the Nrf1 gene in adult mouse leads to nonalcoholic steatohepatitis and hepatic neoplasia. Proc Natl Acad Sci U S A **102** (11): 4120-4125.
- Yang DY and Rogler CE (1991). Analysis of insulin-like growth factor II (IGF-II) expression in neoplastic nodules and hepatocellular carcinomas of

- woodchucks utilizing in situ hybridization and immunocytochemistry. Carcinogenesis **12** (10): 1893-1901.
- Yang SQ, Lin HZ, Mandal AK, Huang J and Diehl AM (2001). Disrupted signaling and inhibited regeneration in obese mice with fatty livers: implications for nonalcoholic fatty liver disease pathophysiology. Hepatology **34** (4 Pt 1): 694-706.
- Yao R and Cooper GM (1995). Requirement for phosphatidylinositol-3 kinase in the prevention of apoptosis by nerve growth factor. Science **267** (5206): 2003-2006.
- Yeh FS, Yu MC, Mo CC, Luo S, Tong MJ and Henderson BE (1989). Hepatitis B virus, aflatoxins, and hepatocellular carcinoma in southern Guangxi, China. Cancer Res **49** (9): 2506-2509.
- Yoder JA and Bestor TH (1998). A candidate mammalian DNA methyltransferase related to pmt1p of fission yeast. Hum Mol Genet **7** (2): 279-284.
- Yoshimizu T, Miroglio A, Ripoché MA, Gabory A, Vernucci M, Riccio A, Colnot S, Godard C, Terris B, Jammes H and Dandolo L (2008). The H19 locus acts in vivo as a tumor suppressor. Proc Natl Acad Sci U S A **105** (34): 12417-12422.
- Younossi ZM, McCullough AJ, Ong JP, Barnes DS, Post A, Tavill A, Bringman D, Martin LM, Assmann J, Gramlich T, Mullen KD, O'Shea R, Carey WD and Ferguson R (2004). Obesity and non-alcoholic fatty liver disease in chronic hepatitis C. J Clin Gastroenterol **38** (8): 705-709.
- Zaina S, Pettersson L, Thomsen AB, Chai CM, Qi Z, Thyberg J and Nilsson J (2003). Shortened life span, bradycardia, and hypotension in mice with targeted expression of an Igf2 transgene in smooth muscle cells. Endocrinology **144** (6): 2695-2703.

-
- Zemel S, Bartolomei MS and Tilghman SM (1992). Physical linkage of two mammalian imprinted genes, H19 and insulin-like growth factor 2. Nat Genet **2** (1): 61-65.
- Zhang JY, Chan EK, Peng XX and Tan EM (1999). A novel cytoplasmic protein with RNA-binding motifs is an autoantigen in human hepatocellular carcinoma. J Exp Med **189** (7): 1101-1110.
- Zhang JY, Zhu W, Imai H, Kiyosawa K, Chan EK and Tan EM (2001). De-novo humoral immune responses to cancer-associated autoantigens during transition from chronic liver disease to hepatocellular carcinoma. Clin Exp Immunol **125** (1): 3-9.

9. Publications

9.1 Abstracts

Kiemer AK, Tybl E, Shi FU, Wieland S, Chisari F, Tan EM. Upregulation of IGF2 and H19 in livers transgenic for the tumor-associated autoantigen *p62*. Boston, 2006, Scientific Conference, poster presentation, AASLD, Hepatology supplement.

Tybl E, Shi FD, Walter J, Tierling S, Bohle RM; Wieland S, Chisari F, Tan EM, Kiemer AK. Metabolic alterations in mice overexpressing the tumor-associated autoantigen *p62*. 3. Mildred Scheel Cancer Conference der Deutschen Krebshilfe, 18.-20.06.2008, poster presentation.

Tybl E, Shi FD, Walter J, Tierling S, Bohle RM; Wieland S, Chisari F, Tan EM, Kiemer AK. Possible roles of the tumor-associated autoantigen *p62* in Hepatocellular Carcinoma (HCC). 50. Jahrestagung der Deutschen Gesellschaft für Experimentelle und Klinische Pharmakologie und Toxikologie, Mainz, 10.-12.03.2009, Lecture, Naunyn-Schmiedeberg's Archives of Pharmacology supplement.

9.2 Original Publications

Tybl E, Shi F-D, Tierling S, Walter J, Bohle RM, Wieland S, Zhang J, Tan EM, Kiemer AK. Liver-specific overexpression of the IGF2 mRNA binding protein *p62* induces a fatty liver disease phenotype. submitted

Bouayed J, Desor F, Rammal H, Kiemer AK, Tybl E, Schroeder H, Rychen G, Soulimani R. Effects of lactational exposure to benzo[alpha]pyrene (B[alpha]P) on postnatal neurodevelopment, neuronal receptor gene expression and behaviour in mice. Toxicology 2009; **259** (3): 97-106.

Hoesl E, Stieber J, Herrmann S, Feil S, Tybl E, Hofmann F, Feil R, Ludwig A. Tamoxifen-inducible gene deletion in the cardiac conduction system. J Mol Cell Cardiol 2008; **45** (1): 62-69.

Dünschede F, Tybl E, Kiemer AK, Dutkowski P, Erbes K, Kircher A, Gockel I, Zechner U, Schad A, Lang H, Junginger T, Kempfski O. Bcl-2 upregulation after 3-nitropropionic acid preconditioning in warm rat liver ischemia. Shock 2008; **30** (6): 699-704.

10. Curriculum vitae

Name: Tybl

Vorname: Elisabeth

Geburtstag und -ort: 23.05.1979 in Neunkirchen/Saar

Familienstand: unverheiratet

Staatsangehörigkeit: deutsch

Theoretische Ausbildung:

1986-1990 Grundschule Wemmetsweiler

1990-1993 Illtal- Gymnasium Illingen

1993-1998 Gymnasium Ottweiler

1999-2003 Studium der Pharmazie an der Universität des Saarlandes

2004 Abschluss: 3. pharmazeutisches Staatsexamen

2006 Diplomarbeit in Pharmazie in der Arbeitsgruppe von Prof. Dr. A. Ludwig am Lehrstuhl von Prof. Dr. F. B. Hofmann, Institut für Pharmakologie und Toxikologie, TU München, München

2005- 2009 Dissertation zum Dr. rer. nat. am Lehrstuhl von Frau Prof. Dr. Alexandra K. Kiemer, Institut für Pharmazeutische Biologie, Universität des Saarlandes, Saarbrücken

12. Acknowledgement

Die vorliegende Arbeit wurde am Institut für Pharmazeutische Biologie, Fakultät für Pharmazie der Universität des Saarlandes angefertigt.

An dieser Stelle möchte ich mich bei Frau Prof. Dr. Alexandra K. Kiemer bedanken, die es mir ermöglicht hat, an diesem interessanten und komplexen Thema an Ihrem Institut arbeiten zu können und die durch ihre Diskussionen und Anregungen zum Entstehen dieser Arbeit beigetragen hat.

Herrn Prof. Dr. Rainer M. Bohle und den Mitarbeitern seines Instituts, vor allem Gertrud Walter, danke ich besonders für die gute Betreuung, die vielfältigen Ratschläge und vielen freundlichen Gespräche.

Herrn Prof. Dr. Jörn Walter und Dr. Sascha Tierling gilt mein Dank für Ihre hilfreiche und tatkräftige Unterstützung bei der Durchführung der Imprinting Analysen.

Ebenfalls ein großes Dankeschön gilt den Tierpflegern Sven Oliger und Eva-Maria Dilly, die mich mit viel Gefühl in das Arbeiten mit den Mäusen einweihten.

Marga Sand-Hill und Herrn Prof. Dr. Jürgen Geisel danke ich für deren Hilfe bei der Durchführung der Serumanalysen.

Mein Dank geht auch an Klaus Gladel und Theo Ransweiler, die mir bei der Hepatozytenisolierung und in technischen Dingen eine große Stütze waren und die mir mit Ihrer herzlichen Art über schwierige Phasen der Arbeit hinweggeholfen haben. Nadège Ripoché danke ich dafür, dass sie immer ein offenes Ohr für Diskussionen hatte und mich durch ihre nette und kollegiale Art unterstützt hat. Simon Räsch, Anna Erschens, Oliver Blank und Marion Welsch danke ich für deren Hilfe bei der Durchführung praktischer Arbeiten und das witzige Arbeitsklima.

Zuletzt gilt mein ganz besonderer Dank meinen Eltern, Barbara und Rainer, weil sie immer für mich da sind und mich bei allem unterstützen.